BOMEM

NGST

Next Generation Space Telescope

Final Report

Volume 1 - Executive Summary

Document Number: **SP-BOM-005/99**

Issue: **1** **Revision:** B

Issue Date: **13 October 1999** **Document Name:** Annex B1.doc

	Function	Name	Signature	Date
Prepared by				
Prepared by				
Approved by	Project Manager	André Villemaire		
Approved by	Director, SPR division	Jean Giroux		

BOMEM Inc. • a unit of Elsag Bailey Process Automation N.V.

450 Saint-Jean-Baptiste Avenue • Québec, Québec G2E 5S5 Canada • Phone (418) 877–2944 • Fax (418) 877–2834

TABLE OF CONTENTS

DOCUMENT CHANGE RECORD

Issue	Rev.	Date	Chapter/Paragraph Number, Change Description (and Reasons)
1	-	30 March 1999	First release of document
1	A	20 August 1999	New revision to remove references to cost, for inclusion with final report to NASA
1	B	13 October 1999	New revision to remove proprietary notices.

1. INTRODUCTION

The Next Generation of Space Telescope (NGST) project of NASA is intended to provide continuity and new focus for research following the success of the Hubble Space Telescope. It is considered to be a technologically challenging project as the technology needed is not necessarily available. It challenges the innovation of the scientific and technological community to come up with an affordable technology to carry out the scientific goals of the mission.

Canada has a strong astronomical community and they have ranked the participation of this project as the priority in their LTSP III submission. In order for Canada to participate, the areas of technical expertise and competence necessarily has to match the required technologies of the NGST project.

At the end of 1998, CSA awarded a number of contracts to Canadian firms in order to define the nature and scope of the potential Canadian contribution to NGST. Bomem was awarded a contract (9F007-8-3007/001/SR) to study the potential use of a Fourier Transform Imaging Spectrometer as a science instrument for NGST. Bomem has been building Fourier Transform spectrometers for more than 25 years and has several thousands commercial units installed world-wide. Very early, Bomem also established itself as a world leader of advanced IR instrumentation, developing state-of-the-art spectrometers for balloon-borne, aircraft as well as spacecraft. Today Bomem is involved in several major space Fourier Transform programs, including the ESA MIPAS, CNES IASI, NPOESS CrIS and JPL TES programs, to name a few.

The purpose of this document is to summarise the results from the CSA funded NGST study. This document is Volume 1 – *the Executive Summary* - of the final report. The other deliverables of the study contract are listed in Table 1.

Table 1: Deliverables of the study contract

Volume	Document Number	Document	Description
1	SP-BOM-005/99	Executive Summary	5-page summary of the findings of the contract
2	SP-BOM-006/99	Planning Report	Report on the scheduling and cost of the proposed Canadian participation. The planning report also includes the risk assessment and mitigation plan
3	SP-BOM-007/99	Trade Analyses	Report on the trade analyses performed to arrive at a credible baseline for the proposed Canadian participation.
4	SP-BOM-008/99	Performance Analyses	Report on the sensitivity analyses performed to evaluate the suitability of the proposed Canadian participation for NGST
5	SP-BOM-009/99	Technology Report	Report on some proposed novel technology approaches to the specific NGST environment for the proposed Canadian participation.

Bomem is currently conducting a follow-on contract (9F007-8-1136/001/SR) to build a prototype interferometer to study key technological challenges identified in the first study. The documents listed in Table 1 and the test results from the prototype will be included in the Canadian Imaging Fourier Transform Spectrometer final report, due 1 October 1999.

1.1 REFERENCE DOCUMENTS

RD 1 Bomem Proposal No:SPIR180898, issue 1, revision -, dated 8 September 1998, in response to solicitation No 9F007-8-3007/A.

RD 2 Volume 2 - Planning Report, SP-BOM-006/99

RD 3 Volume 3 - Trade Analyses, SP-BOM-007/99

RD 4 Volume 4 - Performance Analyses, SP-BOM-008/99

RD 5 Volume 5 - Technology Report, SP-BOM-009/99

2. SUMMARY OF THE STUDY CONTRACT

Figure 1 shows the structure of the study contract as it was presented in the Bomem proposal (RD 1). This work flow was followed closely during the execution of the project. The labels on the left hand side of the boxes in Figure 1 refer to the items requested by the government in Section 2 of the statement of work. As can be seen a number of additional tasks were added to complement and enhance the suggested work.

In the task "Explore IFTS trade space", we explored the trade space of the NGST IFTS to arrive at a technical baseline. The results of the trade studies are described in Volume 3 (RD 3) and summarised in Section 3. This technical baseline raises the fundamental design issues on one hand and proposes a baseline with a representative level of complexity of the final instrument on the other, with enough details to be able to build a realistic cost and schedule estimate.

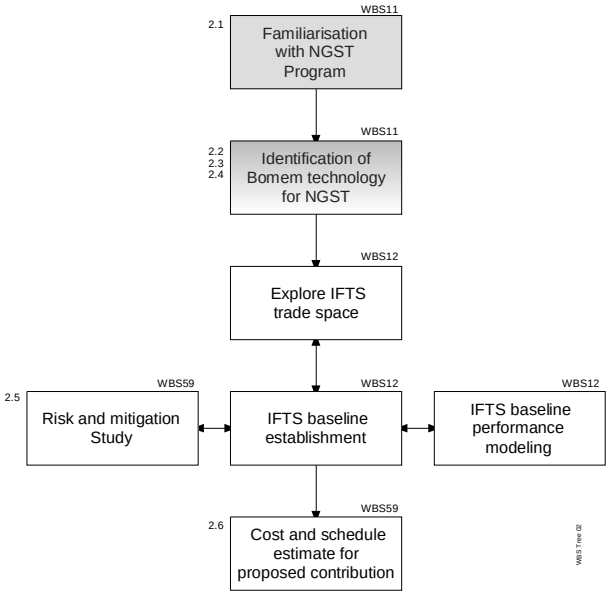

Figure 1 Structure of the Bomem lead study contract.

The spectrometric performance of this baseline was evaluated to verify compliance with the science requirements. The results from the simulations can be found in Volume 4 (RD 4). The IFTS technology was found to not only to satisfy the scientist requirements but also to enable more science because of the wealth of information conveyed by this type of integral field system.

After completing the technical investigations, a risk analysis was performed and a mitigation plan was drafted as reported in Volume 2 (RD 2) and are summarised in Section 4. The cost and schedule estimates were produced and are described in the same volume and are summarised in Sections 5 and 6.

3. PROPOSED PARTICIPATION

The proposed Bomem participation in NGST is the interferometer subsystem of an Imaging Fourier Transform Spectrometer (IFTS) for NGST. Given the very broad wavelength range of NGST, it is believed that the subsystem will actually be composed of three separate interferometer modules and one dichroic module to steer the light into them. **This constitutes the baseline for the schedule and cost estimates presented in this report**.

The interferometer modules are defined as complete subsystems capable of operating by themselves. The subsystem includes the opto-mechanical components (mirrors, beamsplitters and possibly collimating and condensing lenses or mirrors, depending on the primeship of these items) interferometer structural and thermal control assemblies, metrology assembly (metrology source, optics, detector and electronics) and interferometer control electronics. Figure 2 illustrates these components.

We propose a development approach that uses basically three key models, 1) a breadboard which is currently under development, 2) an engineering model which will be form, fit and function compatible with the flight model but may use lower grade of space qualification on the electronics, and 3) a flight model.

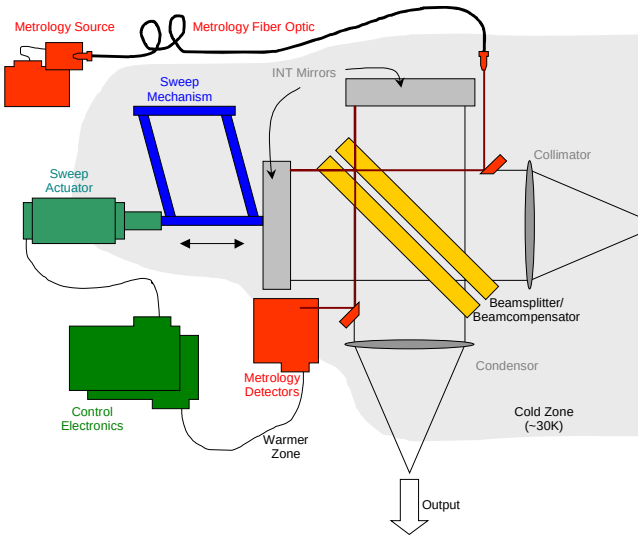

Figure 2 Schematic of NGST IFTS Components

4. RISK ANALYSIS AND MITIGATION PLAN

The risk associated with the proposed development was analyzed using a standard method proposed by DSMC (Defense Systems Management College, www.dsmc.dsm.mil). The method was used on other Bomem/ITT projects as a relative risk assessment method. It analyze the probability of development failure by looking at 3 different causes of failure and evaluate the importance of three type of consequences in case of failure. By selecting the appropriate weighting factors between each item, one can evaluate the overall risk. The formulae used to calculate the final risk factor are given in RD 2. The table shall be used to compare each component and to assess the risk mitigation priority.

Table 2: NGST IFTS Risk Factor

Risk No.	Item / Weighting Factors	Maturity (Pm) a 0.33	Complexity (Pc) b 0.34	Dependency (Pd) c 0.33	Probability of Occurrence (Pf) Pf = a Pm + b Pc + c Pd	Technical Factor (Ct) d 0.3	Cost Factor (Cc) e 0.15	Schedule Factor (Cs) f 0.55	Consequence (Cost of Occurrence) (Cf) Cf = d Ct + e Cc + f Cs	Total Risk (Rf) Rf = Pf + Cf - (Pf * Cf)
1	Metrology Source qualification	0.3	0.1	0.5	**0.30**	0.5	0.7	0.9	**0.75**	**0.825**
2	Cryogenic Metrology Fiber Optic Qualification	0.3	0.1	0.5	**0.30**	0.5	0.2	0.5	**0.46**	**0.617**
3	Metrology Detector qualification	0.1	0.3	0.2	**0.20**	0.5	0.3	0.5	**0.47**	**0.577**
4	Sweep actuator performance	0.8	0.5	0.5	**0.60**	0.7	0.5	0.9	**0.78**	**0.912**
5	Sweep Mechanism performance	0.5	0.5	0.3	**0.43**	0.7	0.2	0.3	**0.41**	**0.663**
6	Sweep technique performance (step scan)	0.9	0.7	0.3	**0.63**	0.5	0.3	0.5	**0.47**	**0.806**
7	Dynamic alignment performance	0.9	0.7	0.3	**0.63**	0.7	0.1	0.5	**0.50**	**0.817**
8	Dicroic system qualification	0.3	0.3	0.5	**0.37**	0.7	0.5	0.7	**0.67**	**0.791**
9	Interferometer beamsplitter qualification	0.3	0.1	0.5	**0.30**	0.7	0.4	0.3	**0.44**	**0.603**
10	Mirror qualification	0.1	0.1	0.5	**0.23**	0.5	0.3	0.3	**0.36**	**0.508**
11	input/output optics qualification	0.1	0.1	0.5	**0.23**	0.7	0.3	0.5	**0.53**	**0.639**
12	Control electronics qualification	0.3	0.5	0.5	**0.43**	0.7	0.5	0.5	**0.56**	**0.751**
13	Calibration source performance	0.9	0.8	0.3	**0.67**	0.3	0.5	0.5	**0.44**	**0.814**
14	Control software & algorithm performance	0.7	0.5	0.2	**0.47**	0.7	0.3	0.8	**0.70**	**0.837**

The summary of the analysis for the development of an interferometer subsystem for the NGST IFTS is given in Table 2. The three most important risk elements are found to be: 1) the sweep actuator performance, 2) the control algorithms and software and 3) the metrology source qualification. Table 3 presents the result of the risk analysis and drafts a mitigation plan. A part of the mitigation plan is currently underway with the breadboard contract (pre-phase A activities). This will give Bomem the ability to validate some of the technology planned for the interferometer. In fact the breadboard tests will address some of the crucial aspects of risk # 4, 5, 6, 7, and 15 which include the two top risk elements. For items # 1, 3 and 10 to 13, space qualification has already been performed on similar components on previous space instruments.

Table 3: NGST IFTS Risk Factor and Mitigation

No.	Level	Risk Identified	Risk Mitigation planned during phase A
1	**0.825**	**Metrology Source qualification**	Assess requalification of diodes from programs with less stringent PA requirements.
2	0.617	Cryogenic Metrology Fiber Optic Qualification	Perform transmission and polarization tests at cryo temperatures
3	0.577	Metrology Detector qualification	Assess requalification of diodes from programs with less stringent PA requirements.
4	**0.912**	**Sweep actuator performance**	Perform testing on current breadboard prior to instrument design and select alternate technologies if necessary
5	0.663	Sweep Mechanism performance	Study several designs and run test on current breadboard
6	0.806	Sweep technique performance (step scan)	Perform extended testing on breadboard version
7	0.817	Dynamic alignment performance	Perform alignment by iterative optimization techniques
8	0.791	Dicroic system qualification	Research past cryogenic programs for mirror performance
9	0.603	Interferometer beamsplitter qualification	Research past cryogenic programs for mirror performance
10	0.508	Mirror qualification	Research past cryogenic programs for mirror performance
12	0.639	input/output optics qualification	Research past cryogenic programs for mirror performance
13	0.751	Control electronics qualification	Select space qualified components
14	0.814	Calibration source performance	Perform extended study and simulation of various approaches
15	**0.837**	**Control software & algorithm performance**	Test uncompiled high level version on breadboard.

5. PROPOSED COST

The cost estimate was built using a bottom-up methodology. The work breakdown was first constructed using a classic project model composed of two models (engineering model and flight model) and the usual development cycles bounded by the kickoff, PDR, CDR and TRR milestones. Next a detail work form was filled out for every task. This level of detail is sufficient to produce a realistic and solid cost estimate. The level of efforts were entered based on experience on similar projects and based on the work already completed and the risk analysis described in Section 4. For a detailed discussion on the methodology and cost drivers see RD 2. Table 4 shows the summary of the cost estimate for the development of the interferometer module for the NGST IFTS.

To make things clear and simple, this cost estimate covers only the IFTS interferometer subsystem. However there are a number of other subsystems or components that Bomem is interested in developing and for which Bomem possesses a unique, world-class expertise. Table 5 lists the three main areas where Bomem could also contribute, along with rough-order-magnitude cost estimates. Bomem would be pleased to present the relevant capabilities and past experience and to hold discussions with CSA on these additional developments.

Table 4: Cost estimate summary

TABLE REMOVED

Table 5: Cost estimates for items not part of the proposed contribution

TABLE REMOVED

6. SCHEDULE

A schedule was constructed around the four milestones provided by CSA, namely the NGST IFTS Kickoff, FM PDR, FM CDR and delivery. The resulting schedule was found to be quite aggressive and is thought to increase the risk of the development, considering that a large team (>25) has to be built in a very short time. The work performed on the breadboard (pre-phase A) will help quickly come to a technological baseline for the EM, but the proposed schedule is still considered to be restrictive. Bomem would recommend to increase the timeframe by 20-40% if it is possible, by example starting the EM program earlier, even at a reduced effort.

7. CONCLUSION

The work performed under this study contract clearly identifies an exciting Canadian involvement in the NGST program, the development the heart of the NGST IFTS. We found that the technology has enormous science returns and could be developed completely in Canada for less than [**COST INFORMATION REMOVED**]. This cost was found to be compatible with the development of similar space instruments. The risk identified are relatively low considering the sophistication of the NGST mission, partly due to the expertise and solutions put forward by Bomem.

— End of document —

BOMEM

NGST

Next Generation Space Telescope

Final Report

Volume 2 - Planning Report

Document Number: **SP-BOM-006/99**

Issue: **1** **Revision:** B

Issue Date: **13 October 1999** **Document Name:** Annex B2 .doc

	Function	Name	Signature	Date
Prepared by	Scientist	André Villemaire		
Prepared by	Administrative	Julie Bergeron		
Approved by	Scientist	Frédéric Grandmont		
Approved by	Director, SPR division	Jean Giroux		

BOMEM Inc. • a unit of Elsag Bailey Process Automation N.V.

450 Saint-Jean-Baptiste Avenue • Québec, Québec G2E 5S5 Canada • Phone (418) 877–2944 • Fax (418) 877–2834

TABLE OF CONTENTS

LIST OF FIGURES

LIST OF TABLES

DOCUMENT CHANGE RECORD

Issue	Rev.	Date	Chapter/Paragraph Number, Change Description (and Reasons)
1(draft)	-	25 March 99	Draft of document
1	-	6 April 99	First release of document
1	A	28 sept. 99	Modified version to remove references to cost and schedule to include in the final report to NASA.
1	B	13 October 1999	New revision to remove proprietary notices.

1. INTRODUCTION

1.1 BACKGROUND INFORMATION

The Next Generation of Space Telescope (NGST) project of NASA is intended to provide continuity and new focus for research following the success of the Hubble Space Telescope. It is considered to be a technologically challenging project as the technology needed is not necessarily available. It challenges the innovation of the scientific and technological community to come up with an affordable technology to carry out the scientific goals of the mission.

Canada has a strong Space Astronomy community and they have ranked the participation of this project as the priority in their LTSP III submission. In order for Canada to participate, the areas of technical expertise and competence necessarily has to match the required technologies of the NGST project. The nature and scope of the Canadian contribution to the NGST are neither identified nor defined. The CSA sees the Canadian contribution as one that matches the industrial capability, an area that would result in industrial and economic growth and provide a sound base for competitiveness in the international market.

At the end of 1998, CSA awarded a number of contracts to Canadian firms. Bomem was awarded such a contract to study the potential use of a Fourier Transform Imaging Spectrometer as a science instrument for NGST.

1.2 SCOPE OF PROJECT

This work was carried out under contract no 9F007-8-3007/001/SR.

Bomem proposed to study the potential use of a Fourier Transform Imaging Spectrometer as a moderate spectral resolution camera for NGST. The approach was to first investigate the trade space of the instrument design. Next the performance of the instrument was predicted to confirm the suitability of the technology for the NGST mission. The risk analysis and mitigation plans were then completed. Finally the Cost and Schedule estimates were drafted based on the previous findings.

1.3 SCOPE OF DOCUMENT

This document is Volume 2 of the final report. The deliverables of the study contract are listed in Table 1.

Volume 2 covers the scheduling and cost estimates of the Canadian participation proposed by Bomem for the NGST program. This participation is described in Section 2. This report also includes the risk assessment and mitigation plan to support the level of effort proposed and described in Section 4.

Table 1: Deliverables of the study contract

Volume	Document Number	Document	Description
1	SP-BOM-005/99	Executive Summary	5-page summary of the findings of the contract
2	SP-BOM-006/99	Planning Report	Report on the scheduling and cost of the proposed Canadian participation. The planning report also includes the risk assessment and mitigation plan
3	SP-BOM-007/99	Trade Analyses	Report on the trade analyses performed to arrive at a credible baseline for the proposed Canadian participation.
4	SP-BOM-008/99	Performance Analyses	Report on the sensitivity analyses performed to evaluate the suitability of the proposed Canadian participation for NGST
5	SP-BOM-009/99	Technology Report	Report on some proposed novel technology approaches to the specific NGST environment for the proposed Canadian participation.

1.4 PROJECT METHODOLOGY

Figure 1 shows the structure of the project as it was presented in the Bomem proposal (see RD 1). This work flow was followed remarkably closely during the execution of the project. The labels on the left hand side of the boxes in Figure 1 refer to the items requested by the government in Section 2 of the statement of work. As can be seen a number of additional tasks were added to complement and enhance the suggested work.

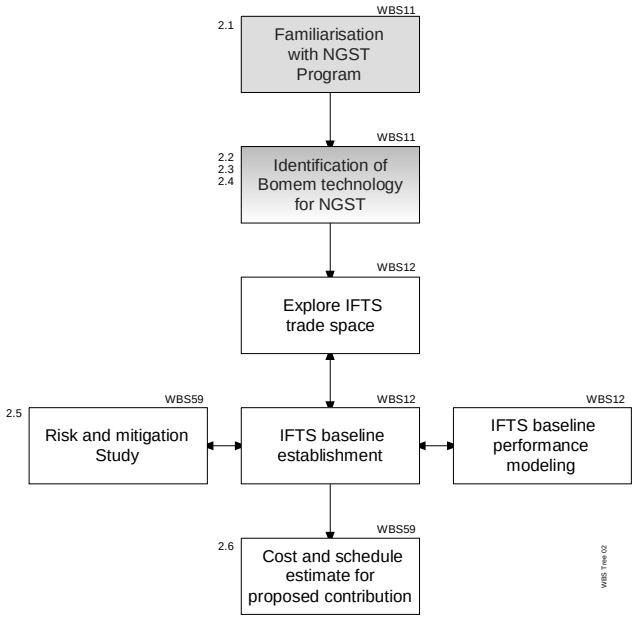

Figure 1 Structure of the Bomem lead study contract.

In the task "Explore IFTS trade space", we explored the trade space of the NGST IFTS to finally arrive at a technical baseline. The results of the trade studies is described in RD 2. This technical baseline raises the fundamental design issues on one hand and proposes a baseline with a

representative level of complexity of the final instrument on the other, with enough details to be able to build a realistic cost and schedule estimate.

The spectrometric performance of this baseline was evaluated to verify compliance with the science requirements. The results from the simulations can be found in RD 3.

Next a risk analysis was performed and a mitigation plan was drafted (see Section 4). Finally the cost and schedule estimates were produced and are described in Sections 5 and 6.

1.5 REFERENCE DOCUMENTS

RD 1 Bomem Proposal No:SPIR180898, issue 1, revision -, dated 8 September 1998, in response to solicitation No 9F007-8-3007/A.

RD 2 Volume 3 - Trade Analyses, SP-BOM-007/99

RD 3 Volume 4 - Performance Analyses, SP-BOM-008/99

RD 4 Volume 5 - Technology Report, SP-BOM-009/99

2. PROPOSED PARTICIPATION

In this section we describe the scope of the proposed Bomem participation in NGST. The proposed contribution is the interferometer subsystem of an Imaging Fourier Transform Spectrometer (IFTS) for NGST.

Given the very broad wavelength range of NGST, it is believed that the subsystem will actually be composed of three separate interferometer modules and one dichroic module to steer the light into them. **This constitutes the baseline for the schedule and cost estimates presented in this report**.

The interferometer modules are complete subsystems capable of operating by themselves. The subsystem includes the opto-mechanical components (mirrors, beamsplitters and possibly collimating and condensing lenses or mirrors, depending on the primeship of these items) interferometer structural and thermal control assemblies, metrology assembly (metrology source, optics, detector and electronics) and interferometer control electronics. Figure 3 illustrates these components.

To make things clear and simple, this report focuses only on the IFTS interferometer subsystem. However there are a number of other subsystems or components that Bomem is interested in developing and for which Bomem possesses a unique, world-class expertise. Table 2 lists the three main areas where Bomem could contribute, along with rough-order-magnitude cost estimates. Bomem would be pleased to present the relevant capabilities and past experience and to hold discussions with CSA on these additional developments.

Table 2: Cost estimates for items not part of Baseline

Item	Number	Cost
Flight Calibration sources	3	REMOVED
Ground Segment - Data processing algorithms and software (level 1b)	1	REMOVED
Special test Equipment for instrument-level validation – Includes calibration sources and cryogenic collimator	1	REMOVED

3. DEVELOPMENT APPROACH FOR NGST IFTS

3.1 MODELS

Various approaches are possible for the development of space hardware as far as models are concerned. The model philosophy typically flows down from the risk analysis which can be done in a quantitative way, with targets set for the various models and to achieve an acceptable risk for the flight unit. Obviously, the mission criticality of the sensor, the overall mission (launch and platform) costs also fold in. We expect that the NGST expectations will be very high, typical of the larger science missions like EOS or ENVISAT. A for high probability of success is a must. This assessment implies that:

- Strict PA requirements will be enforced
- Rigorous development methods must be followed
- Reviews, control boards etc. will be implemented
- Risk reduction programs will be developed
- Mass models will be supplied
- Simulators will be used for verification throughout

We propose a development approach that uses basically three key models, 1) a breadboard which is currently under development, 2) an engineering model which will be form, fit and function compatible with the flight model but may use lower grade of space qualification on the electronics, and 3) a flight model.

To maintain reduced cost and accelerated development, the development approach will reuse available components as much as possible and make use of synergies with other space programs.

3.2 DEVELOPMENT CYCLES

3.2.1 Preliminary Design

The preliminary design phase is the first step in the project. It is concluded by the preliminary design review (PDR). At this review, there is an exhaustive review of all aspects of the system down to detailed subsystem concepts with all the required technical analysis to give confidence in the feasibility of the approach and its risk level. We present revised plans for the development, as well as plans for the manufacturing and testing of the various units. Action items are generated and the milestone is closed when these are resolved to the satisfaction of the customer. After closing, the manufacturing of the EM is released as well as long lead items for the FM as required. Finally, the results of risk reduction activities (breadboards and analysis) are presented.

3.2.2 Detailed Design

The detailed design phase pushes the design to the level where manufacturing can be started:

- The detailed drawings are produced
- The plans are turned into procedures
- The change control board is implemented
- Configuration control management is implemented

The phase is concluded after successful completion of the Critical Design Review (CDR) where the documentation is presented along with the EM test results. At this point, there must be great confidence in the probability of success of the instrument.

3.2.3 Manufacturing

Following the CDR, the manufacturing phase is started, first by the procurement of parts, their assembly into sub-assemblies and integration into the final sensor. As the work process, subsystem testing is performed, key and mandatory inspection points are met. The test readiness review (TRR) milestone is used to clear the way to final testing which will include the performance verification as well as the environmental qualification of the unit. Upon successful completion of the test plan, acceptance is granted by the customer and the unit is delivered.

3.3 TOOLS, TECHNIQUES AND METHODOLOGIES

Bomem uses several tools in the development process for its projects. They cover performance assessments, requirements flowdown and project management.

In the course its 25 years of experience in development Fourier Spectrometers, Bomem has gained a thorough understanding of the performance aspects of these instruments. Furthermore, we have integrated these tools in a formal software package for internal use and select customers. These allow:

- Rapid assessment of performance and performance drivers for FTS instruments including noise, accuracy and line shape aspects
- Simulation of the instrument to study the effect of various instrument parameters and abnormal operation. It also allows the creation of realistic data sets for training and verification of the ground segment software.

For more information on these tools, please refer to:

http://www.bomem.com/spectro/index.htm

We also intend to make use of a requirements flowdown tool called DOORS (Dynamic Object Oriented Requirements System see: http://www.qssinc.com/products/doors/introduction.html) for the systematic allocation of requirements to subsystems and generation of the various procedures and verification assessment.

Bomem uses for all its operations an integrated project management system that provides weekly information on the effort levels required and earned value status of all projects as well as new upcoming projects. This allows very accurate assessments of schedule and cost status for the program.

3.4 REVIEWS AND AUDITS

3.4.1 Formal Reviews

Reviews will be the formal tool to present a detailed insight of the actual status of the project. PA engineer shall ensure traceability of requirements through each phase during reviews. PA Engineer shall participate directly or with an inspection report to formal reviews. The following formal reviews shall be held at dates specified in the Development Schedule.

- Kick-off meeting
- Preliminary Design Review (PDR)
- Critical Design Review (CDR)
- Test readiness Review (TRR)
- Acceptance review

The scope of the various reviews is covered in section 3.2.

3.4.2 Peer Reviews and Audits

Peer reviews will be held regularly to provide an internal verification of the development activities within the group. Peer reviews will be led by the PA Engineer. The peer reviews shall provide a means for reducing the number of problems and enhance the performance of the product by mutual assistance. Peer reviews are expected throughout the project duration. Peer reviews will be held at contractor's place. The reviews will be pre-scheduled and material distributed in advance.

Audits shall be held when required. Initiated by the PA Engineer, they will be held in order to verify that the tools and techniques are in accordance to the requirements. Audit reports will be kept at the PA Engineers desk.

3.5 PRODUCT ASSURANCE ACTIVITIES

To ensure that the contractual requirements of the project are systematically achieved, deficiencies are detected, corrected and prevented from recurrence, a Product Assurance program will be implemented.

The following Quality Assurance activities shall be performed:

- participation in writing coherent development, analysis, production and test plans for QA related issues,
- participation in reviews, audits and meetings,
- ensuring adherence to standards and procedures,

- liaison with configuration management,
- involvement in problem reporting and resolution,
- validation and acceptance tests follow-up including non-conformance control.

Status list of QA activities will be maintained at the PA Engineer desk. It will be provided upon request for review.

3.5.1 Product Assurance Organisation

The contractor in charge of the NGST IFTS development should have Program Assurance activities in place. The organisation should be qualified to an external program as ISO9001. The PA organisation is under the responsibility of a Management Committee. The PA manager reports directly to the Project Manager and to this committee.

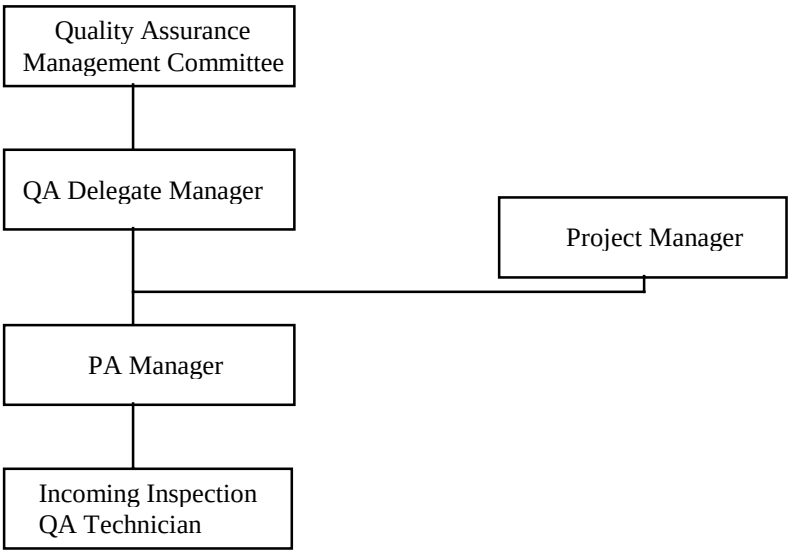

Figure 2: PA Organisation

The PA manager is responsible for implementation of the requirements in the project organisation and his contractors/suppliers.

Higher level contractors shall have right to access to PA activities as long as it is in respect with proprietary rights.

3.5.2 Review of documents

PA manager will participate in the review of documents and release cycle of specifications, plans, procedures and other documents related to the project. PA manager will review documents based on their conformance with quality assurance aspects.

This applies particularly to the Test Procedures.

3.5.3 Progress Reports

PA activities are reported in the monthly progress reports. These reports present problem areas and recommended solutions, if any. Non-conformance statuses are reported. PA documentation status is also reported.

3.5.4 Non-Conformance Reports

Non-conformance reports follow the procedure for Non-Conformance Control. When a non-conformance is detected, a non-conformance report is prepared on an in-house report. Non-Conformance Reports are presented in the monthly progress report.

3.5.5 Tests Witnessing

During testing, PA manager attends selected tests and/or attends testing activities to confirm that Test Procedures are followed correctly.

3.6 VERIFICATION STRATEGY

The verification strategy derives directly from the system and subsystem requirements through the establishment of the verification approach for each of the specific requirements. Specific approaches, in order of decreasing preference are:

1. By test. A direct measurement of the requirement to be met. The mass is measured on a scale.
2. By test and analysis. A direct measurement is not possible and some calculations are required to achieve the verification from system level measurements.
3. By analysis. A direct measurement is not possible and the compliance can only be determined from a model
4. By inspection. A simple visual inspection of a feature is required. Applies to markings, for example.
5. By design. When no other way of insuring that the requirement will be met is a design review. Applies to safety features and failure cases.

The verification strategy is determined early in the program for the system and similarly are defined for the subsystems as they get defined. They are reviewed at the major review to achieve a reasonable balance of cost and risk.

4. RISK ANALYSIS AND MITIGATION PLAN

4.1 METHODOLOGY

While there are many ways to assess the risk in the course of a project we favour the DSMC (Defense Systems Management College) approach that we used on several NOAA programs. A team surveys the project and determine the list of all risks including both technical and management risks. The consequences of problems in terms of costs and schedules are assessed independently and the some qualitative scores are combined for each of the identified components. It therefore becomes possible to sort the risk items in priority, assign targets levels as a function of time and finally put together a risk mitigation plan

The risk analysis can be performed as part of trade-off studies early in the design.

4.2 DESCRIPTION OF SUBSYSTEM

Figure 3 is a schematic illustration of the NGST IFTS interferometer subsystem. Clearly identified are the various components.

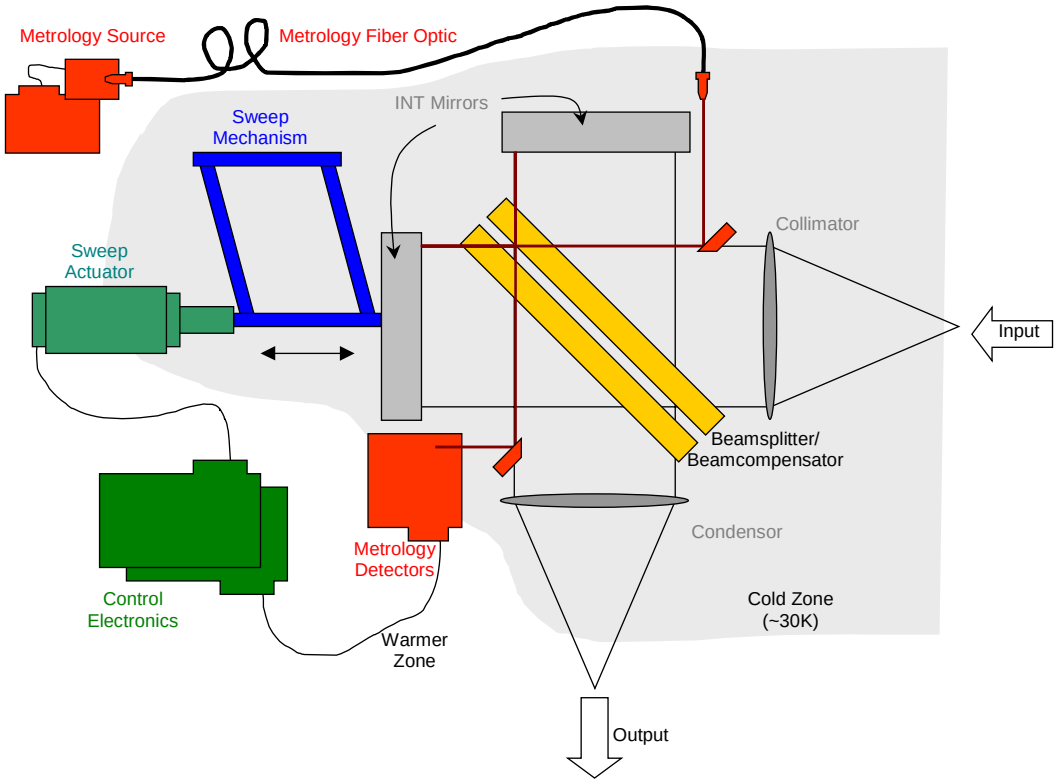

Figure 3 Schematic of NGST IFTS Components

4.3 LEVEL OF DIFFICULTY

As a complement to the formal risk analysis described above, Table 3 presents a first assessment of the risks associated with IFTS broken down against the key problem factors for a space-based cryogenic instrument. The rather low risk approach of the technologies involved with the interferometer doesn't require us to worry about the basic feasibility.

Table 3: Level of Difficulty matrix for the various interferometer components

Component \ Environment	Thermal	Radiation	Vibration	Lifetime
Collimator	Low	Low	Low	Low
Condensor	Low	Low	Low	Low
Beamsplitter / compensator	Medium	Low	Medium	Low
Interferometer Mirrors	Low	Low	Low	Low
Sweep Mechanism	Low	Low	Medium	High
Sweep Actuator	Hard	Low	Medium	High
Metrology Source	Medium	Medium	Low	High
Metrology Fibre Optic	Hard	Medium	Medium	High
Metrology Detectors	Medium	Medium	Low	Low
Control Electronics	Low	Medium	Low	Medium

4.3.1 Thermal Environment Considerations

We assume that the instrument is divided in a number of thermal zones. In Figure 3, we only show two zones, the coldest thought to be around 30 K, and another one labelled Warmer Zone. Some components will undoubtedly be located in the warmer environment. The main reason for placing a component in the warmer zone are is that 1) their function allows them to be located away from the cold optics such as electronic boards and 2) they generate heat. There is a high cost to place heat-dissipating components in the coldest environment. Current heat budgets supplied by NASA allow a few hundreds of mW to be dissipated by the interferometer subsystem in the 30 K area. For some components, it is not yet decided if they will be placed in the coldest zone or not. In this case they are illustrated in Figure 3 with the thermal zone border passing through them. One such example is the Sweep Actuator. From the point of view of the interferometric actuation, it would be ideal to have the actuator placed close to the sweep mechanism. However if an actuator with sufficiently low power dissipation cannot be found, a high dissipation device could be placed in the warmer area and transfer

the mechanical motion using a stiff, insulating member, with possibly degraded actuation performance. The components for which the location is not yet known, a worst case in terms of risk is assumed, namely that they sit in the coldest zone.

Another example of component location to be determined is the Metrology Detectors. The detector themselves will lie in the coldest zone but the associated preamplifiers may be required to be very close to the detectors to minimise noise pickup. In this case low-power design and components will be required.

The Beamsplitter and Beamcompensator are made of visible light and infrared light transmitting elements. Many of these materials, especially in the infrared, are relatively soft or brittle, making their mounting much harder than, say monolithic metal mirrors. This is even more so in the case of cryogenic mounting and mounts appropriate for vibration (launch) environment. Both of these problems have been solved for a number of space instruments though. The level of difficulty score is thus considered medium.

The sweep mechanism would normally get a high to very high level of difficulty score, however in our baseline we assume the use of dynamic alignment that alleviates the problem of distortion of the thermal structure. On the down side, this choice complicates the metrology.

The Metrology Fibre Optic will be submitted to a high thermal gradient and this may place mechanical stresses that may change the light transmission characteristics but also that may produce mechanical failure.

The thermal environment imposes three types of constraints on components. The first one is the difficulty of operation in a very cold environment. The second difficulty is the testing of the devices in the cryogenic chambers and the increased complexity of such operations. The third constraint is the low-dissipation requirement, almost always associated with low temperature environments.

4.3.2 Radiation Environment Considerations

The radiation environment has very a low level of difficulty score for all mechanical components such as mirrors (the Collimator and Condensor are thought to be made of mirrors and not lenses) and the sweep mechanism. The transmission properties of materials used in transmission such as the Metrology Fibre Optic and Beamsplitter/recombiner may be affected by cosmic radiation. However we consider that only the Fibre Optic carries a certain level of difficulty because of the long optical path and the limited choices of fibre material. As it is the case for all space development, the electronic components potentially carry a high level of difficulty associated to space radiation but we assume that we can find a solution appropriate for the level of NGST cosmic radiation. This solution will be similar to that found for the rest of the NGST system.

4.3.3 Vibration Considerations

Most of the vibration considerations in space systems are usually centred around the initial launch perturbations. This is the case for the NGST IFTS, however a Fourier Transform spectrometer requires interferometric alignment requires tolerance to vibration during operation also. When an interferometer gets out of alignment, it efficiency, and consequently its sensitivity, degrades very rapidly.

The vibration environment and the thermal distortions are the factors most often cited by critics to say that the operation of a FTS in space is a risky business. This is true of FTS that *passively* rely on their structure to maintain alignment through the initial launch vibrations and through the structural deformations caused by spatial and temporal thermal gradients. The situation is different however if a FTS equipped with a *dynamically* aligned system is used.

The baseline Bomem NGST IFTS has a dynamic alignment subsystem which is shares components with the metrology. The dynamic alignment utilises the light from the metrology source and adds a number of detectors alongside the metrology detectors to sense the interferometric alignment. The dynamic alignment electronics sends a signal to a pair of short-stroke actuators (like single element piezo) to correct the alignment. This subsystem allows the system to readjust after a launch perturbation and allows to compensate thermal distortions. It allows us to design a much cheaper interferometer structure with traditional space materials, to save mass and greatly reduce the "interferometer in space" risk. It also generates significant saving during testing by having this sensing device built-in the interferometer subsystem, allowing to "see" what perturbations are experienced while the system is cooled down to 30 K. Cryogenic interferometer systems such as the CIRS on CASSINI is a good example of the problems encountered (see papers 04 and 24-26 of the SPIE Vol. 2814, Cryogenic Optical Systems and Instruments VII, Denver August 1996) during the testing of a passive system.

Bomem invented the dynamic alignment more than 25 year ago.

4.3.4 Lifetime Considerations

Lifetime in space issues affect 1) components with moving parts, 2) electronic components and 3) optical components in transmission. Lifetests will definitely be performed on the sweep mechanism, sweep actuator and dynamic alignment mechanism and actuators, all of which are moving parts.

The lifetime of electronic components in general is of concern, but the selection of space qualified electronic components is routinely performed for all space developments and does not carry excessive risk. Special attention is to be devoted to the metrology source which is thought to be a solid state laser diode at 1.55 μm. We plan to select a laser diode tested for another space program at Bomem (or elsewhere) or conduct lifetests in the lab during the development.

The darkening of optical components used in transmission because of radiation is a potential problem. The material will be selected form published space qualified lists to take care of this effect.

4.4 RISK ESTIMATE

The risk associated with the development of an interferometer subsystem for the NGST IFTS was analyzed using a standard method proposed by DSMC (Defense Systems Management College, www.dsmc.dsm.mil). The method was used on other Bomem/ITT projects as a relative risk assessment method. It analyze the probability of development failure by looking at 3 different causes of failure and evaluate the importance of three type of consequences in case of failure as defined in Table 4. By selecting the appropriate weighting factors between each item, one can evaluate an overall risk for a specific action. The formulae used to calculate the final risk factor Rf is given in Table 6. The table shall be used to compare each action item relative to another one to assess priority.

It is important to highlight the fact that this evaluation is performed on the risk of development process failure and not on the risk of failure of the instrument in flight. An example would be, that midway in the project the optical fiber selected cannot be space qualified for cryogenic space operation. The method evaluate the risk and consequence associated with such an event and the impact of a work around solution. It is therefore assumed that the instrument will work properly once in space.

Table 4: DSMC Probability & Consequence Definitions

Probability Definitions (Pf)			
Magnitude	**Maturity (Pm)**	**Complexity (Pc)**	**Dependency (Pd)**
0.1	Existing	Simple design	Independent of existing system, facility, or associated contractor
0.3	Minor redesign	Minor increases in complexity	Schedule dependent on existing system, facility, or associate contractor
0.5	Major change feasible	Moderate increase in complexity	Performance dependent on existing system performance, facility, or associated contractor
0.7	Technology available, complex design	Significant increase	Schedule dependent on new system schedule, facility, or associate contractor
0.9	State of art, some research complete	Extremely complex	Performance dependent on new system schedule, facility, or associate contractor

Table 5 DSMC Consequence Definitions

Consequence Definitions (Cf)			
Magnitude	**Technical (Ct)**	**Cost (Cc)**	**Schedule (Cs)**
0.1	Minimal or no consequences, unimportant	Budget estimate not exceeded, some transfer of money	Negligible impact on program, slight development schedule change compensated by available schedule slack
0.3	Small reduction in technical performance	Cost estimates exceed budget by 1 to 5 percent	Minor slip in schedule (less than 1 month), some adjustment in milestones required
0.5	Some reduction in technical performance	Cost estimates increased by 5 to 20 percent	Small slip in schedule
0.7	Significant degradation in technical performance	Cost estimates increased by 20 to 50 percent	Development schedule slip in excess of 3 months
0.9	Technical goal can not be achieved	Cost estimates increased in excess of 50 percent	Large schedule slip that affects segment milestones or has possible effect on system milestones

Table 6: DSMC Risk Factor Definition

Risk Factor,	$Rf = Pf + Cf - Pf \times Cf$
Probability of failure,	$Pf = a(Pm) + b(Pc) + c(Pd)$
Consequece of failure,	$Cf = d(Ct) + e(Cc) + f(Cs)$
Pm =	Probability of failure due to hardware maturity
Pc =	Probability of failure due to degree of complexity
Pd =	Probability of failure due to dependence on other items
Ct =	Technical consequences due to failure of selected technology (replacement options)
Cc =	Cost consequences due to failure of selected technology
Cs =	Schedule consequences due to failure of selected technology

The summary of the analysis for the development of an interferometer subsystem for the NGST IFTS is given in Table 7. The three most important risk elements are found to be: 1) the sweep actuator performance, 2) the control algorithms and software and 3) the metrology source qualification. Section 4.5 addresses the mitigation of these risks.

Table 7: NGST IFTS Risk Factor

Risk No.	Item / Weighting Factors	Maturity (Pm) a 0.33	Complexity (Pc) b 0.34	Dependency (Pd) c 0.33	Probability of Occurrence (Pf) Pf = a Pm + b Pc + c Pd	Technical Factor (Ct) d 0.3	Cost Factor (Cc) e 0.15	Schedule Factor (Cs) f 0.55	Consequence (Cost of Occurrence) (Cf) Cf = d Ct + e Cc + f Cs	Total Risk (Rf) Rf = Pf + Cf - (Pf * Cf)
1	Metrology Source qualification	0.3	0.1	0.5	**0.30**	0.5	0.7	0.9	**0.75**	**0.825**
2	Cryogenic Metrology Fiber Optic Qualification	0.3	0.1	0.5	**0.30**	0.5	0.2	0.5	**0.46**	**0.617**
3	Metrology Detector qualification	0.1	0.3	0.2	**0.20**	0.5	0.3	0.5	**0.47**	**0.577**
4	Sweep actuator performance	0.8	0.5	0.5	**0.60**	0.7	0.5	0.9	**0.78**	**0.912**
5	Sweep Mechanism performance	0.5	0.5	0.3	**0.43**	0.7	0.2	0.3	**0.41**	**0.663**
6	Sweep technique performance (step scan)	0.9	0.7	0.3	**0.63**	0.5	0.3	0.5	**0.47**	**0.806**
7	Dynamic alignment performance	0.9	0.7	0.3	**0.63**	0.7	0.1	0.5	**0.50**	**0.817**
8	Dicroic system qualification	0.3	0.3	0.5	**0.37**	0.7	0.5	0.7	**0.67**	**0.791**
9	Interferometer beamsplitter qualification	0.3	0.1	0.5	**0.30**	0.7	0.4	0.3	**0.44**	**0.603**
10	Mirror qualification	0.1	0.1	0.5	**0.23**	0.5	0.3	0.3	**0.36**	**0.508**
11	input/output optics qualification	0.1	0.1	0.5	**0.23**	0.7	0.3	0.5	**0.53**	**0.639**
12	Control electronics qualification	0.3	0.5	0.5	**0.43**	0.7	0.5	0.5	**0.56**	**0.751**
13	Calibration source performance	0.9	0.8	0.3	**0.67**	0.3	0.5	0.5	**0.44**	**0.814**
14	Control software & algorithm performance	0.7	0.5	0.2	**0.47**	0.7	0.3	0.8	**0.70**	**0.837**

4.5 MITIGATION PLAN

Table 8 presents the result of the risk analysis and drafts a mitigation plan. A part of the mitigation plan is currently underway with the breadboard contract (pre-phase A activities). This will give Bomem the ability to validate some of the technology planned for the interferometer revealed to be problematic. In fact the breadboard tests will address some of the crucial aspects of risk # 4, 5, 6, 7, and 15 which include the two top risk elements. For items # 1, 3 and 10 to 13, space qualification has already been performed on similar components on previous space instruments. These items are present in the risk evaluation because the ones required for the NGST IFTS may differ from existing space-qualified versions. It is thought that the instrument design can be modified to accommodate space qualified components.

Table 8: NGST IFTS Risk Factor and Mitigation

No.	Level	Risk Identified	Risk Mitigation planned during phase A
1	**0.825**	**Metrology Source qualification**	Assess requalification of diodes from programs with less stringent PA requirements.
2	0.617	Cryogenic Metrology Fiber Optic Qualification	Perform transmission and polarization tests at cryo temperatures
3	0.577	Metrology Detector qualification	Assess requalification of diodes from programs with less stringent PA requirements.
4	**0.912**	**Sweep actuator performance**	Perform testing on current breadboard prior to instrument design and select alternate technologies if necessary
5	0.663	Sweep Mechanism performance	Study several designs and run test on current breadboard
6	0.806	Sweep technique performance (step scan)	Perform extended testing on breadboard version
7	0.817	Dynamic alignment performance	Perform alignment by iterative optimization techniques
8	0.791	Dicroic system qualification	Research past cryogenic programs for mirror performance
9	0.603	Interferometer beamsplitter qualification	Research past cryogenic programs for mirror performance
10	0.508	Mirror qualification	Research past cryogenic programs for mirror performance
12	0.639	input/output optics qualification	Research past cryogenic programs for mirror performance
13	0.751	Control electronics qualification	Select space qualified components
14	0.814	Calibration source performance	Perform extended study and simulation of various approaches
15	**0.837**	**Control software & algorithm performance**	Test uncompiled high level version on breadboard.

5. SCHEDULE

Figure 4 shows the NGST IFTS schedule (bottom - ID 20 and higher) along with the NGST milestones (top – ID 1-19). The task listed in Figure 4 are described in Section 6.1. The schedule was constructed around four milestones provided by CSA, the NGST IFTS Kickoff, FM PDR, FM CDR and delivery.

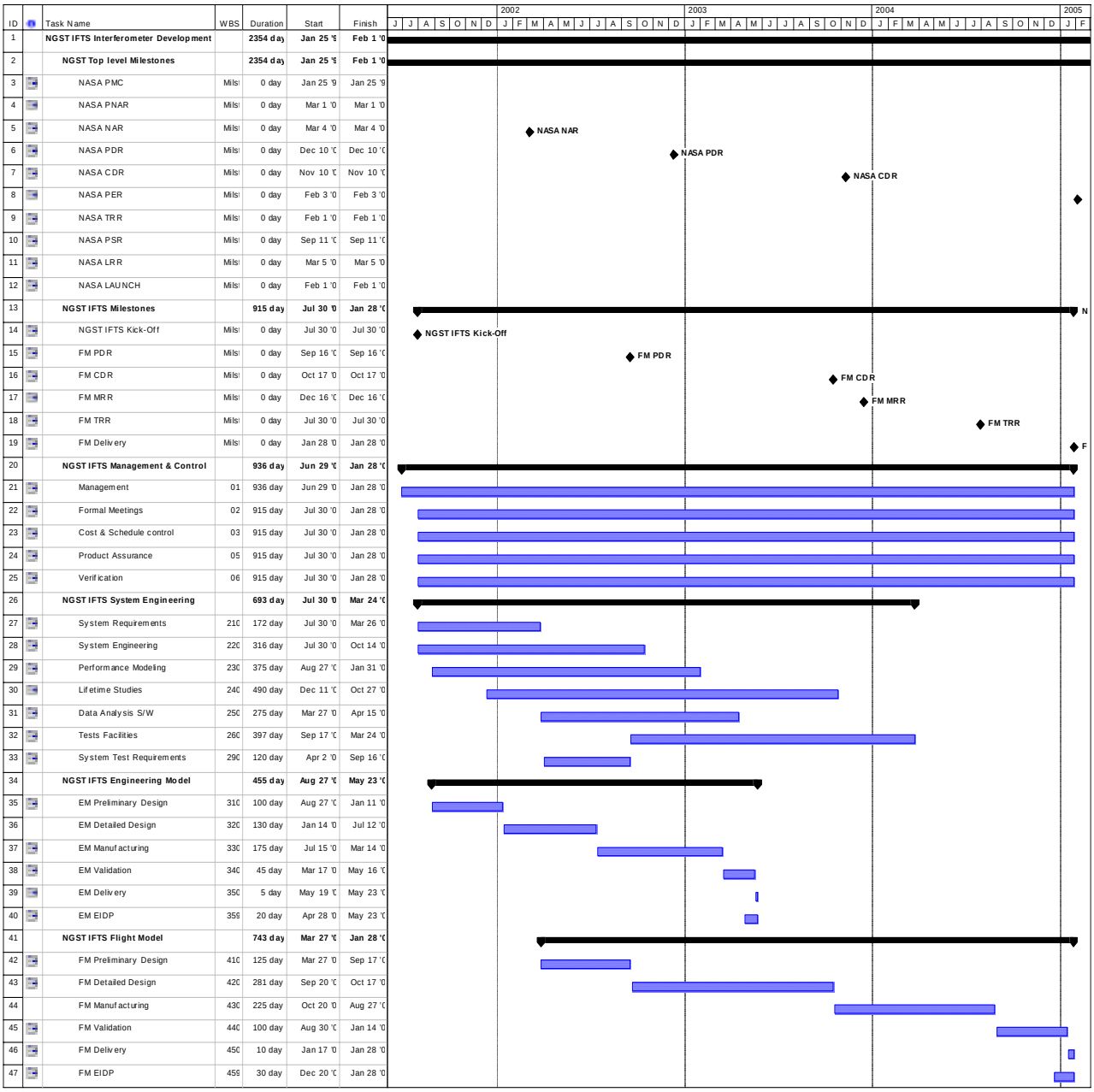

ID	Task Name	WBS	Duration	Start	Finish
1	**NGST IFTS Interferometer Development**		**2354 day**	**Jan 25 '9**	**Feb 1 '0**
2	**NGST Top level Milestones**		**2354 day**	**Jan 25 '9**	**Feb 1 '0**
3	NASA PMC	Mils	0 day	Jan 25 '9	Jan 25 '9
4	NASA PNAR	Mils	0 day	Mar 1 '0	Mar 1 '0
5	NASA NAR	Mils	0 day	Mar 4 '0	Mar 4 '0
6	NASA PDR	Mils	0 day	Dec 10 '0	Dec 10 '0
7	NASA CDR	Mils	0 day	Nov 10 '0	Nov 10 '0
8	NASA PER	Mils	0 day	Feb 3 '0	Feb 3 '0
9	NASA TRR	Mils	0 day	Feb 1 '0	Feb 1 '0
10	NASA PSR	Mils	0 day	Sep 11 '0	Sep 11 '0
11	NASA LRR	Mils	0 day	Mar 5 '0	Mar 5 '0
12	NASA LAUNCH	Mils	0 day	Feb 1 '0	Feb 1 '0
13	**NGST IFTS Milestones**		**915 day**	**Jul 30 '0**	**Jan 28 '0**
14	NGST IFTS Kick-Off	Mils	0 day	Jul 30 '0	Jul 30 '0
15	FM PDR	Mils	0 day	Sep 16 '0	Sep 16 '0
16	FM CDR	Mils	0 day	Oct 17 '0	Oct 17 '0
17	FM MRR	Mils	0 day	Dec 16 '0	Dec 16 '0
18	FM TRR	Mils	0 day	Jul 30 '0	Jul 30 '0
19	FM Delivery	Mils	0 day	Jan 28 '0	Jan 28 '0
20	**NGST IFTS Management & Control**		**936 day**	**Jun 29 '0**	**Jan 28 '0**
21	Management	01	936 day	Jun 29 '0	Jan 28 '0
22	Formal Meetings	02	915 day	Jul 30 '0	Jan 28 '0
23	Cost & Schedule control	03	915 day	Jul 30 '0	Jan 28 '0
24	Product Assurance	05	915 day	Jul 30 '0	Jan 28 '0
25	Verification	06	915 day	Jul 30 '0	Jan 28 '0
26	**NGST IFTS System Engineering**		**693 day**	**Jul 30 '0**	**Mar 24 '0**
27	System Requirements	210	172 day	Jul 30 '0	Mar 26 '0
28	System Engineering	220	316 day	Jul 30 '0	Oct 14 '0
29	Performance Modeling	230	375 day	Aug 27 '0	Jan 31 '0
30	Lifetime Studies	240	490 day	Dec 11 '0	Oct 27 '0
31	Data Analysis S/W	250	275 day	Mar 27 '0	Apr 15 '0
32	Tests Facilities	260	397 day	Sep 17 '0	Mar 24 '0
33	System Test Requirements	290	120 day	Apr 2 '0	Sep 16 '0
34	**NGST IFTS Engineering Model**		**455 day**	**Aug 27 '0**	**May 23 '0**
35	EM Preliminary Design	310	100 day	Aug 27 '0	Jan 11 '0
36	EM Detailed Design	320	130 day	Jan 14 '0	Jul 12 '0
37	EM Manufacturing	330	175 day	Jul 15 '0	Mar 14 '0
38	EM Validation	340	45 day	Mar 17 '0	May 16 '0
39	EM Delivery	350	5 day	May 19 '0	May 23 '0
40	EM EIDP	359	20 day	Apr 28 '0	May 23 '0
41	**NGST IFTS Flight Model**		**743 day**	**Mar 27 '0**	**Jan 28 '0**
42	FM Preliminary Design	410	125 day	Mar 27 '0	Sep 17 '0
43	FM Detailed Design	420	281 day	Sep 20 '0	Oct 17 '0
44	FM Manufacturing	430	225 day	Oct 20 '0	Aug 27 '0
45	FM Validation	440	100 day	Aug 30 '0	Jan 14 '0
46	FM Delivery	450	10 day	Jan 17 '0	Jan 28 '0
47	FM EIDP	459	30 day	Dec 20 '0	Jan 28 '0

Figure 4 NGST IFTS Schedule

The resulting schedule is quite aggressive and is thought to increase the risk of the development. There is only a four month period between the kickoff and PDR of the EM. This is especially short considering that during that time a large team (>25) has to be built. The work performed on the breadboard (pre-phase A) will help quickly come to a technological baseline for the EM, but the proposed schedule is thought to be restrictive, Bomem would recommend to increase the timeframe by 20-40% if it is possible, by example starting the EM program earlier, perhaps at a reduced effort.

Bomem has the required expertise, size and is growing at a rate compatible with the staffing requirement of NGST. The SPIR division of Bomem is the world largest development team of Fourier Transform spectrometers.

6. BUDGET ANALYSIS

6.1 METHODOLOGY

The cost estimate was built using a bottom-up methodology. The work breakdown was first constructed using the models and development cycles described in Sections 3.1 and 3.2. The resulting work breakdown structure is shown in Figure 5. The work is divided in four classes of tasks. The 00X tasks pertain to project control and quality assurance. The 2XX tasks pertain to system engineering. The 3XX tasks pertain the to engineering model development and the 4XX tasks pertain to the flight model development.

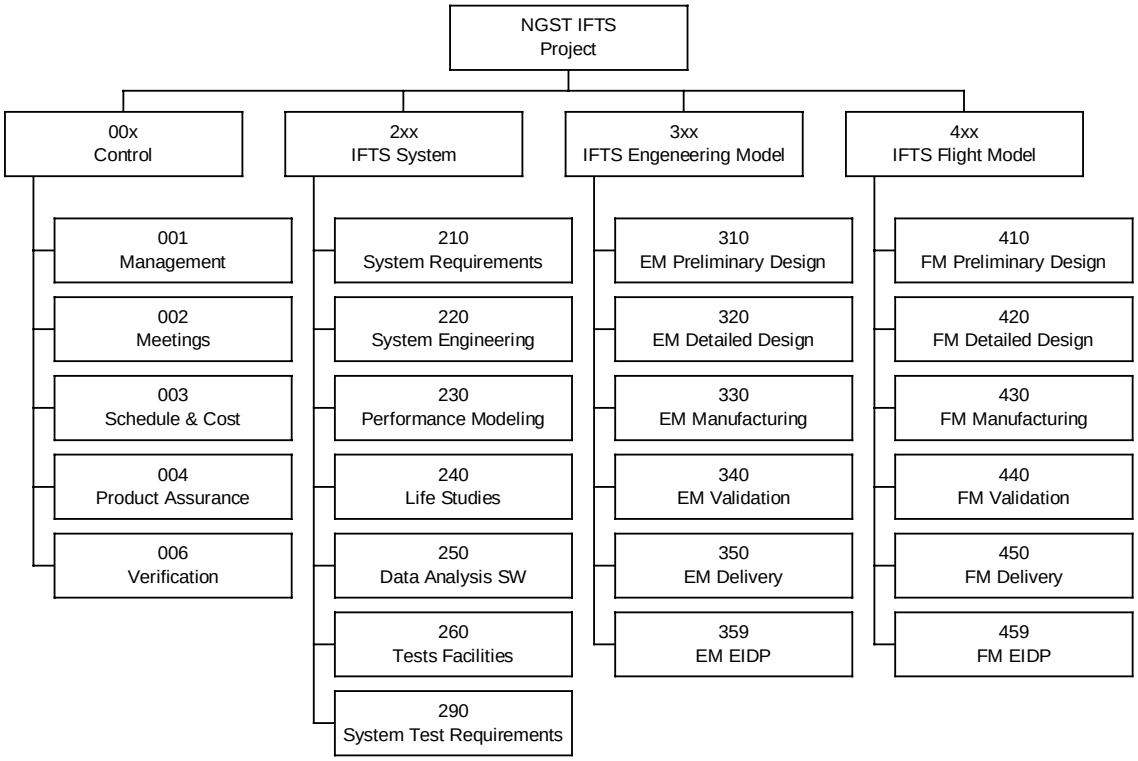

Figure 5 Work breakdown structure

Next a detail work form (Bomem F240 form) was filled out for every task (also known as WBS). Table 9 shows an example of the detail work form for WBS310 – EM preliminary design. The work in the WBS is broken down in easily identifiable subtasks requiring no more than a few weeks. This level of detail is sufficient to produce a realistic and solid cost estimate. The hours and material, contract, travel costs are wrapped up in a single summary page (see Table 10).

The level of efforts are entered based on experience on similar projects and based on the work already completed (See RD 2 and RD 3) and the risk analysis described in Section 4. The complete workbook (Excel) can be provided upon request.

Table 9: Example of a WBS detail work form. The I3S, I2S, T3S and T1S refer to labor categories and the entries are hours.

Task Title: *[NGST IFTS EM] Preliminary Design*
Task Objective: *EM Preliminary Design*

Start Date: August 27, 2001
End Date: January 11, 2002

Responsable

Description	I3S	I2S		T3S	T1S					MAT	CONT	VOY	Aut
Establish interferometer req. From instrument req.	150												
Sensor req. Draft	150	150											
Flowdown req. To subsystem	75	75											
Flowdown req. To ass'y	75	75											
NGST IFTS Interferometer General Concept	60	60											
NGST IFTS Interferometer Radiometric Concept/Analysis	60												
NGST IFTS Interferometer Optical Concept	150	150		150									
NGST IFTS Interferometer Mechanical Concept	225	300		450	450								
NGST IFTS Interferometer Electrical Concept	300	300		300									
NGST IFTS Interferometer Interface Concept	150												
NGST IFTS Interferometer Alignment Concept	150												
Alignment and Test Bench Concept	50			150									
NGST IFTS Interferometer Optical Performance Analysis	225												
NGST-P Instrument Radiance Analysis	150	100											
NGST IFTS Interferometer Prelim. Thermal Analysis	150	100											
NGST Interferometer preliminary structural analysis	150	100											
Mass & Power & Heat diss. budget first eval.	200	150											
Temperature Control System Design	160												
NGST IFTS Interferometer prelim. procurement specification	100												
Component and Material Evaluation	300												
Prelim Electronic Schematics				225	225								
Sweep Control algorithms	200	300											
PDR Engineering Documentation and Data List	150	300		150	150								
Total	**3380**	**2160**	**0**	**1425**	**825**	**0**	**0**	**0**	**0**	**0**	**0**	**0**	**0**

6.2 COST DRIVERS

Several aspects of the development of the NGST IFTS have a significant impact on the overall cost.

6.2.1 Schedule

As discussed in Section 5 the schedule is thought to be very short and forces us to form a large NGST IFTS team which would not be as efficient as a smaller team. Increased communication between the team members will be required, because each member will be assigned to smaller, more specific tasks, limiting their view of the system-level requirements. This risk will be mitigated by the use of requirement control tools such as DOORS (see Section 3.3).

6.2.2 Testing

The testing of the NGST IFTS is a substantial effort because of the cleanliness requirement and more importantly because of the *cryogenic operation temperature*. Bomem has designed, built and tested two cryogenic interferometers in the past, but these where limited to liquid nitrogen temperatures (77 K). For the NGST IFTS, we are required to perform the testing in a chamber fitted with liquid nitrogen *and liquid helium* cooling equipment to reach the 30 K operation temperature. This type of test facility is significantly more difficult to design, built and operate. Cooling times are longer and operation costs (cryogens) are higher.

6.2.3 Temperature

The cost of design of the NGST IFT is significantly increased compared to standard earth orbiting Fourier Transform spectrometers because of its operating temperature. Significant thermal modeling and design will need to be performed. Although the thermal variations are thought to be smaller than for standard earth orbiting platforms, the absolute temperature is very low (30 K) requiring a significant effort spent on thermal management. In particular ultra-low dissipation devices will need to be used in the 30 K temperature environment.

6.2.4 Interfacing

Since the proposed Bomem contribution is the interferometer *subsystem* to the instrument, itself which is one *system* of the instrument suite (named the NGST ISIM – integrated science instrument module), itself which must comply with the platform interfaces, it is expected that the interface issues and the interface requirement flowdown process will drive a significant portion of the design effort.

6.2.5 Radiation, vibration, contamination

Finally the NGST IFTS development is significantly impacted by issues of radiation hardening, ruggedization against vibration and contamination control, all of which are standard development efforts for space hardware.

6.3 BUDGET ESTIMATE

Table 10 shows the summary of the cost estimate for the development of the interferometer module for the NGST IFTS, as described in Section 2. Table 11 provides the breakdown by task category. Table 12 provides the cost breakdown by WBS.

Table 10: Cost estimate summary

TABLE REMOVED

Table 11: Cost breakdown by task category

TABLE REMOVED

Table 12: Cost breakdown by WBS

TABLE REMOVED

7. REFERENCE MISSIONS

7.1 MIPAS, AIRS, IASI AND TES

The above thee missions are current on-going programs in which Bomem is involved and where similar technologies to IFTS are used. They include ESA, EUMETSAT/CNES and NASA/EOS programs. The cost for the development and production of the first flight unit is remarkably similar, in the vicinity of INFORMATION RELATIVE TO COST REMOVED. This includes the cost of the detectors, which represents typically 20-25% of the cost. These instruments are representative of the IFTS as being key instruments on a world class satellite program. They are however burdened by large industrial teams, frequent replanning (as NGST could be) and led by prime contractors with little initial experience in this type of instrumentation. INFORMATION RELATIVE TO COST REMOVED

7.2 CRIS

The Cross-track IR sounder (NPOESS) is the next generation low earth orbit IR sounder for operational meteorology. Bomem is part of the ITT team and is in charge of the interferometer, the calibration hardware and algorithms. This work is in a competitive Phase A and after a down-selection process, we expect an award for multiple units. This opportunity is an important long-term prospect for space-borne interferometers. Very aggressive cost targets are provided given the long-term nature of these weather programs and the relative simplicity of the instrumentation. INFORMATION RELATIVE TO COST REMOVED.

7.3 ACE

Bomem, ITT and NASA Langley are collaborating on FTS design in the ACE (Atmospheric Chemistry Experiment) program. This instrument is proposed for the Canadian SciSAT-1 mission to be flown in 2001. The instrument concepts derives directly from the Langley WEB interferometer with its highly efficient folded optical path and moving cube corners. An ACE prototype has been put together by the team during the summer of 1998 and can serve as the basis for further prototyping. The instrument will also make use of miniature frequency stable lasers.

INFORMATION RELATIVE TO COST REMOVED

7.4 SUMMARY

While this type of analysis can only provide a rough assessment of cost credibility, we see that the IFTS costs should lie in the INFORMATION RELATIVE TO COST REMOVED bracket (including detector), excluding ground-processing hardware or software.

8. ABBREVIATIONS AND ACRONYMS

CDR	Critical Design Review
CIF	Change Implementation Form
CIRS	Composite Infrared Spectrometer
DOORS	Dynamic Object Oriented Requirements
DSMC	Defense Systems Management College
EM	Engineering Model
ESA	European Space Agency
FM	Flight Model
H/W	Hardware
IFTS	Imaging Fourier Transform Spectrometer
ISIM	Integrated Science Instrument Module
IT	Integration Test
NGST	Next Generation Space Telescope
PA	Product Assurance
PDR	Preliminary Design Review
QA	Quality Assurance
QM	Qualification Model
RD	Reference Document
S/W	Software
TPR	Test Procedures & Reports
TRR	Test Readiness Review
WBS	Work breakdown Structure

— End of document —

BOMEM

NGST

Next Generation Space Telescope

Final Report

Volume 3 - Trade Analyses

Document Number: **SP-BOM-007/99**

Issue: **1** **Revision:** A

Issue Date: **13 October 1999** **Document Name:** Annex B3.doc

	Function	Name	Signature	Date
Prepared by	Scientist	Louis Moreau		
Prepared by	Scientist	Frédéric Grandmont		
Approved by	Project Manager	André Villemaire		
Approved by	Director, SPR division	Jean Giroux		

BOMEM Inc. • a unit of Elsag Bailey Process Automation N.V.

450 Saint-Jean-Baptiste Avenue • Québec, Québec G2E 5S5 Canada • Phone (418) 877–2944 • Fax (418) 877–2834

TABLE OF CONTENTS

LIST OF FIGURES

LIST OF TABLES

DOCUMENT CHANGE RECORD

Issue	Rev.	Date	Chapter/Paragraph Number, Change Description (and Reasons)
1		12 April 1999	Draft of document
1			First release of document
1	A	13 October 1999	New revision to remove proprietary notices.

1. INTRODUCTION

1.1 BACKGROUND INFORMATION

The Next Generation of Space Telescope (NGST) project of NASA is intended to provide continuity and new focus for research following the success of the Hubble Space Telescope. It is considered to be a technologically challenging project as the technology needed is not necessarily available. It challenges the innovation of the scientific and technological community to come up with an affordable technology to carry out the scientific goals of the mission.

Canada has a strong Space Astronomy community and they have ranked the participation of this project as the priority in their LTSP III submission. In order for Canada to participate, the areas of technical expertise and competence necessarily has to match the required technologies of the NGST project. The nature and scope of the Canadian contribution to the NGST are neither identified nor defined. The CSA sees the Canadian contribution as one that matches the industrial capability, an area that would result in industrial and economic growth and provide a sound base for competitiveness in the international market.

At the end of 1998, CSA awarded a number of contracts to Canadian firms. Bomem was awarded such a contract to study the potential use of a Fourier Transform Imaging Spectrometer as a science instrument for NGST.

1.2 SCOPE OF PROJECT

This work was carried out under contract no 9F007-8-3007/001/SR.

Bomem proposed to study the potential use of a Imaging Fourier Transform Spectrometer as a moderate spectral resolution camera for NGST. The approach was to first investigate the trade space of the instrument design. Next the performance of the instrument was predicted to confirm the suitability of the technology for the NGST mission. The risk analysis and mitigation plans were then completed. Finally the Cost and Schedule estimates were drafted based on the previous findings.

1.3 SCOPE OF DOCUMENT

This document is Volume 3 of the final report. The other deliverables of the study contract are listed in Table 1.

Volume 3 covers the *Trade Analyses* performed on the contribution proposed by Bomem, namely an Imaging Fourier Transform Spectrometer (IFTS) module as one of the central science instrument for NGST. The goal of a trade study is to evaluate the advantages and disadvantages of the various technical options available to implement a component of the system. For example, Fourier Transform Spectrometers can be constructed using flat mirrors or cube-corner retroreflectors. Both of these approaches have advantages and disadvantages. The goal of the flat vs. cube-corner retroreflectors trade study is to find out which is more advantageous for NGST. After the main trade studies are completed a coherent concept for the system, *named a baseline,* appears.

It is important to note however that the trade analyses presented in this volume are first and foremost motivated by the desire to derive an IFTS baseline for the purpose of *cost and schedule estimates*. These trades are only indicative of the type of studies the designers will conduct during the development of this sophisticated spectrometer module. In fact, when a doubt existed in these preliminary trade studies, the choice was motivated by spectrometric performance in the first place, before cost, practicality or maturity of the technology. This may have led to a technical baseline which is more complex and ambitious than usually encountered. This has the consequence of generating a conservative cost and schedule estimate.

Table 1: Deliverables of the study contract

Volume	Document Number	Document	Description
1	SP-BOM-005/99	Executive Summary	5-page summary of the findings of the contract
2	SP-BOM-006/99	Planning Report	Report on the scheduling and cost of the proposed Canadian participation. The planning report also includes the risk assessment and mitigation plan
3	SP-BOM-007/99	Trade Analyses	Report on the trade analyses performed to arrive at a credible baseline for the proposed Canadian participation.
4	SP-BOM-008/99	Performance Analyses	Report on the sensitivity analyses performed to evaluate the suitability of the proposed Canadian participation for NGST
5	SP-BOM-009/99	Technology Report	Report on some proposed novel technology approaches to the specific NGST environment for the proposed Canadian participation.

The trade analyses covered in this document cover the following trade analyses:

- Wavelength coverage, Section 2
- Metrology separation, Section 4
- Two ports vs. Four ports, Section 5
- Corner reflectors vs. Flat mirrors, Section 6
- Spectral bands separation, Section 7
- Sweeping method, Section 8

The radiometric calibration strategy is discussed in Section 9 but due to limited time, no hard conclusion could be reached. NGST poses a substantially different set of conditions from ordinary earth-observing IFTS (where most of the calibration expertise exists) that it is expected that dramatically different calibration approach will be required. Bomem has a unique expertise in design and fabrication of calibration sources and is very interested in this subsystem. However because no baseline could be established, it was decided to leave the calibration sources out of the proposed contribution for the moment.

1.4 REFERENCE DOCUMENTS

RD 1 Bomem Proposal No:SPIR180898, issue 1, revision -, dated 8 September 1998, in response to solicitation No 9F007-8-3007/A.

RD 2 Volume 4 - Performance Analyses NGST performance studies, SP-BOM-008/99

RD 3 Wolf W. L. and G. J. Zissis Ed., The Infrared Handbook, ERIM, 1989.

RD 4 Stockman H. S. & al., Cosmic ray rejection and image processing aboard the next generation space telescope, UCB Astronomy.

RD 5 Handbook of Optics, Volume 1, McGraw Hill, edited by Michael Bass, sponsored by optical society of America, 1995.

1.5 DEFINITIONS

Étendue	The product of the limiting collection area and the solid angle of the limiting field of view. Often called throughput.
Irradiance	Incident radiant energy per unit surface per unit time. Spectral irradiance is the irradiance at a given wavenumber (or wavelength or frequency) per unit wavenumber (or unit wavelength or unit frequency). Usual symbol is *E*.
Jansky	Units of spectral irradiance. Symbol is Jy (1 Jy = 10^{-26} W m^{-2} s).
Radiance	Radiant energy per unit surface per unit solid angle per unit time. Spectral radiance is the radiance at a given wavenumber (or wavelength or frequency) per unit wavenumber (or unit wavelength or unit frequency). Usual symbol is *L*.
Wavenumber	The inverse of the wavelength. Usual symbol is σ (σ=1 /λ).

1.6 ACRONYMS

AC	Alternating Current
CCD	Charge-Coupled Device
CSA	Canadian Space Agency
DC	Direct Current
DF	Dispersive Filter
DFT	Discrete Fourier Transform
DN	Detector Noise
DSI	Double-Sided Interferogram
FFT	Fast-Fourier Transform
FOV	Field Of View
FOV	Field Of View
FPA	Focal Plane Array

FPA	Focal Plane Array
FSR	Free Spectral Range
FTS	Fourier Transform Spectrometer
FTS	Fourier-Transform Spectrometer
FWHM	Full-Width at Half Maximum
IFIRS	Integral Field Infrared Spectrograph
IFS	Integral Field Spectrograph
IFTS	Imaging Fourier Transform Spectrometer
IR	Infrared
MIR	Middle Infrared
MOS	Multi-Object Spectrograph
MPD	Maximum path difference
NEP	Noise Equivalent Power
NESI	Noise Equivalent Spectral Irradiance
NESR	Noise Equivalent Spectral Radiance
NGST	New Generation Space Telescope
NGST	Next Generation Space Telescope
NIR	Near Infrared
OPD	Optical path difference
PN	Photon Noise
RMS	Root-Mean Square
RN	Read-Out Noise
SNR	Signal to Noise Ratio
SNR	Signal to Noise Ratio
SSI	Single-Sided Interferogram
TF	Tuneable Filter
VIS	Visible
ZPD	Zero Path Difference

1.7 LEGEND FOR THE SCHEMATICS

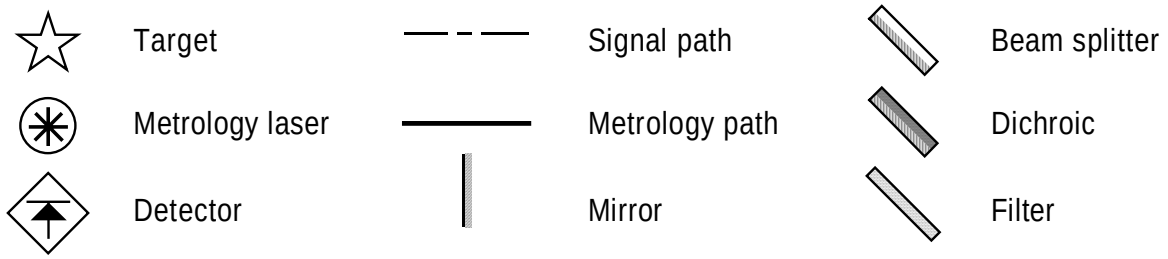

2. GENERAL GUIDELINES

The activity of performing a trade analysis can be summarised as:

1. List all relevant approaches to implement the component or the mode of operation of interest.

2. List the discriminating criteria for each component or the mode of operation. Determine the score of each approach for each criteria in the context of the specific instrument or program.

3. Elect a baseline approach, based on the overall score.

The third step is based on the relative importance of each criteria. There is often insufficient information to determine the relative importance weighting factors and the results are somewhat subjective and lead to discussions. As much as possible the trade studies should be established on quantifiable grounds and associated with engineering studies.

At this early stage in the design of the NGST IFTS we rely on the information available and previous studies. The mission requirements of NGST and the conclusions of RD2 impose the following constraints on the IFTS design:

- The instrument will cover a broad spectral range from visible to MIR.
- The efficiency should be as close to 100% as possible.
- The Etendue should only be limited by the primary telescope and the detector array.
- The instrument must be sensitive to extremely small fluxes in a relatively high noise environment. A SNR of 10 for Irradiance of the order of one nJ is sought.
- A position accuracy of 1% of the step size is sufficient to make sure that the noise caused by position errors is much smaller than the photon noise for small incoming flux.
- Precision and accuracy on absolute radiance output should be close to 1%.
- Calibration should not have to be perform on period shorter than 2 weeks to keep output measurement within 1% stability.
- The observation time required to achieve a high SNR is very long (approx. 12 days) and should not be unnecessarily increased.
- The instrument must be fully space compliant.
- Weight and space should be kept to a minimum.
- The total cost of the design is also limited.

3. WAVELENGTH COVERAGE

Sensitivity range of 1 to 5 micron had been primarily selected for the first definition of the NGST instrument. However, current evolution of the NGST project shows that extended range is becoming a requirement as it is a feature wanted by most end users of the space telescope. Extension of this primary selected wavelength range for NGST operation, must be carefully studied. Any change in the detection range of the instrument spectral coverage could have serious implication on the design and cost. Sensitivity in the visible spectrum (0.4 to 1 micron) and in the MIR (5 to 30 micron) tend to become new targeted characteristics. In this brief discussion, a study for extending the wavelength range is presented.

First, enlarging the instrument waveband means that more than 1 set of detector arrays is needed to collect all the light. The only detectors that cover the full NGST extended waveband are thermal detector and they have non-optimal responsivity to noise ratio as compared to quantum detector. Moreover, it wouldn't be suitable anyway for the following reason. One unfavourable property of Fourier transform spectrometers is that they generate spectra with uniform noise on the spectral scale. This feature tends to promote the breaking up of the full bandwidth into smaller bands where the signal doesn't vary too much in intensity. Otherwise the area of weak signal tend to be drowned by the average noise level caused in part by the high signal area. At this stage it is thought that the spectrum will be covered in 3 slightly overlapping regions (visible, NIR, MIR) forcing the need for 3 separate FPA. As it will be shown in section 6, dichroic beamsplitters are proposed to separate distinct wavebands and direct them on appropriate FPA. Trade studies are also conducted to evaluate the use of separate interferometers instead of using a single one for all waveband. Having separate interferometers is suitable for optimising sensitivity at the desired wavebands but this raise cost somewhat.

At the short end of the wavelength waveband, adding the visible spectrum involves using a different type of detector (probably CCD camera). It also prevent the use of common visible laser for metrology as it would produce a great amount of stray light coinciding with the sensitivity zone of the detector. The absolute calibration of the visible band also brings certain concerns. Calibration source for the visible are much harder to use than the blackbodies used in the thermal IR. Calibration lamps with some kind of scattering mechanism to reduce the intensity will probably have to be developed. Such lamp produces a fair amount of heat that has to be evacuated by proper thermal management system.

At the other end of the spectrum, extension to long wavelength mainly causes problem on stray light control. At such long wavelength (30 μm), insufficiently cooled surfaces show strong emission that could completely mask the target signal. Care must then be taken to cool the instrument enough to reduce the stray light coming from thermal emission of the surroundings. Extending the upper bound from 5 micron to 30 micron could mean having to cool down to temperature close to 20K instead of 80K to reduce stray light contamination. Much more capable cooling system must then be chosen though the spacecraft sunshield should considerably help lower the temperature. The problem mainly consists in evacuating heat generated by electronics, mechanical and calibration devices.

With such a large waveband, spectral separation of metrology become almost impossible, forcing the development of new ideas. Space qualified laser of wavelength lower than 30 μm or higher than 0.4 μm are less common. All these topics are studied in more details in the following sections.

4. METROLOGY SEPARATION

4.1 DESCRIPTION

The metrology system is used to monitor the optical path difference between the two arms of the interferometer. The same metrology signal can also be used to monitor the alignment of the mirrors and instruct an alignment mechanism to correct misalignments. The metrology of FTS instrument is one of the highly desirable components of these instruments as it provides a high fidelity spectral scale by virtue of the frequency standard (laser) used for the interferogram sampling. The metrology makes sure that the system is continuously spectrally stable but the radiation from the metrology signal, usually a laser, can also be a source of pollution as photons from the metrology signal can reach the science detector. This contamination can be particularly important for small flux applications like deep space astronomy where the typical metrology laser can have an energy flux several orders of magnitude higher than the flux of the observed astronomical object. It is thus important to separate the metrology signal from the target signal. In this section, different method of separation is presented and their relative advantages and disadvantages, considering NGST special conditions, are discussed.

The fact that the power of the metrology light should be so much higher that the science light is disturbing at first sight. If the science detector can detect a few photons per second, why would the metrology require, say 10^{15} photons per second? The answer lies in the difference in bandwidth requirement for both systems. The science light interferograms has a very low bandwidth since it requires 10^5 seconds for an acquisition. The bandwidth of the metrology is much higher. In a simplistic way we can look at the feedback time we expect for the typical tasks assigned to the metrology. In the case of a step-scan system, the most basic task for the metrology is to provide position feedback while moving the interferometer mirror from one fixed OPD position to the next. In order to preserve a good measurement duty cycle we want to minimise the amount of time devoted to transitioning the mirror because no science light is collected. If we want to perform the OPD transition in a few seconds, we need a metrology feedback on the order of few tens to hundred of seconds, which is a much higher bandwidth than the science light. This very large bandwidth admits more noise in the electrical system and thus requires more optical power to achieve adequate position servoing.

4.1.1 No metrology

One of the most radical method, to make sure that the signal from the metrology does not contaminate the signal of the target, is to design a system without metrology. Such a system is spectrally calibrated prior to launch. However, post-launch variations of the spectral calibration cannot be directly monitored. Periodic alignment of the mirrors of the interferometer is also impossible without an interferometric metrology

4.1.2 Temporal separation

The metrology signal and the target signal can be separated in time. For instance the metrology signal can be on only when the moving mirror is displaced to a new sampling position and off when the target signal acquisition at a given OPD begins. When the metrology signal is off, all the optical elements that were used to direct the metrology signal can be removed from the optical path

(potentially at a certain cost in precision) or they can remain in place (potentially causing some obscuration). Since the metrology is off when the acquisition is made, the target signal cannot be contaminated by stray photons from the metrology.

This method is particularly appropriate for a step scan interferometer. During the acquisition, the moving mirror is at rest. The stability of the position can be estimated by comparing the position measurement before and after the acquisition to monitor any drift in position.

4.1.3 Spatial separation

The metrology signal can be spatially separated from the target signal. In this case, optical elements are positioned in the optical path to make sure that the metrology signal does not reach the detector. The OPD can thus be monitored and the sweep controlled at all time even during the acquisition. These optical elements usually cause some obscuration and block a fraction of the target signal. The metrology signal can be placed off the centre of the optical path (Figure 1 b), reducing or eliminating the obscuration but causing some coupling between tilt errors and OPD position error thus making the alignment and positioning less accurate. An annular separation (Figure 1c) where the metrology signal is all around the target signal can solve that accuracy problem but may results in even larger obscuration.

The photon flux from a visible laser with a power of the order of the mW is of the order of 10^{15} photons per second. For signals of the order of a few nJ, the photon flux from the target is only a few photons per second. Even if a small fraction of the metrology signal is deviated by scattering, diffraction, or multiple reflections the contamination can be of several orders of magnitude larger than the signal from the target. Even if we consider only the multiple reflections within the beamsplitter, the photon contamination exceeds the signal of the target by several orders of magnitude (see Annex A).

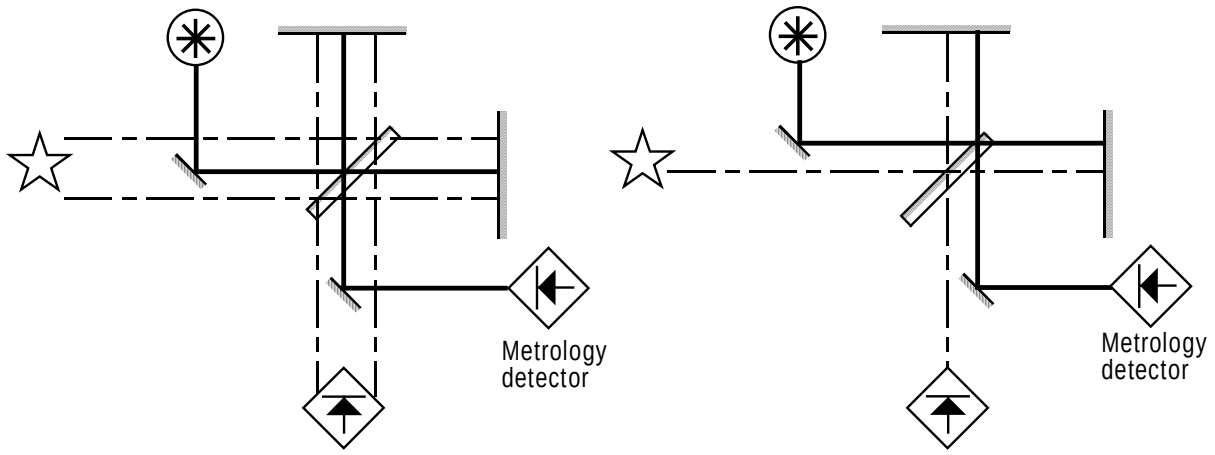

a) b)

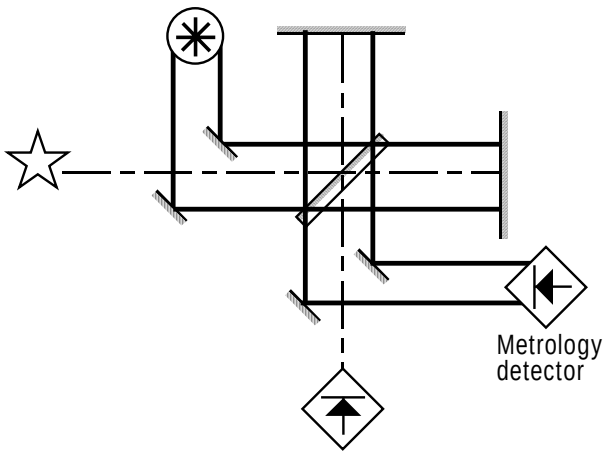

c)

Figure 1: Metrology spatially separated. a) Centred. b) Off centre c) Annular

4.1.4 Spectral separation

The metrology signal can also be spectrally separated from the signal of the target, by choosing a metrology source with a wavelength outside the waveband of the detector. If the wavelength of the metrology is longer than the longest wavelength of response, it is often believed that the stray light from the metrology will not contaminate the signal and will not increase the photon noise because the detectors are not sensitive to such long wavelength. However because we aim at attenuating the amount of stray light by several order of magnitudes, there is not guarantee that this approach will work. The cut-off (transition to longer wavelength) of semiconductor materials are usually only characterised over a few order of magnitude. Figure 2 shows the relative spectral response of various semiconductor detectors around the cutoff wavelengths. The cutoff of GaN is characterised over four orders of magnitudes while the longer wavelength material is only characterised over two orders of magnitude. Over the very wide dynamic range required for NGST, we expect second order phenomena to take place such as phonon-photon interactions. More investigations are required to conclude on this topic.

If the wavelength of the metrology is shorter than the shortest wavelength of response, stray light from the metrology will not contaminate the signal (in the sense that the target and the metrology are spectrally distinct) but will certainly increase the photon noise. Quantum efficiency at short wavelength decreases somewhat but does not reach zero. Because the photon flux from the metrology is much higher than the photon flux from the target (15 order of magnitude higher in the case of a 1 mW visible laser), even if the quantum efficiency is very low the increase of the photon noise can be significant. For the same reason, high-pass optical filters are probably not a solution. An imperfect filter will not completely remove the stray light from the metrology and may also reduce the transmission efficiency of the target signal.

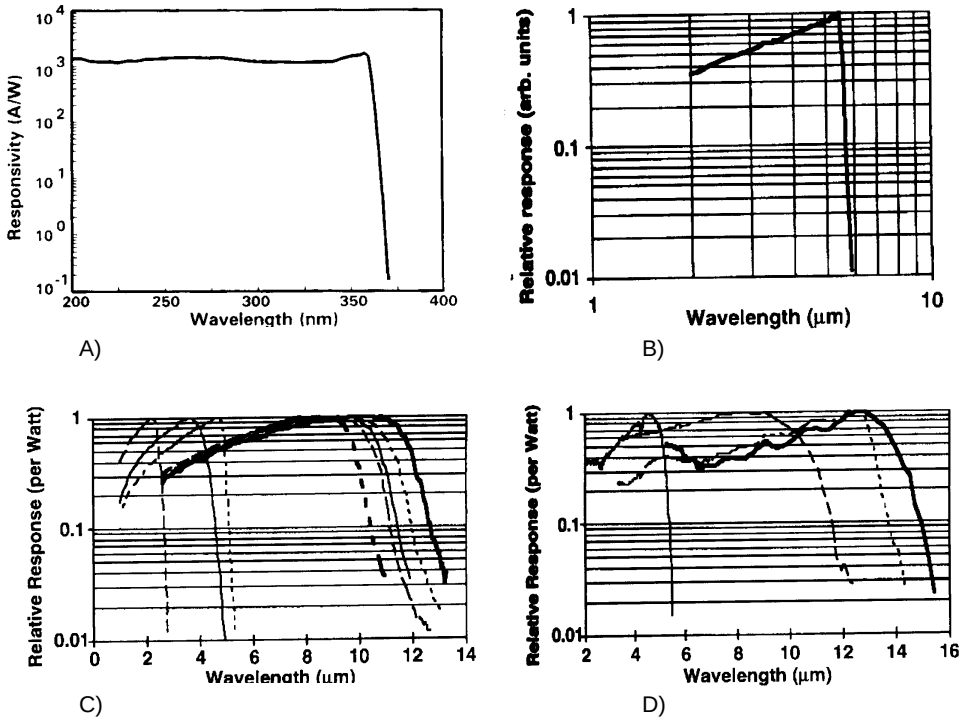

Figure 2: Examples the spectral variation of the relative response per watt (directly related to quantum efficiency times wavelength), for A) GaN photodiode (no AR coating), B) InSb photodiode (no AR coating), C) HgCdTe photodiodes with various cutoff wavelengths (no AR coating), and D) HgCdTe photoconductors with various cutoff wavelengths (with AR coating). Data taken from RD 5

If spectral separation is chosen, some form of spatial separation is also required to inject the metrology signal in the interferometer and direct it to the metrology detectors. The techniques then deals with some of the advantages and disadvantages of spatial separation alternatives (see Section 4.1.3). Spectral separation is merely a way to reduce the contamination of the signal by the metrology. Moreover, spectral separation limits the metrology sources that can be used. If NGST is to be used from the beginning of the visible, around 400 nm, to the thermal infrared, around 30 μm, the choices of metrology sources are drastically limited. There are not many types of lasers available at short wavelengths and most of them, such as Excimer lasers, are unsuited for such operation. At longer wavelengths, the choice of lasers is slightly larger but whether they are suitable or can be space qualified is doubtful. Moreover, at longer wavelengths the period of the reference signal is larger and it may impair the achievement of a fine position resolution.

4.1.5 Indirect metrology

The OPD can also be monitored indirectly. Figure 3 shows an example of such an indirect monitoring. In this example the position of the moving mirror is measured by a second interferometer that uses the

back of the moving mirror as one of its reflectors. Since the metrology and the signal from the target go through completely different optical path, the signal is not obscured. Given the extremely high attenuation required to avoid contaminating the signal of the target, care must be exerted so that no light from the metrology source "leaks" from the metrology interferometer to the science interferometer, particularly around the edge of the moving mirror. The process illustrated on Figure 3 is only an example of indirect metrology. There are other possible configurations. For instance an inductive or capacitive sensor can be used to monitor the position of the moving mirror.

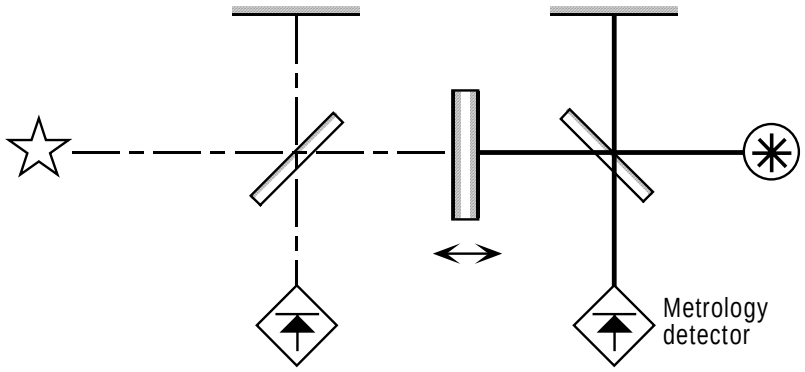

Figure 3: Example of indirect OPD monitoring

4.2 COMPARISONS

Table 2: Qualitative comparison of various metrology configuration

Configuration	Advantages	Disadvantages
a) No metrology.	1. No signal contamination. 2. No obscuration. 3. Simplest design.	1. No position monitoring. 2. No dynamic alignment.
b) Temporal separation.	1. No signal contamination. 2. Metrology can be of any wavelength. 3. Having no obscuration is possible.	1. Position monitoring is not continuous. 2. May require actuators to move the injection and retrieval optics in and off the path (if no obscuration is required).
c) Spectral separation.	1. Constant monitoring. 2. No signal contamination if longer wavelength is used.	1. Difficult to realise if NGST is to measure from UV to TIR. 2. May increase the photon noise if the wavelength of the metrology is shorter than the lower wavelength of the band. 3. Not as precise monitoring if a

		long wavelength is used. 4. Must be used with a spatial separation alternatives.
d) Spatial separation: centred.	1. Constant monitoring. 2. Metrology can be of any wavelength.	1. Potential signal contamination caused by scattering, multi-reflections and diffraction. 2. Obscuration.
e) Spatial separation: off centre.	1. Constant monitoring. 2. No or small obscuration. 3. Metrology can be of any wavelength.	1. Potential signal contamination caused by scattering, multi-reflections and diffraction. 2. Some coupling between OPD errors and tilt errors.
f) Spatial separation: annular.	1. Constant monitoring. 2. No or small obscuration. 3. Metrology can be of any wavelength.	1. Potential signal contamination caused by scattering, multi-reflections and diffraction.
g) Indirect	1. Signal contamination can be prevented. 2. No obscuration. 3. Simultaneous observations. 4. Metrology can be of any wavelength.	1. Does not monitor the position directly (e.g. sensitive to differential thermal distortion). 2. More complex design.

4.3 CONCLUSIONS

The question of contamination is a serious one which dismiss option c), d), e) and f). Solution a) does not provide true OPD or alignment monitoring capabilities and is, thus, less interesting. The temporal separation does not have such problems. The worst limitation of that option is the lack of information while the metrology is off. Whether such a system can work and allow a reliable monitoring of the position and the alignment remains to be seen. The accuracy may depend on the sweeping method used; this option is probably more suited to a step scan sweep than a continuous sweep. Breadboarding activities is a very good approach at mitigating this risk.

Option g) on the other hand present some interesting features. Even if it does not provide true OPD, the deviation from real values can be strongly minimised by controlling the environment temperature which will certainly be the case in NGST instrument environment. This option also allows some form of indirect alignment monitoring. However, it would be risky to think of this option as a stand alone option for providing metrology for the instrument as the metrology signal does not run through all optical elements to account for misalignment or OPD.

Temporal separation seems to be the most appropriate option for NGST and it worth being tested and investigated further. This is the method chosen for this baseline instrument but hybrid version of

option b) and g) might become handy in solving some of the problems associated with temporal separation.

5. TWO PORTS VS. FOUR PORTS

5.1 DESCRIPTION

Every Michelson interferometers and its derivatives have two input ports and two output ports. However, for the most common implementation of the Michelson interferometers, the second output port is superposed to the first input port (returning 50% of the incoming light back to the target) and the second input port is superposed to the first output port (see Figure 5b). With such interferometers, the second output port cannot be directed to a detector without blocking the signal from the target and the second input port is occupied by the detector, making them, for all practical purposes, two ports interferometers.

There exists a few ways to make the four ports available. Two such ways are shown on Figure 4, one using cube corner mirrors and one using flat mirrors. The first method separates the beam in the system pupil, while the second method separates the beam in a system field image. In both cases, the second output port can be occupied by a second detector. This is equivalent to doubling the efficiency of the interferometer, thus increasing the signal to noise ratio by a factor $\sqrt{2}$. Comparing the signal from the first detector with the signal from the second detector may also allow the detection and correction of soft failures due to cosmic rays. In this dual port configuration, light coming from the second input must be controlled as it is added to the first input. This input will have to be blocked by a cold stop or it could be used to estimate the background radiation.

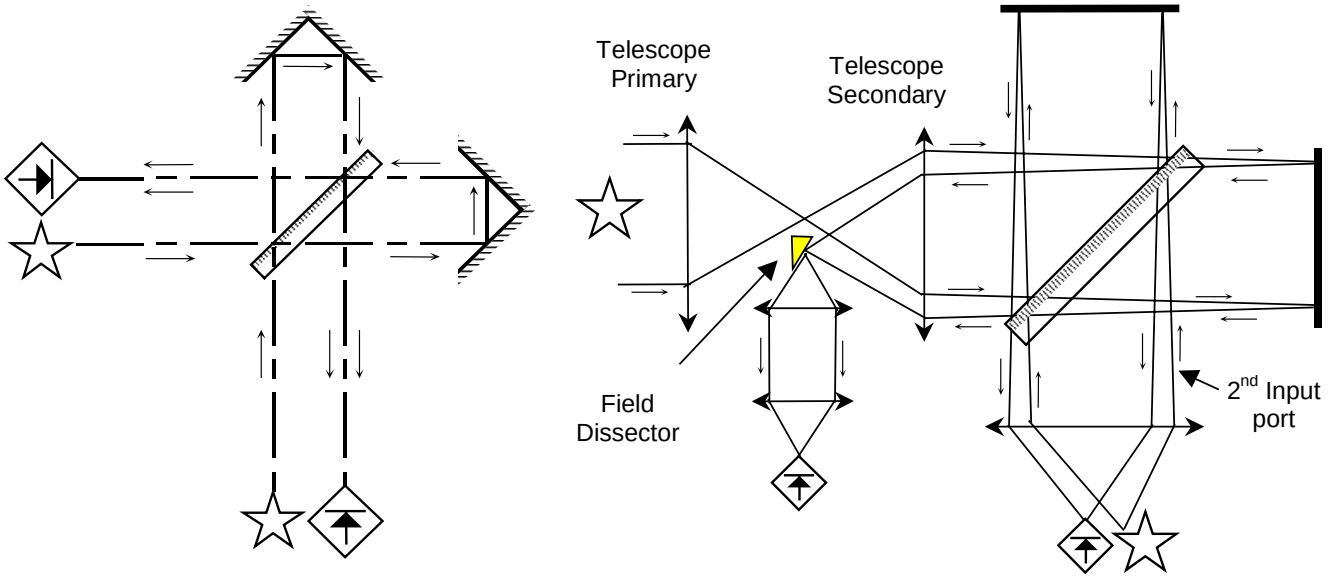

Figure 4: Two examples of a four ports interferometer a) with corner reflectors b) with flat mirrors

No matter if the interferometer has two or four distinct ports, the principle is similar. The beam incident from the left input hits the beamsplitter where it is divided into reflected and transmitted wavefronts. These wavefronts are reflected back to the beamsplitter (acting as a recombiner) by the interferometer mirrors, to recombine and interfere. Due to the nature of the beamsplitter, two such recombinations are obtained, one reflected and one transmitted. In fact, the interferometer can be seen as a sinusoidal chopper with a certain modulation frequency that depends on the wavelength of the light. The light is not destroyed but rather switched from one output port to the other.

5.2 COMPARISONS

Table 3: Qualitative comparison of the single and dual port configuration

Configuration	Advantages	Disadvantages
a) Two ports	1. Requires only one set of detectors. 2. Simpler design. Lower cost.	1. Lower efficiency.
b) Four ports	1. Increase the SNR by a factor $\sqrt{2}$. 2. Redundancy. 3. Simultaneous measurements with two detectors make the correction of glitches and spikes easier.	1. Requires two sets of detectors. 2. More complicated design. Higher cost.

5.3 CONCLUSIONS

As mentioned in RD 2, NGST will requires the highest efficiency possible to achieve a high SNR for small incoming flux. This reason alone is sufficient to justify the selection of the four-port option over the two-port option.

From the point of view of the interferometer, the four-port configuration is only marginally more expensive than the two-port configuration. Obviously, the same thing cannot be said for the detector subsystem, as the four-port configuration implies a duplication of that subsystem. For the purpose of evaluating the feasibility, cost and schedule of the interferometer module of NGST, we will use the four-port configuration, so as to consider the worst case.

6. CORNER REFLECTORS VS. FLAT MIRRORS

6.1 DESCRIPTION

Most of today's Fourier transform spectrometer (FTS) are still based on the interferometer designed by Michelson and Morlay in the early 20th century and shown on Figure 5b. These FTS use flat mirrors. One notable exception is the retroreflector spectrometer marketed by Bomem and Brucker, such as the cube corner interferometer shown on Figure 5a. With the flat mirror configuration, the optical path of one of the interferometer arm is usually changed by moving one mirror. With the Bomem MB interferometer, a system with a corner cube configuration, an optical path difference between the two arms is achieved by rotating the two retroreflectors around a central pivot.

Both configuration has its advantages and disadvantages. A partial list of these characteristics is given in Table 4.

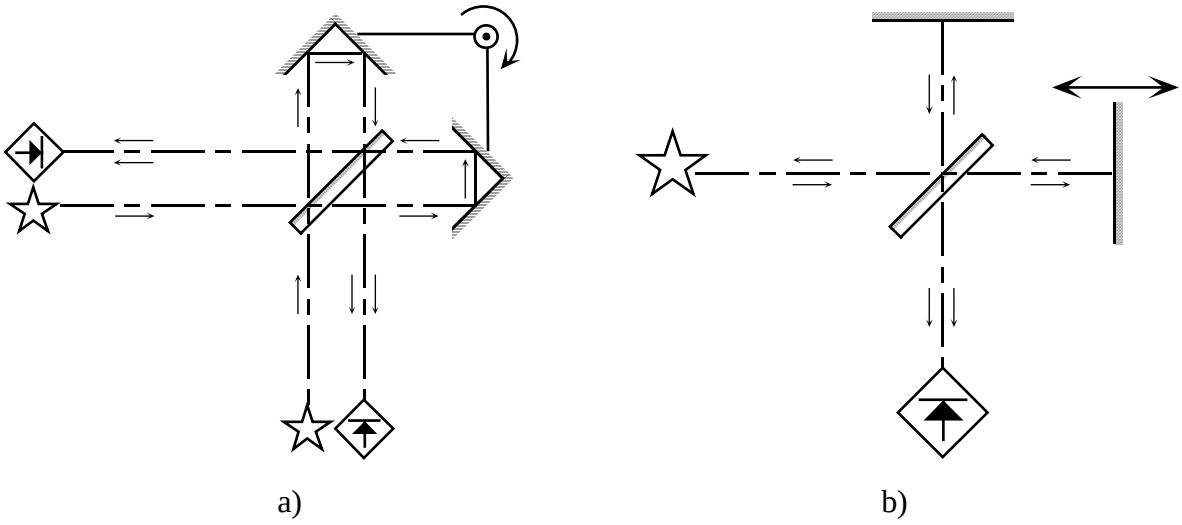

Figure 5: a) Interferometer with corner reflectors. b) Interferometer with flat mirrors.

6.2 COMPARISONS

Table 4: Qualitative comparison of the flat mirrors and corner reflectors configuration

Configuration	Advantages	Disadvantages
a) Corner reflectors	1. Only small residual tilt error. 2. Easier to construct a passive mechanism.	1. Lower ultimate modulation efficiency. 2. Possible shear error. 3. Three reflections: reduced transmission efficiency. 4. Composite assembly with cemented parts; fragility & stability concerns.
b) Flat mirrors	1. Better ultimate modulation efficiency. (No shear error) 2. Better transmission. (Only one reflection) 3. Robust monolithic component.	1. Possible tilt error. 2. Good alignment requires a dynamic alignment system.

6.3 CONCLUSIONS

Because of the stringent sensitivity requirement of NGST we will consider a dynamically aligned flat mirror interferometer design. This option is more apt to produce the highest interferometer efficiency as it potentially has a higher transmission efficiency and higher modulation efficiency than the configuration with corner reflectors.

7. SPECTRAL BANDS SEPARATION

7.1 DESCRIPTION

Given the sensitivity requirement of NGST and its missions, it will probably be a multi-detector system. Each detector need to be optimised for a given spectral band. Most proposed designs suggest at least two spectral bands: one from 1 to 5 μm and another from 5 to 10 μm. Other spectral bands to extend NGST's capabilities in the visible as well as at longer wavelengths (up to 30 μm) are also considered.

Several design options are possible to separate the incoming radiation in spectral bands and direct each band to the appropriate detector. Figure 9 shows six different configurations to spectrally separate the radiation incoming from the target. The first two designs (a and b) use a moving mirror to direct the radiation to every detector in succession, either before or after the interferometer. Acquisition is first performed in the first spectral band, then the mirror is moved to direct the radiation to second detector and so on. The next two designs (c and d) use a reflecting prism to split the incoming radiation in different parts and direct each fraction to a different detector. The last two designs (e and f) use a series of dichroic beamsplitters to separate the incoming radiation in several spectral bands and direct each band to a given detector. A dichroic beamsplitters is an optical component with a coating designed to be highly reflective in a specific spectral band and highly transparent at other wavelengths.

Regardless of the exact method used to spectrally separate the incoming radiation, the separation can be done before the signal enters the interferometer or after it exits the interferometer. If the separation is done after the signal exits, the beamsplitter of the interferometer will have to be designed so as to be effective over the total waveband used by NGST. It is difficult to design a good wideband beamsplitter for various reasons. A typical beamsplitter is usually made of three different parts with different functions: the reflective coating, the bulk substrate, and the anti-reflection coating. The reflective coating is used to split the incoming beam in a reflected and a transmitted part, ideally in equal proportion. The bulk substrate is a thick piece of transparent material to support the reflective and anti-reflection coatings. The anti-reflection coating is used to minimise the reflectance at the second interface of the beamsplitter. These three parts are made of various dielectric materials (often several layers of such materials for the coatings) that are not necessarily effective at all wavelengths. For instance most materials that are transparent in the near-IR have a low transmittance in the visible and the middle-IR (see Figure 7 for a few examples).

Moreover, it is very difficult to design coatings that are effective over a broad range of wavelengths; these coatings are based on constructive or destructive interference and so, the effects are strongly wavelength dependent. To further complicate the matter, the surface roughness of the material used in the infrared tends to be important compared to the wavelengths in the visible. Figure 8 shows the modulation efficiency considering no wavefront deformations (i.e. equal to four times the product of the beamsplitter transmittance and reflectance) of the reflective side of an extended range caesium iodine (CsI) beamsplitter optimised for the near-infrared.

The difficulty of making a wideband beamsplitter is well illustrated with the CsI example. CsI is one infrared material best transmission range in the long wave (see Figure 7). However, being a alkaline salt, it is a very soft material so it is very difficult to polish flat enough for a good modulation efficiency in the short wave.

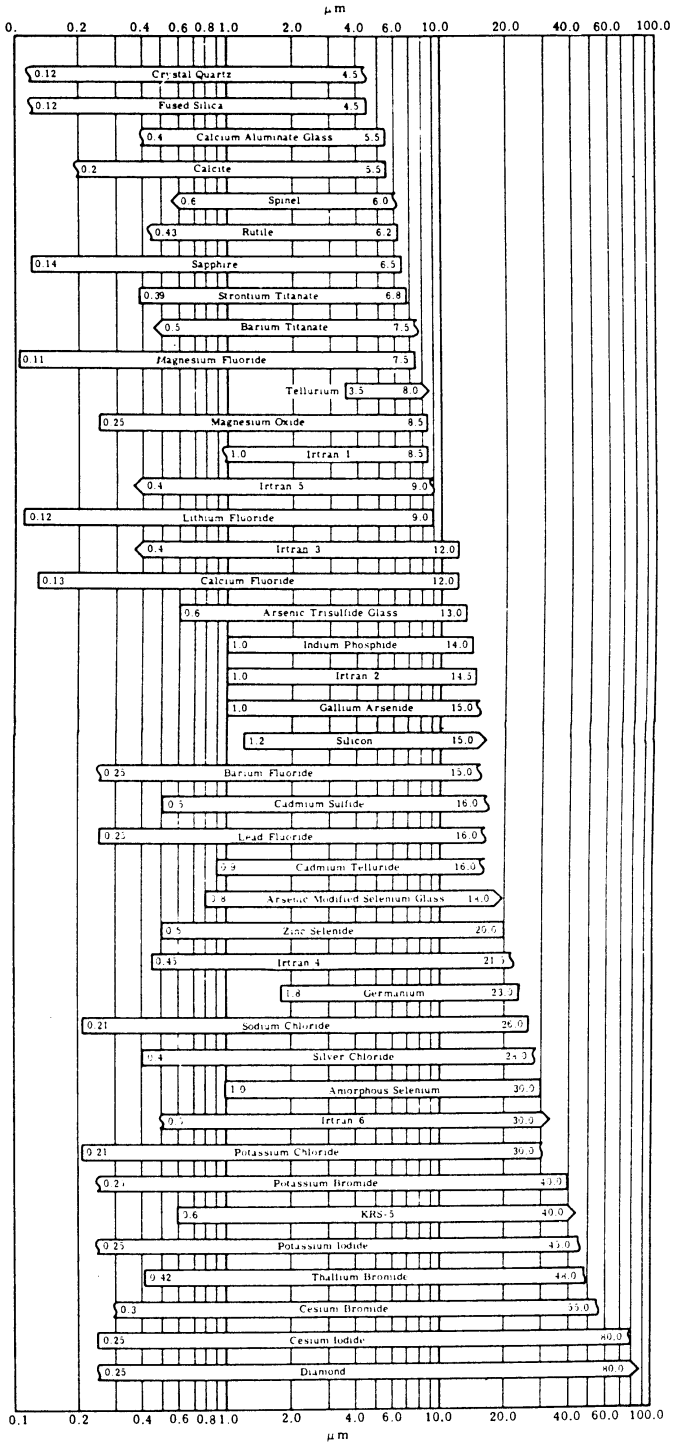

Figure 6: Transmission region (from 100 to 10%) of various optical materials with a thickness of 2mm (RD 3).

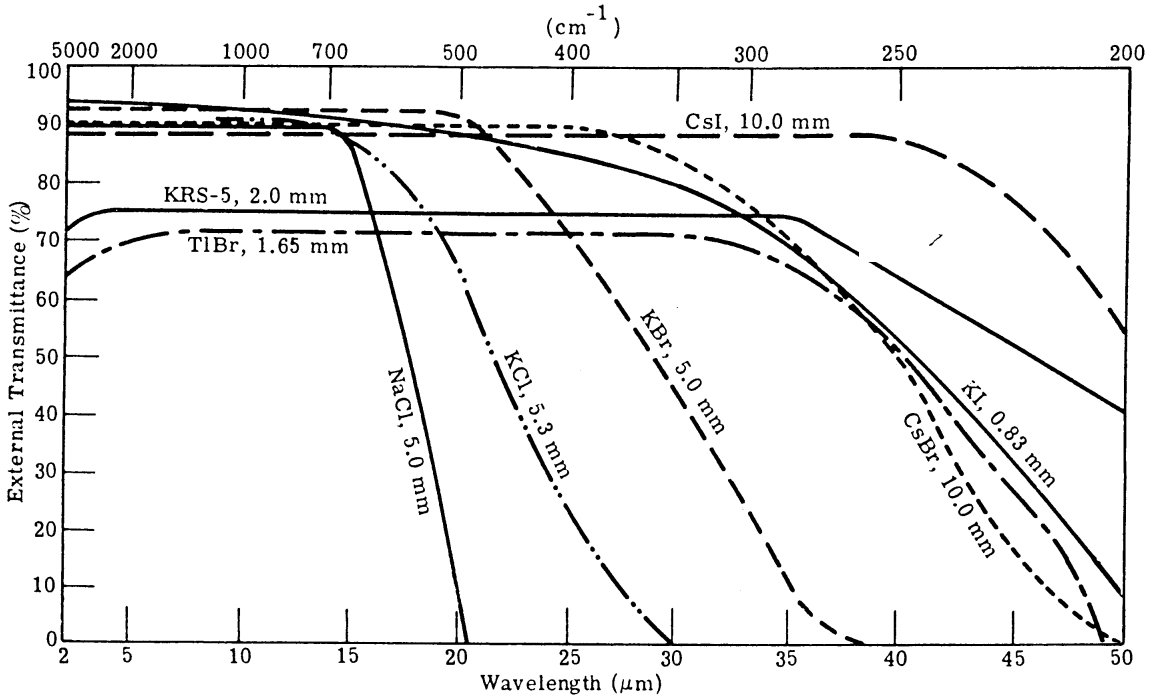

Figure 7: The spectral transmittance of caesium iodine, potassium iodine, potassium bromide, thallium bromide, KRS-5, caesium bromide, sodium chloride, and potassium chloride (RD 3) .

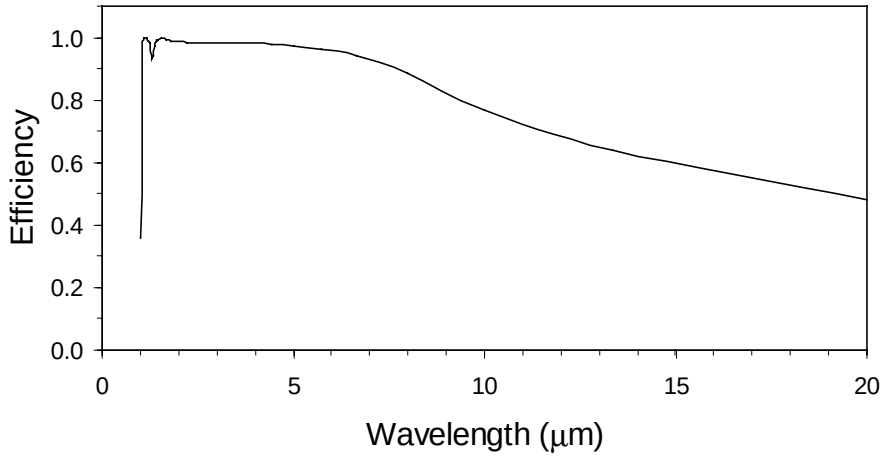

Figure 8: Modulation efficiency at angle of incidence of 30º for extended range NIR-MidIR CsI beamsplitter.

On the other hand, if the separation is made before the signal enter the interferogram, each spectral band will be directed to a different interferometer. Each beamsplitter can then be optimised for that

particular narrower band. Of course, that second option is more costly and take up more space and weight. At this point, we will put sensitivity ahead of the cost, and adopt a split before the interferometers in order to have several optimised interferometer

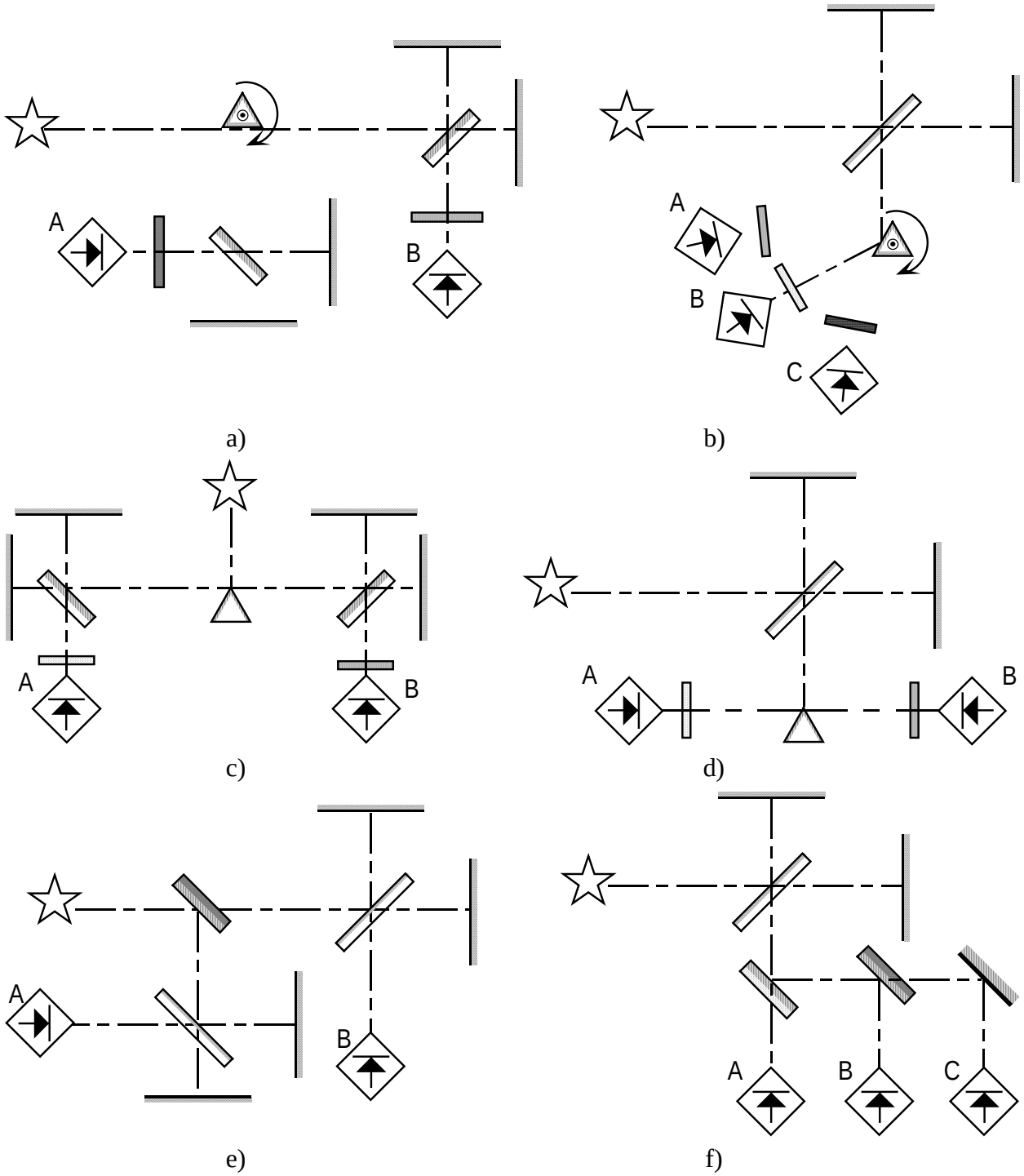

Figure 9: Example of band separations. a) Pointing mirror at the entrance. b) Pointing mirror at the exit. c) Wedge at the entrance. d) Wedge at the exit. e) Dichroic beamsplitters at the entrance. f) Dichroic beamsplitters at the exit.

7.2 COMPARISONS

Table 5: Qualitative comparison of various band separation configurations

Configuration	Advantages	Disadvantages
a) Pointing mirror at the entrance	1. Small transmission loss. 2. The beamsplitters can be optimised for each band. 3. Can accommodate several bands. 4. Less components.	1. Non-continuous operation – longer observation time. 2. Requires one interferometer per band (increased cost and weight). 3. Moving parts. 4. Differential polarisation effects.
b) Pointing mirror at the exit	1. Small transmission loss. 2. Can accommodate several bands.	1. Non-continuous operation – longer observation time. 2. Requires a broadband beamsplitter. 3. Moving parts. 4. Differential polarisation effects.
c) Reflective prism at the entrance. (field separation)	1. The beamsplitters can be optimised for each band. 2. Simultaneous observations.	1. Transmission efficiency is divided by the number of prism faces. 2. Requires one interferometer per band (increased cost and weight).
d) Reflective prism at the exit (field separation).	1. Simultaneous observations.	1. Requires a broadband beamsplitter. 2. Transmission efficiency is divided by the number of prism faces.
e) Reflective prism at the entrance. (pupil separa-tion)	1. The beamsplitters can be optimised for each band. 2. Simultaneous observations.	1. Each detector sees a slightly different field of view. 2. Require a larger primary telescope to achieve the same FOV size.
f) Reflective prism at the exit. (pupil separation)	1. Simultaneous observations.	1. Requires a broadband beamsplitter. 2. Each detector sees a slightly

		different field of view. 3. Require a larger primary telescope to achieve the same FOV size.
g) Dichroic at the entrance	1. The beamsplitters can be optimised for each band. 2. Can accommodate several bands. 3. Simultaneous observations.	1. Transmission loss due to imperfect dichroic beamsplitters. 2. Requires one interferometer per band (increased cost and weight).
h) Dichroic at the exit	1. Simultaneous observations. 2. Can accommodate several bands.	1. Requires a broadband beamsplitter. 2. Transmission loss due to imperfect dichroic beamsplitters.

7.3 CONCLUSIONS

Since it is difficult to design a beamsplitter efficient over a wide spectral range and a high efficiency is required to obtain a good enough SNR for the small flux of expected NGST's targets, the options that requires a broadband beamsplitter should be rejected. In other words, the spectral separation should be performed at the entrance of the instrument and every band directed to a different interferometer optimised for that particular band. Spectral separation before the instrument also allows to optimise sweeping patterns, stroke and speed for each band but it necessarily implies higher cost and larger weight and space.

The total acquisition time required to achieve a good SNR is already very long, of the order of 10 days (see RD 2). For that reason the configuration using a pointing mirror should also be rejected because it does not allow simultaneous observation.

The remaining design options are c), e) and g). A high efficiency cannot be achieved with option c). Using option e) will result in smaller FOV unless a larger primary telescope is used. Since the primary telescope is already a very challenging and costly component of NGST, it is doubtful that its planned diameter can be increased further. If the FOV seen by every detector array is smaller, the total time required to cover a given portion of the sky will be larger. because of these two factors, option e) is not interesting. The remaining option is g): separating the various spectral bands with a series of dichroic at the entrance of the sensor. Although this option is not ideal in terms of transmission efficiency, cost, weight and power consumption it is the best compromise.

8. SWEEPING METHOD

8.1 DESCRIPTION

Three main sweeping methods may be considered.

Step scan: The interferometer mirror is moved from one OPD position to another by monitoring the metrology signal. Once the correct sampling position is found, the system is stopped. The detector is then exposed to light from the target. The system keeps on running through this sequence until the maximum path difference is reached. Output gives only one interferogram per sweep.

Continuous scan:
- 1 sweep
- Low speed

The speed of OPD variation is servo-controlled at a constant low value. The integration of the detector occurs while the mirror is moving. Only one sweep is needed to conclude measurement. Multiple interlaced interferograms may be acquired in one sweep.

Continuous scan:
- multiple sweeps
- High speed

The speed of OPD variation is servo-controlled at a constant high value. The integration of the detector occurs while the mirror is moving. Multiple sweeps are needed to conclude measurement and achieve the required SNR. Each sweep leads to one or more interferogram.

Figure [10] shows the evolution of the moving mirror as a function of time for all three techniques. The number of steps and the OPD range have been reduced on the graph to highlight the aspect of various sweep method. The number of sweep for the high speed continuous scan is for illustration only.

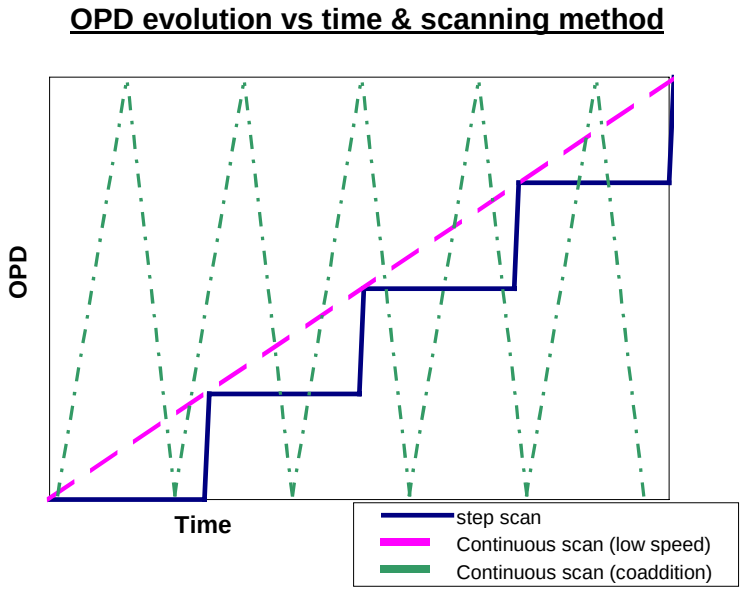

Figure 10: Sweeping methods studied

Regardless of the techniques chosen, one will have to integrate light from the target over similar periods of time to achieve the required SNR since a minimal number of photon (and hence time) must be received from the source. Typical integration time for a complete acquisition is of the order of 10^6 seconds ($2X10^6$ s. = 23.2 days in our RD2 example) to achieve reasonable SNR for incoming flux of the order of 10^{-9} Jy as mentioned in RD2. Therefore, the stop and stare approach (step scan) is worth considering as it is normally rejected for faster acquisition system because of its inefficient duty cycle.

The duty cycle of the step scan method is known to present some inefficiency partly because no acquisition occurs while the system is positioning itself to the next sampling position. However in a system driven by conclusions of RD2, assuming that single sided interferogram are acquired, 100 sampling positions would be needed to complete the overall time of $2X10^6$ with R=100, leading to individual step of $2X10^4$ second (5.5 hours). With such long integration, it is believed that the transit time (likely to be of the order of one second) will represent less than 0.01 % of the total integration time removing the argument of inefficiency. Also, one of the greatest advantage of this technique is that it is fully compatible with temporal separation of metrology since it may be possible to not monitor the OPD when it is stationary. On the other hand having to keep a mirror stable over such long acquisition time presents a challenge that may be addressed by using a hybrid metrology system (temporal and indirect metrology) and proper positioning device.

If the second method is chosen, a sensitive servoing mechanism will have to be designed. For example, let us calculate the speed needed in our RD2 case study. The total optical path difference needed to achieve the stated 80 cm^{-1} spectral resolution can be calculated by the following relation:

$$Resolution\,in\,wavenumber \approx \frac{1}{Total\,OPD}$$

$$80\,cm^{-1} = \frac{1}{Total\,OPD} \rightarrow Total\,OPD = 0.0125\,cm$$

Assuming that the interferometer used has 2:1 optical vs mechanical movement ratio, the total travel of the moving mirror corresponding to a MPD of 0.0125 cm, is 62 μm. One will have to servo the movement of the moving mirror to a speed of 1.88 nm/min to conduct a single sweep in $2X10^6$ seconds. Different metrology design have already been studied to provide sufficient feedback to servo control loop to accomplish such a task.

At this speed the interferogram smear caused by mirror movement during acquisition can be minimised by using shorter individual integration time. In this second method, a series of N interlaced interferograms would be acquired during a single sweep, each having the same sampling interval Δx but being spaced apart by $\Delta x/N$. At the end of the sweep, the N spectra derived from the N interferograms can be averaged, increasing the SNR by a factor $N^{0.5}$. The advantage is that the camera is acquiring at every instant of the total measurement time and lead to a perfect duty cycle efficiency.

For the second continuous scan variant, which is the technique used in most Bomem instruments, the velocity is higher and several sweeps (say N) are used to read the interferogram. The N interferograms acquired are then averaged, also increasing the SNR by a factor $N^{0.5}$. Smearing effect can be more important with this method if no interlaced interferograms are acquired during each sweep. Doing so would however increase the processing power needed as well as the amount of data storage space.

To carefully study the individual aspects of each method, an important fact has to be considered. The conclusions of RD4 indicate that some limits have to be considered relative to the integration time used in the NGST instrument. A too short integration time gives too few photons compared to the readout noise which is a constant for readout operation. On the other hand, an integration time too long makes it impossible to determine the flux because ionising cosmic event that change detector count (see Figure [11]). One way to readout rapidly (to avoid cosmic spikes) while minimising the readout noise is to perform successive non-destructive readout cycles. For the case of NGST, an integration time of 10^3 seconds with 64 non-destructive readouts is assumed to be an optimised way of sampling the science signal. This not only reduces the total effective readout noise well below the background noise, but it also permits the detection and removal of cosmic ray event (reference RD4). Figure 11 shows the aspect of a typical acquisition. A slope fitting algorithm where cosmic ray jump can easily be removed, is used to evaluate the incoming flux which correspond to the slope on the graph. It is important to note that this 10^3 integration time lead to only one point on the interferogram as one flux measurement is extracted from the graph. Also note that any offset is remove automatically with this method. In fact the slope extract operation removes some of the 1/f noise problems usually associated with DC measurements.

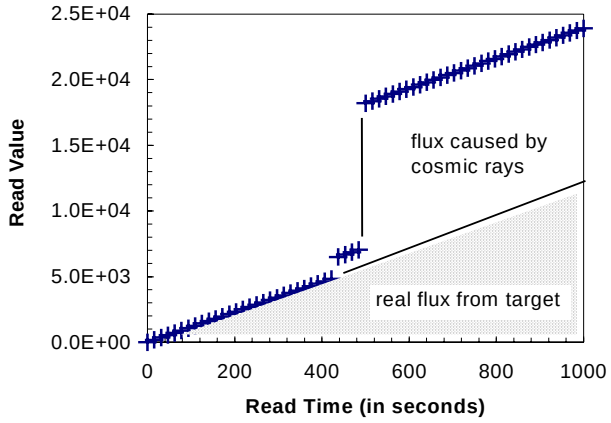

Figure 11: Example of non-destructive readout in presence of cosmic events

This conclusion sets a constraint on the different sweeping alternatives studied. For the step scan technique, it means that several acquisitions will be collected at every sampling position. In our example where the step integration time is of 2X104 seconds, 20 acquisitions of 103 seconds could take place at each of the 100 sampling positions. It also mean that 20 interlaced interferogram would be collected if the second method was used. The third sweeping method is slightly handicapped by this time constraint. If only one data can be pulled out of the algorithm every 103 second, one can't think about having a very fast multiple sweep sequence. For a 100 point interferogram, this would lead to a minimum time for a complete sweep of 100 X 103 seconds = 105 seconds, close to the 2X106 required for the complete measurement. Then 20 interferograms could be obtained in the total integration time, increasing the SNR by a factor of 200.5 = 4.47, a result similar to the one obtained with the second method.

8.2 COMPARISONS

Table 6: Qualitative comparison of various sweeping methods

Configuration	Advantages	Disadvantages
a) Step scan	1. Optimal modulation at fixed OPD. 2. Easy to use with temporal separation of metrology 3. Lower processing power needed. 4. Minimal storage space.	1. Duty cycle inefficiency; transit time is lost. 2. 1/f noise may couple to spectra.
b) 1 scan at low velocity	1. Best duty cycle.	1. Modulation may be limited by interferogram smear during integration. 2. High storage space required. 3. 1/f noise may couple to spectra. 4. Not easy to use with temporal separation of the metrology.
c) Continuous scan with coaddition	1. 1/f noise rejection.	1. Modulation limited by interferogram smear during integration. 2. High storage space required. 3. Not easy to use with temporal separation of the metrology.

8.3 CONCLUSIONS

All three method may show similar SNR performance in operating conditions like the NGST environment. The step scan has some duty cycle inefficiency, but the two others are suffering from smear as they integrate while the output signal is changing. It is not obvious however that this smearing effect has a dramatic influence over the quality of the measurement obtained since the calibration of the instrument will account for this behaviour.

On the other hand, in Section 4, we selected the temporal separation of the metrology to avoid any risk of contaminating the signal of the target. Sweeping method b) and c) are difficult to adapt with this separation option. They would most likely require the indirect metrology approach which is less accurate because the laser beam does not go through the full system; it can't account for beamsplitter or static mirror small movement and thermal deformation. The remaining option (step scan) present all advantages of static acquisition and will be easily integrated with the temporal separation of metrology.

From the point of view of the interferometer also, the step scan approach has the advantage of offering the ultimate flexibility in terms of positioning and dwell times offering infinite possibilities of non traditional sweep pattern such as uneven integration times or uneven sampling intervals.

9. RADIOMETRIC CALIBRATION STRATEGY

9.1 DESCRIPTION

Several strategies exist for radiometric calibration. The list includes in-flight calibration with internal calibration targets, pre-launch calibration on ground, and in-flight calibration using known celestial bodies.

Regardless of the calibration strategy used, the goal is always the same: to obtain the necessary information to convert the electric signal of the detector (integrated change, current or voltage) into equivalent radiometric units. The traditional method of calibration uses two measurements: one acquired while the instrument is looking at a target with a high energy flux (a "warm" target) and a second one while the instrument is looking at a target with a small energy flux (a "cold" target). For linear instrument, a straight line is then used between these two points (see Figure 12). The slope of that line for a given wavelength gives the gain of the instrument at that wavelength and the ordinate at the origin gives the offset of the instrument at that wavelength.

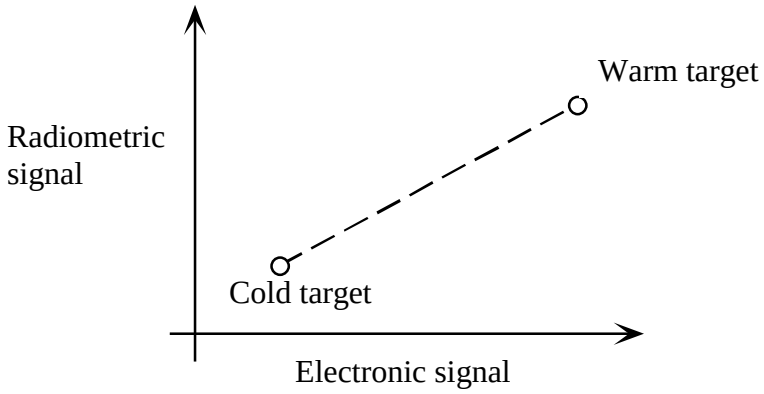

Figure 12: Two points calibration

The spectral gains, the spectral offsets and the exact calibration equation (including fine tuning such as non-linearity correction) can be determined on the ground, prior launch, in well controlled conditions. However, no matter how precise this preliminary calibration is, nothing guarantees that the instrument performance and response will remain the same after launch and through the lifetime of the instrument. Degradation of the optics and electronics, due to contamination, thermal stress, cosmic particles, exposure to ultraviolet radiation, etc. are likely to cause modifications that will affect the calibration. The most common source of radiometric calibration change are thermally induced gain and offset drifts. Detectors responsivity can change with operating temperatures. Thermal drift and spatial gradient can also affect the interferometric alignment which translates into change of modulation efficiency (visibility) or instrument responsivity. For the FTS operating in the thermal IR, the drift most frequently corrected for is the instrument self radiance, or the offset. On the other hand, for the NIR and visible, where the thermal emission is negligible, the offset may not be needed at all, only a measure of the response is required. Astronomers working on NGST requirements are asking for a radiometric accuracy on the order of a few percent on absolute flux measurements. Such a

precision can be achieved on the ground but to maintain the accuracy after the launch, other calibration processes are likely to be required.

Calibration with internal calibration targets uses sources of controlled emission; blackbodies for infrared and lamps for the visible/near infrared. These targets are periodically inserted in the optical path at the entrance of the interferometer in order to monitor the evolution of the sensor and obtain calibration coefficients (spectral gains and offsets). They are usually used to illuminate uniformly the whole field of view so that the response of each individual pixel can be evaluated simultaneously and in the same conditions. However, such system cannot include the fore optics (the telescope) in the calibration process, as it would be impossible to insert a calibration target in front of NGST to illuminate uniformly the primary mirror. The response of the telescope is not necessarily constant since contamination due to outgassing and interplanetary dust can affect its spectral reflectance after the launch.

After launch, calibration information can also be obtained by observing celestial bodies with known and stable (over the lifetime of the instrument) spectral flux. This method relies on models and cross-referencing with other observatories. Since this calibration process includes the fore optics it can be used to monitor the evolution of the performance of the telescope. The major drawbacks of this method are that it will probably be necessary to reorient the telescope to point at the appropriate calibration targets and that these targets cannot cover the whole field of view. Another problem stems from the fact that such calibration processes depends on observations from the ground that include atmospheric effects, especially absorption in the infrared by water vapour, CO_2 and other molecules. This alters the accuracy with which the real spectrum is estimated.

There is a proposal that IFIRS only needs to be precise (repeatable) but not necessarily accurate (absolute). IFIRS could derive then its absolute accuracy from using known reference standards contained within the measurements. This approach is probably viable but requires some level of validation. For example the additional uncertainty introduced by the limited knowledge of the radiance of those standards.

However there exists a simple argument why there is negligible additional cost from hardware to provide absolute calibration sources as compared to allowing only relative calibration.

A relative calibration requires only stable reference sources, rather than known sources. In general, reference sources in the IR are bodies heated at a temperature suitably hot to provide enough photons in the spectral range used. A stable source thus requires its temperature to be monitored precisely and controlled accurately via heaters and/or coolers. At first sight the stability requirement does not imply knowing the source emissivity neither does it imply having a good emissivity. It is not the case however. By virtue of Kirchoff's law, a source with less than perfect emissivity also reflects the radiation from its surrounding in the instrument being calibrated. This situation generates additional requirements, albeit less stringent, on the knowledge of the temperature of the environment. Any change in the temperature of the environment around a grey but otherwise perfectly stable source translates into calibration errors.

The difficulty in assessing the temperature of the environment around a calibration source is great. Not only must the temperature of each surface in the field of view of the source be measured to some level of accuracy, but in the case where these surfaces are not perfectly black themselves (which is overwhelmingly so), the temperature of every surface in the field of view of these secondary surfaces must also be measured to some level of accuracy. In many cases these secondary surfaces cannot be black (for ex. a mirror) so that high order "scattering" must be considered.

For these reasons it is much simpler to work with a calibration source that does not reflect the environment, i.e. a blackbody with high emissivity. However a blackbody with high emissivity is also what is needed for achieving absolute calibration. The only extra work involved in achieving absolute calibration is that the temperature metrology must be absolute rather than relative – a relatively easy and straightforward task.

As for the telemetry, the heat source should be turned off during measurement. Cool down may take several hours/days.

9.2 COMPARISONS

Table 7: Qualitative comparison of various calibration strategies

Configuration	Advantages	Disadvantages
Pre-flight calibration / characterisation only	Simpler system design. Less expensive (no need for space qualified source) Less stringent weight, space, time and power requirement. Controlled environment.	Less reliable if used alone. Difficult to reproduce all space operating conditions. No capability to track instrument ageing.
In-flight calibration with internal calibration targets (blackbodies and lamps)	Ability to characterise and monitor the evolution of the individual response of the pixels of each array. Calibration can be optimised for target. Always available. No need to re-point the telescope. Accuracy of calibration over the entire FOV.	Complicates system design Requires calibration sources that generate heat in the system (risk of stray light contamination). Consumes power. Calibration does not include telescope fore optics.
In-flight calibration with astronomical references	Include fore optics. Simpler system design. Less expensive (no need for space qualified source) Weight, space, and power economy.	Satellite of telescope movement needed to point at calibration body. Availability of sources (2) within the pointing range of telescope may depend on spacecraft position. Only a few pixels at a time can be calibrated because the astronomical references do not cover the 3.3' X 3.3' FOV. Non-uniform calibration over all pixels, i.e. difficulties to find calibration source with uniform brightness. Cross-referencing with other observatories is required.

9.3 CONCLUSIONS

A combination of the three calibration strategies will likely be used for NGST. Each method has its own unique advantages and they fill out different tasks and purposes.

Pre-launch characterisation and calibration is always performed for testing purposes and to evaluate the sensor performance. It is performed in a controlled environment and is useful to evaluate the sensor parameters that affect the calibration, such as the non-linearity of the detectors, and that are more difficult to evaluate after launch.

On board calibration with tuneable blackbodies and lamps allows to monitor the evolution of the sensor response. The frequency of the calibration can be set according to the radiometric stability requirements, every two weeks for the gain and every couple hours for the offset. The internal calibration targets are always available without having to point the telescope and they can cover the whole field of view uniformly. Proper cooling and shielding should eliminate the risks of target signal contamination.

Calibration using celestial references can be used to verify the validity of calibration parameters obtained with the internal calibration targets. It is also useful to track the evolution of the onboard calibration targets and the fore optics. It is envisaged to perform such a measurement using on astronomical reference on a few pixels only. Using the on-board data, a fore optic (telescope) degradation variation can be inferred and applied to the whole array. Plus note that a body with known controlled emission will be needed for the interferometer second input port. These bodies tend to be blackbodies in the IR and light traps in the visible.

10.SUMMARY

In this section we present the baseline found for the NGST IFTS. We must remind the reader that this work is first and foremost motivated by the desire to derive an IFTS baseline for the purpose of *cost and schedule estimates*. These trades are only indicative of the type of studies the designers will conduct during the development of this sophisticated spectrometer module. In fact, when a doubt existed, the choice was motivated by spectrometric performance in the first place, before cost, practicality or maturity of the technology. This may have led to a technical baseline that is more complex and ambitious than usually encountered.

The resulting baseline is illustrated schematically in Figure 13.

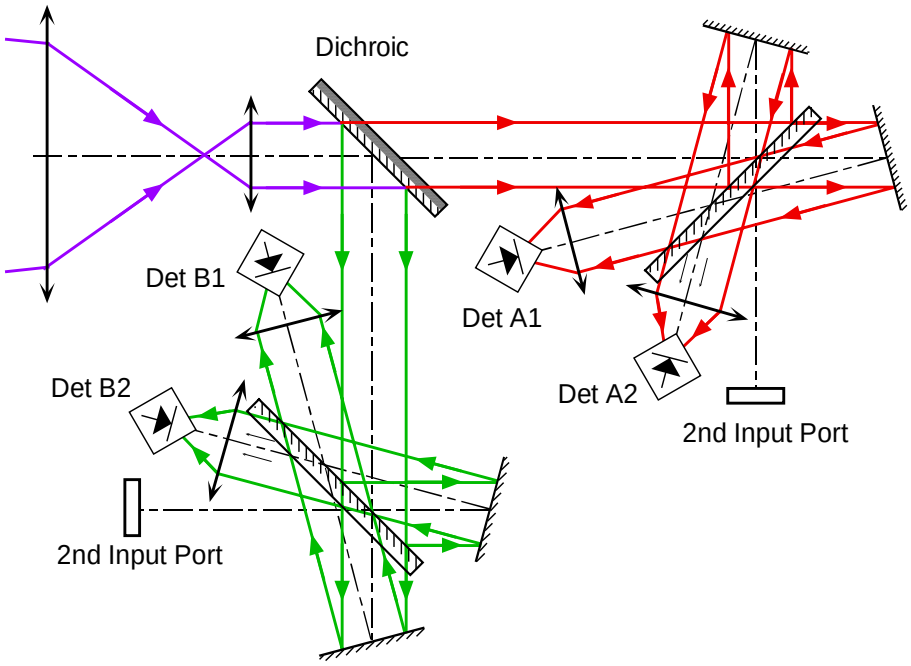

Figure 13: Baseline NGST IFTS

This instrument has the following characteristics.

- Flat mirror system (higher efficiency)
- Four port design (higher efficiency)
- Temporally separated metrology with dynamic alignment and possible hybrid system (no contamination, no obscuration)
- NIR or VIS laser diode.
- Dichroic at the input with multiple interferometers (optimised performance over broad spectrum, higher efficiency than a single interferometer).
- The system performs the sweep using the step scan approach

11.ANNEX

11.1 ANNEX A: ESTIMATION OF AMOUNT OF STRAY LIGHT FROM THE METROLOGY

We here only consider the stray light that is due to multi-reflections in the beamsplitter. Scattering by particles in the optical path, scattering on reflective optical surfaces, scattering within optical components and diffraction effects are not considered. Figure 14 is schematics of the multi-reflections in a beamsplitter. The calculations are based on the figure. Only the beams that exit the beamsplitter toward the primary output port (i.e. at the bottom of the figure) are considered. These beams are given a number that corresponds to the order of scattering. Order 0 is the main beam. Positive number are for "ghost" beams that are reflected only once by the interferometer mirror (exiting at the left of the main beam on the figure) and negative numbers for "ghost" beam that have been reflected twice by a mirror (exiting at the right of the main beam on the figure).

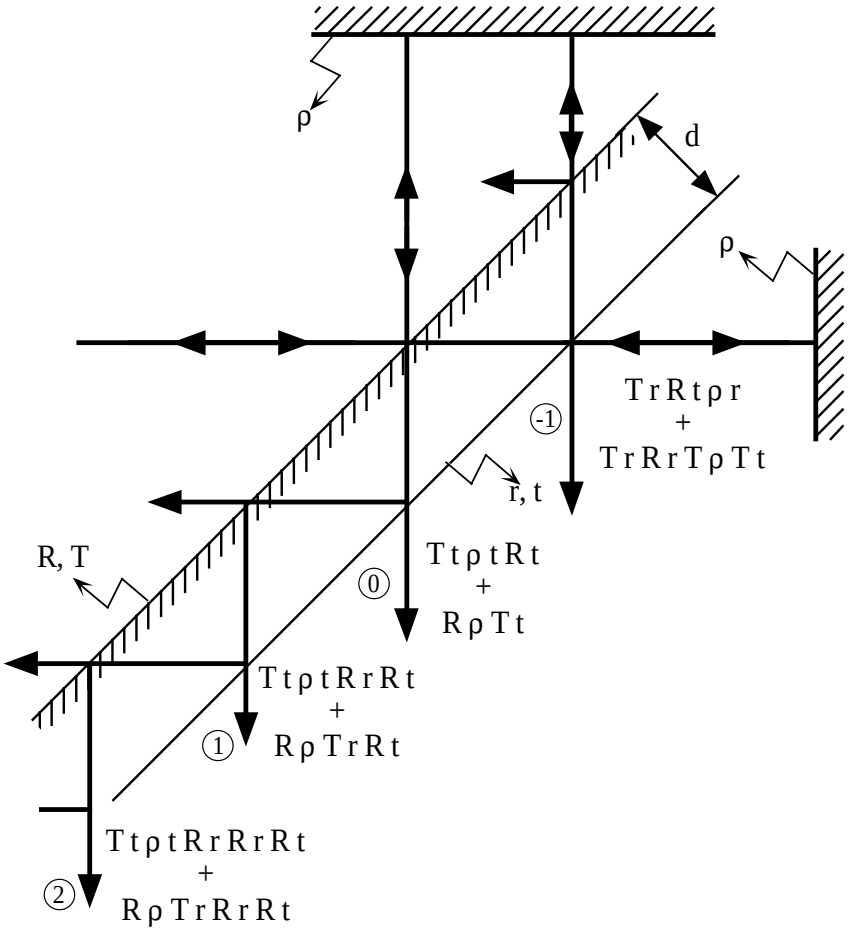

Figure 14: Schematics of the multi-scattering in the beam-splitter

For an incidence angle of 45º, the reflectance and transmittance at the first surface of the beamsplitter are, respectively, *R* and *T*. At the second interface they are, *r* and *t*. The reflectance of

both mirrors at an incidence angle of 0º, is ρ. The fraction of radiation exiting the beamsplitter toward the output port after N reflections in the beamsplitter is:

$$R\,T\,t\,\rho\,(\mathrm{r}\,R)^{N}\,(t+1) \qquad \text{for } N>0$$

$$T\,r^{2}\,R\,(r\,R)^{-(N+1)}\,\rho\,t\,(1+T) \quad \text{for } N<0$$

and the Nth reflection exits the beamsplitter at a distance $\sqrt{2}\,|N|$ d from the centre of the beamsplitter (assuming the incoming beam hits the beamsplitter in the centre), where d is the thickness of the beamsplitter.

Let's suppose a circular beamsplitter with a diameter of 10 cm and central metrology mirror of 3 cm, corresponding to an obscuration of about 10%. The metrology mirror will only "catch" the light that exits within a radius of 1.5 cm from the centre of the beamsplitter. For a particularly thin beamsplitter of 5 mm of thickness, only the light from the first two multi-reflections (N=-2,-1,1 and 2) will be blocked by the metrology mirror, the other "metrology ghosts" will reach the detector.

Assuming that we have a very good beamsplitter and the following values for the reflectances and transmittances:

$R = 0.5$

$T = 0.5$

$r = 0.01$

$t = 0.99$

$\rho = 0.98$

the total fraction of the incoming metrology signal reaching the detector because of multi-reflections in the beamsplitter is:

$$R\,T\,t\,\rho\,(t+1)\sum_{N=3}^{14}\left[(r\,R)^{N}\right]+T\,r^{2}\,R\,\rho\,t\,(1+T)\sum_{N=-3}^{-14}(r\,R)^{-(N+1)}$$

or about 6×10^{-8}. For a laser with a wavelength of 850 nm and a power of 1 mW, this fraction represents about 3×10^{8} photons/s. To compute this value a nearly-perfect beamsplitter was used and several other causes of scattering (surface scattering, volume scattering, scattering by particles in the optical path, etc.) have been neglected. For these reasons, the value obtained should be regarded as a minimal value.

— End of document —

BOMEM

NGST

Next Generation Space Telescope

Final Report

Volume 4 - Performance Analyses

Document Number: **SP-BOM-008/99**

Issue: **1** **Revision:** A

Issue Date: **13 October 1999** **Document Name:** Annex B4.doc

	Function	Name	Signature	Date
Prepared by	Scientist	Louis Moreau		
Prepared by	Scientist	Pierre Tremblay		
Approved by	Project Manager	André Villemaire		
Approved by	Director, SPR division	Jean Giroux		

BOMEM Inc. • a unit of Elsag Bailey Process Automation N.V.

450 Saint-Jean-Baptiste Avenue • Québec, Québec G2E 5S5 Canada • Phone (418) 877–2944 • Fax (418) 877–2834

TABLE OF CONTENTS

LIST OF FIGURES

LIST OF TABLES

DOCUMENT CHANGE RECORD

Issue	Rev.	Date	Chapter/Paragraph Number, Change Description (and Reasons)
1(draft)	-	15 February 1999	Draft of document
1	-	16 March 1999	First release of document
1	A	13 October 1999	New revision to remove proprietary notices.

1. INTRODUCTION

1.1 BACKGROUND INFORMATION

The Next Generation of Space Telescope (NGST) project of NASA is intended to provide continuity and new focus for research following the success of the Hubble Space Telescope. It is considered to be a technologically challenging project as the technology needed is not necessarily available. It challenges the innovation of the scientific and technological community to come up with an affordable technology to carry out the scientific goals of the mission.

Canada has a strong Space Astronomy community and they have ranked the participation of this project as the priority in their LTSP III submission. In order for Canada to participate, the areas of technical expertise and competence necessarily has to match the required technologies of the NGST project. The nature and scope of the Canadian contribution to the NGST are neither identified nor defined. The CSA sees the Canadian contribution as one that matches the industrial capability, an area that would result in industrial and economic growth and provide a sound base for competitiveness in the international market.

At the end of 1998, CSA awarded a number of contracts to Canadian firms. Bomem was awarded such a contract to study the potential use of a Fourier Transform Imaging Spectrometer as a science instrument for NGST.

1.2 SCOPE OF PROJECT

This work was carried out under contract no 9F007-8-3007/001/SR.

Bomem proposed to study the potential use of a Imaging Fourier Transform Spectrometer as a moderate spectral resolution camera for NGST. The approach was to first investigate the trade space of the instrument design. Next the performance of the instrument was predicted to confirm the suitability of the technology for the NGST mission. The risk analysis and mitigation plans were then completed. Finally the Cost and Schedule estimates were drafted based on the previous findings.

1.3 SCOPE OF DOCUMENT

This document is Volume 4 of the final report. The other deliverables of the study contract are listed in Table 1.

Volume 4 covers the *Performance Analyses* performed on the contribution proposed by Bomem, namely an Imaging Fourier Transform Spectrometer (IFTS) module as one of the central science instrument for NGST. The goal of a performance analyses is to evaluate the performance of the proposed IFTS against the science objectives of NGST. The document examines several performance-related issues. In Section 2 we estimate the basic sensitivity of the NGST IFTS. Photon noise and sampling position noise is studied. The sampling position noise is a type of noise not usually encountered in standard Fourier Transform Spectrometer (FTS) and is due to the very slow operation of the NGST IFTS. Section 3 covers the spectral characteristics such as spectral resolution and lineshape characteristics. In Section 4, the sensitivity of Fourier Transform Spectrometers is compared to competing spectrometer technologies such as dispersive systems and filter systems. This is of great

interest in the debate aiming to elect the best spectrometer for NGST. Finally Section 5 addresses some FTS-specific modes of operation, in order to optimise the IFTS sensitivity.

Table 1: Deliverables of the study contract

Volume	Document Number	Document	Description
1	SP-BOM-005/99	Executive Summary	5-page summary of the findings of the contract
2	SP-BOM-006/99	Planning Report	Report on the scheduling and cost of the proposed Canadian participation. The planning report also includes the risk assessment and mitigation plan
3	SP-BOM-007/99	Trade Analyses	Report on the trade analyses performed to arrive at a credible baseline for the proposed Canadian participation.
4	SP-BOM-008/99	Performance Analyses	Report on the sensitivity analyses performed to evaluate the suitability of the proposed Canadian participation for NGST
5	SP-BOM-009/99	Technology Report	Report on some proposed novel technology approaches to the specific NGST environment for the proposed Canadian participation.

1.4 REFERENCE DOCUMENTS

RD 1 Bomem Proposal No:SPIR180898, issue 1, revision -, dated 8 September 1998, in response to solicitation No 9F007-8-3007/A.

RD 2 Volume 4 - Performance Analyses NGST performance studies, SP-BOM-008/99

OPP89 A. V. Oppenheim and R. W. Schafer, “Discrete-time signal processing”, Prentice-Hall International, London, 1989, p. 530.

PAP91 A. Papoulis, “Probability, Random Variables and Stochastic Processes”, 3rd edition, McGraw-Hill, New York, 1991.

PRI97 A. T. Pritt, Jr., P. N. Kupferman, S. J. Young, R. A. Keller, “Imaging LWIR spectrometers for remote sensing applications”, SPIE Proceedings 3063, 1997.

1.5 DEFINITIONS

Étendue — The product of the limiting collection area and the solid angle of the limiting field of view. Often called throughput.

Irradiance — Incident radiant energy per unit surface per unit time. Spectral Irradiance is the irradiance at a given wavenumber (or wavelength or frequency) per unit wavenumber (or unit wavelength or unit frequency). Usual symbol is *E*.

Jansky — Units of spectral irradiance. Symbol is Jy (1 Jy = 10^{-26} W m^{-2} s).

Radiance — Radiant energy per unit surface per unit solid angle per unit time. Spectral radiance is the radiance at a given wavenumber (or wavelength or frequency)

per unit wavenumber (or unit wavelength or unit frequency). Usual symbol is *L*.

Wavenumber — The inverse of the wavelength. Usual symbol is σ (σ=1 /λ).

1.6 ACRONYMS

AC	Alternating Current
CCD	Charge-Coupled Device
CSA	Canadian Space Agency
DC	Direct Current
DF	Dispersive Filter
DFT	Discrete Fourier Transform
DN	Detector Noise
DSI	Double-Sided Interferogram
FFT	Fast-Fourier Transform
FOV	Field Of View
FOV	Field Of View
FPA	Focal Plane Array
FPA	Focal Plane Array
FSR	Free Spectral Range
FTS	Fourier Transform Spectrometer
FTS	Fourier-Transform Spectrometer
FWHM	Full-Width at Half Maximum
IFIRS	Integral Field Infrared Spectrograph
IFS	Integral Field Spectrograph
IFTS	Imaging Fourier Transform Spectrometer
IR	Infrared
MIR	Middle Infrared
MOS	Multi-Object Spectrograph
MPD	Maximum path difference
NEP	Noise Equivalent Power
NESI	Noise Equivalent Spectral Irradiance
NESR	Noise Equivalent Spectral Radiance
NGST	New Generation Space Telescope
NGST	Next Generation Space Telescope
NIR	Near Infrared
OPD	Optical path difference
PN	Photon Noise
RMS	Root-Mean Squared

RN	Read-Out Noise
SNR	Signal to Noise Ratio
SNR	Signal to Noise Ratio
SSI	Single-Sided Interferogram
TF	Tuneable Filter
VIS	Visible
ZPD	Zero Path Difference

2. IFTS SENSITIVITY

It this section, we perform a sensitivity calculation for the NGST IFTS. The goal is to confirm that the IFTS can indeed meet the scientist requirements.

In our simulations we model two sources of noise: the photon noise and the noise due to errors of position of the moving mirror in the interferometer are evaluated. Other sources of noise such as the detector dark current, the digitisation noise, etc., are not considered because it is expected that the technology used will be such as to make these sources of noise negligible compared to the photon noise.

2.1 PHOTON NOISE

The noise equivalent spectral power due to photon noise is:

$$NEP_\gamma(\sigma) = \frac{I_N \, h \sigma \, c}{\eta(\sigma) \, q} \tag{1}$$

where

h: Planck's constant (6.63×10^{-34} J s)

c: speed of light (3.00×10^{8} m s^{-1})

q: elementary charge (6.19×10^{-19} C)

η: spectral quantum efficiency of the detector

σ: wavenumber (m^{-1})

I_N: Current noise (A s$^{0.5}$)

The current noise is proportional to the square root of the total detector current. For a photovoltaic detector, the current noise is:

$$I_N = \sqrt{2 \, q \, I} \tag{2}$$

where, I is the total detector current (per pixel):

$$I = \int_0^\infty q \, \eta(\sigma) \, \Phi_\gamma(\sigma) \, d\sigma \tag{3}$$

where $\Phi_\gamma(\sigma)$ is the total spectral photon flux reaching a pixel of the detector:

$$\Phi_\gamma(\sigma) = \frac{\Phi(\sigma) + \Phi_z(\sigma) + \Phi_d(\sigma)}{h \, c \, \sigma} \tag{4}$$

where $\Phi(\sigma)$ is the spectral energy flux from the target reaching a pixel of the detector. $\Phi_z(\sigma)$ is the spectral zodiacal energy flux reaching a pixel of the detector. $\Phi_d(\sigma)$ is the spectral energy flux emitted by the instrument reaching a pixel of the detector.

$$\Phi(\sigma) = \xi(\sigma)\Theta L(\sigma) \tag{5}$$

$$\Phi_z(\sigma) = \xi(\sigma)\Theta L_z(\sigma) \tag{6}$$

$$\Phi_d(\sigma) = \Theta L_d(\sigma) \tag{7}$$

where $\xi(\sigma)$ is the interferometer efficiency, Θ is the instrument étendue, $L(\sigma)$ is the spectral radiance of the target, $L_z(\sigma)$ is spectral zodiacal radiance (radiation reflected and emitted by interplanetary dust) and $L_d(\sigma)$ is the radiance emitted by the instrument itself. The interferometer efficiency is:

$$\xi(\sigma) = \frac{\xi_{DC}(\sigma)\xi_{AC}(\sigma)}{2} \tag{8}$$

where $\xi_{DC}(\sigma)$ is the spectral transmission efficiency and $\xi_{AC}(\sigma)$ the spectral modulation efficiency. For this instrument, the étendue is the product of the area of the entrance pupil (taken to be equal to the area of the primary telescope) times the solid angle of the field of view of one pixel:

$$\Theta = \pi R^2\ \Omega = \pi\, r^2\ \theta^2 \tag{9}$$

r is the radius of the telescope is and θ is the edge field of view angle for a pixel, assumed to be square.

For this study the spectral radiance of the target, $L(\sigma)$, is the radiance of a blackbody of temperature T with a red shift of z multiplied by a "fill factor" f to reduce the radiance to appropriate level:

$$L(\sigma) = f\ \frac{2hc^2\left[\sigma(z+1)\right]^3}{e^{\frac{hc\sigma(z+1)}{kT}} - 1} \tag{10}$$

where k is Boltzman constant (1.38×10^{-23} J K^{-1}).

The radiance of the zodiacal light is:

$$L_z(\sigma) = \tau_s \frac{2hc^2\sigma^3}{e^{\frac{hc\sigma}{kT_\odot}} - 1} + \tau_{th} \frac{2hc^2\sigma^3}{e^{\frac{hc\sigma}{kT_{th}}} - 1} \tag{11}$$

with:

$$\tau_{th} = 5.61\times10^{-8}\, d^{-0.8} \quad \text{(unitless)} \tag{12}$$

$$T_{th} = 266\, d^{-0.36} \quad (\text{in K}) \tag{13}$$

$$\tau_s = \frac{\tau_{th}\,\alpha}{1-\alpha}\left(\frac{T_{th}}{T_\odot}\right)^4 \tag{14}$$

where d is the distance between NGST and the sun in astronomical units, α is the albedo of the dust particles and $T_\odot$ is the Sun temperature in Kelvin.

The radiance emitted by the instrument is the radiance emitted by a black body at the instrument's temperature with an emissivity equal to its overall absorptance:

$$L_d(\sigma) = (1-\xi_{DC}) \frac{2hc^2\sigma^3}{e^{\frac{hc\sigma}{kT_d}} - 1} \tag{15}$$

where T_d is the temperature of the instrument.

To covert the spectral NEP into NESR, the étendue of the instrument, Θ, its efficiency, $\varepsilon(\sigma)$, the integration time, t, and the spectral interval, $\Delta\sigma$, must be considered:

$$NESR_\gamma(\sigma) = \frac{NEP_\gamma(\sigma)}{\sqrt{n}\,\Delta\sigma\,\Theta\,\xi(\sigma)\,F\,\sqrt{t}} \tag{16}$$

where F is the apodization factor. F=1 for unapodized spectra. n is equal to 1 for a single-port instruments, and to 2 for a dual port instruments. The spectral resolution is the difference between the maximum and the minimum wavenumber for the band studied divided by the "resolution factor", R:

$$\Delta\sigma = \frac{1}{2MPD} = \frac{\sigma_{\max} - \sigma_{\min}}{R} \tag{17}$$

R corresponds to number of bands sampled. It is an integer number between $\sigma_{\max}$–$\sigma_{\min}$ (corresponding to the finest spectral interval considered, 1 cm^{-1}) and 1 (corresponding to a single broad spectral band). MPD is the maximum optical path difference between the two arms of the interferometer.

2.2 POSITION ERROR

The mirror in the moving arm of the interferometer can be positioned with a finite precision. Position errors cause errors in the sampling of the interferogram and these sampling errors cause artifacts and noise in the acquired spectra. Evaluating this noise will give an idea of the required position accuracy.

The noise due to the position errors cannot easily be evaluated analytically. We have to use a Monte-Carlo simulation. The computation can be described by the following steps:

1) Compute the theoretical total spectral radiance incoming on the detector:

$$L_T(\sigma) = \xi(\sigma)L(\sigma) + \xi(\sigma)L_z(\sigma) + L_d(\sigma) \tag{18}$$

2) Compute the theoretical interferogram as being the real part of the Fourier transform of the incoming radiance:

$$I(x) = \Re\{F\{L_T(\sigma)\}\} \tag{19}$$

3) The theoretical interferogram is interpolated by a Fourier transform process to increase its resolution by a factor 8.

4) A new perturbed interferogram is created by sampling the interpolated interferogram at the selected resolution plus a random position error. The sampling positions are:

$$x = N\,\Delta x + \delta x(s_x)\,\Delta x \tag{20}$$

where N is the sampling position number, Δx is the sampling interval and $\delta x(s_x)$ is a random number from a Gaussian distribution of standard deviation s_x. s_x is the relative position error. A new random number is generated for every sampling position.

5) The perturbed interferogram is Fourier transform to generate a perturbed spectrum.

6) Steps 4 and 5 are repeated a sufficient number of time to generate a good statistics. For this study, the process was repeated 50 times.

7) The standard deviation of all the perturbed spectra generated is computed at every wavenumber. The NESR due to the position error, $NESR_\delta$, is that spectral standard deviation.

2.3 TOTAL NOISE

Neglecting the other sources of noise, the total NESR is simply the root sum squared of the NESR due to the photon noise and the NESR due to the position error:

$$NESR(\sigma) = \sqrt{NESR_\gamma^2(\sigma) + NESR_\delta^2(\sigma)} \tag{21}$$

The signal to noise ratio (SNR) is the radiance of the target divided by the total NESR:

$$SNR(\sigma) = \frac{L(\sigma)}{NESR(\sigma)} \tag{22}$$

2.4 RESULTS

Some results are presented to establish a base performance and to illustrate the effect of the various parameters of interest. The following parameters define the base case and have been keep constant for all tests, unless otherwise mentioned:

Radius of primary telescope:	r = 4 m
FOV of one pixel:	θ = 0.05"
Acquisition time:	$t = 2\times10^6$ s
Resolution factor:	R = 100
Transmission efficiency:	ξ_{DC} = 0.84
Modulation efficiency:	ξ_{AC} = 0.70
N. of output port::	n = 1
Apodization factor:	F = 1
Temperature of instrument:	T_d = 30 K

Minimum wavenumber: σ_{min} = 2000 cm^{-1} (corresponding to 5 μm)

Maximum wavenumber: σ_{min} = 10000 cm^{-1} (corresponding to 1 μm)

Quantum efficiency: η = 0.95 from σ_{min} to σ_{max} , 0 elsewhere

Orbital distance: d = 1 A.U.

Albedo of interplanetary dust: α = 0.102

Sun temperature: $T_{\odot}$ = 5770 K

Temperature of the target: T = 5800 K

Red shift of the target: z = 5

Fill factor: $f = 3.7\times10^{-14}$

Relative sampling position error (rms): s_x = 1%

2.4.1 Photon Noise Only

For this step the position error is set to zero. The only noise present is the photon noise.

The target is a blackbody with a temperature T of 5800 K and a red shift z of 5. The "fill factor" f is set to 3.7×10^{-14} on order to have an irradiance of about 5 nJ at a wavelength of 3 μm. Figure 1 shows the spectral irradiance of the target in nJy. Figure 2 shows the spectral photon flux at the detector. Compared to the zodiacal light, the flux emitted by the instrument is negligible for an internal temperature of 30K. The background photon noise is dominated by the zodiacal light.

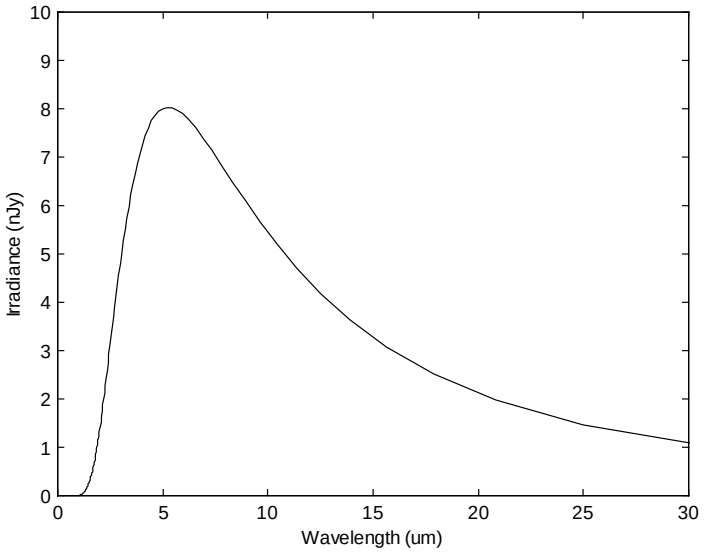

Figure 1 Target spectral irradiance

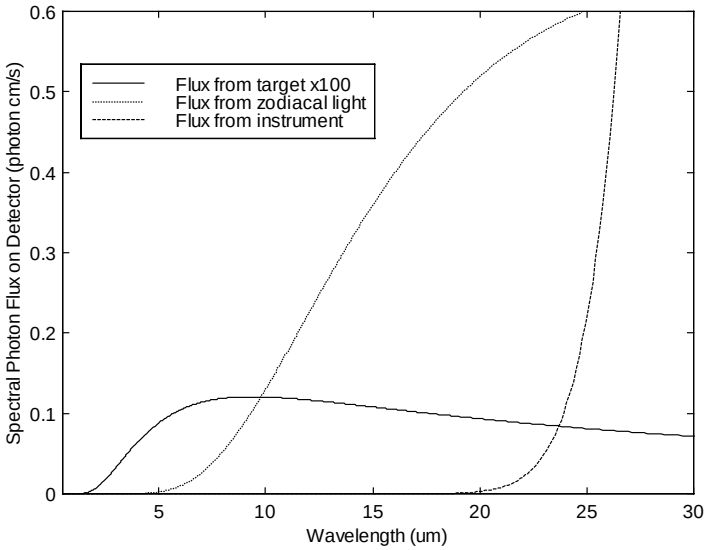

Figure 2 Spectral photon flux on detector

For the first case, the SNR has been computed in the band extending from 1 μm to 5 μm for a resolution factor, *R*, of 100. Figure 3 shows the NESR and the NESI for that case study. Figure 4 shows the SNR as a function of the wavelength. When there is no other noise than the photon noise, Equations 16, 17 and 22 show that the SNR is directly proportional to R^{-1} and directly proportional to $t^{-½}$. There is no need to recalculate different cases to determine the effect of *R* and *t*. For instance at full spectral resolution (R=8000) and every other parameters being constant, the SNR will be 80 time smaller than the SNR plotted on Figure 4. At the broadest spectral resolution (*R*=1), the SNR will be higher by a factor 100 than the SNR of Figure 4.

Similarly, if the flux from emitted by the instrument is negligible, the SNR will be directly proportional to $\sqrt{\xi}$ and to $\sqrt{\Theta}$. Increasing the spectrometer efficiency or the étendue of the instrument increases the SNR. For the current case study, the efficiency is $\xi = 0.3$. Increasing the efficiency to a perfect value ($\xi = 0.5$) will increase the SNR by factor 1.3 compared to the SNR of Figure 4.

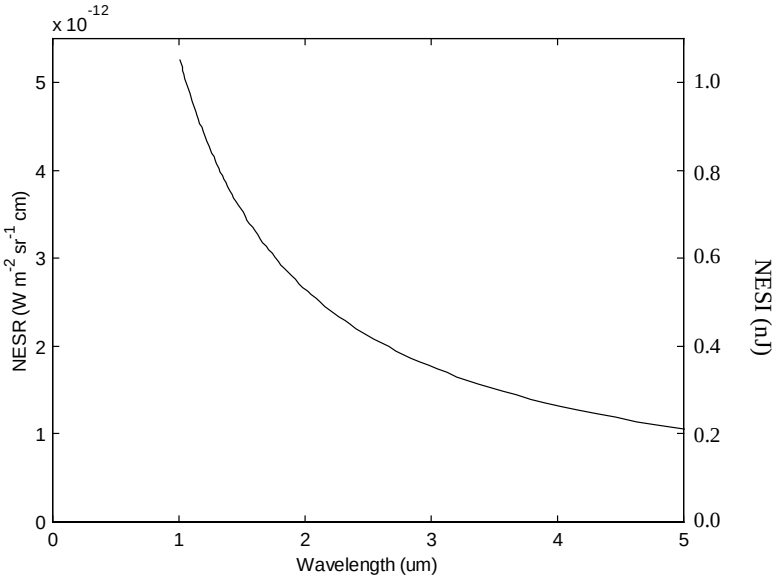

Figure 3 Noise Equivalent Spectral Radiance (NESR) and noise equivalent Spectral Irradiance (NESI) for case 1

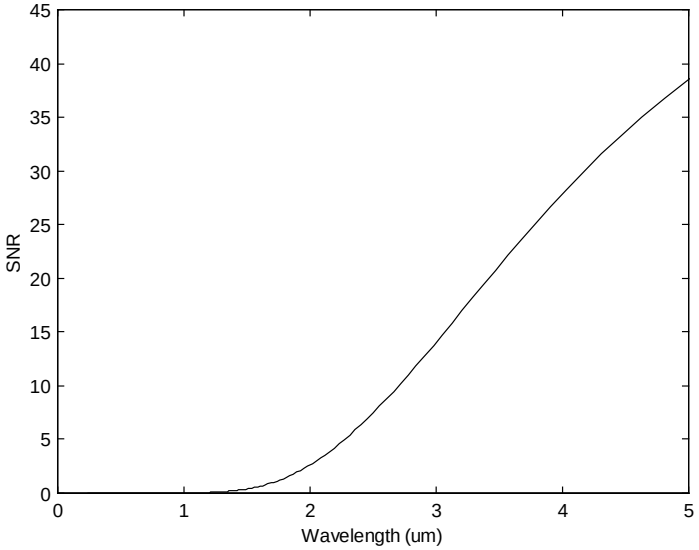

Figure 4 Signal to noise ratio for case 1

The SNR also depends on the incoming radiance, L (i.e. the signal). Because the photon noise is proportional to the square root of the photon flux incoming on the detector, the SNR would be proportional to $\sqrt{L}$ if the background radiation was negligible. In our case, the zodiacal light is important compared to the signal and the dependency of the SNR on L is slightly more complex. Figure 5 compares the SNR of the base case (i.e. Figure 4) compared to the signal for 2*f* and for 0.5*f*.

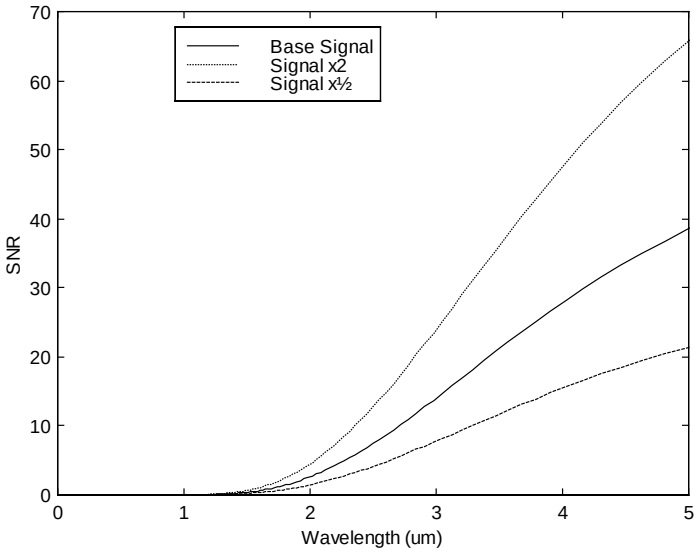

Figure 5 SNR for various signal level

2.4.2 Position Error Noise Only

In this section we describe the effect of errors the position of the sampled interferogram points. Interferograms sampled at the wrong positions appear to have amplitude error which translate into system noise. The process of simulating the sampling position errors is illustrated in Figure 6. The same input parameters listed in Section 2.4.1 were used to compute the total signal.

Figure 7 shows 3 curves of NESR caused by sampling position errors only (i.e. no photon noise) for three different relative rms position errors. $NESR_\delta$ is directly proportional to s_x. Since the signal is not affected by sampling errors, the SNR is thus directly proportional to s_x^{-1}. Because, the noise is computed for relative errors, the calculations are independent of the selected spectral interval. If the absolute error is constant, the SNR will be proportional to R^{-1}.

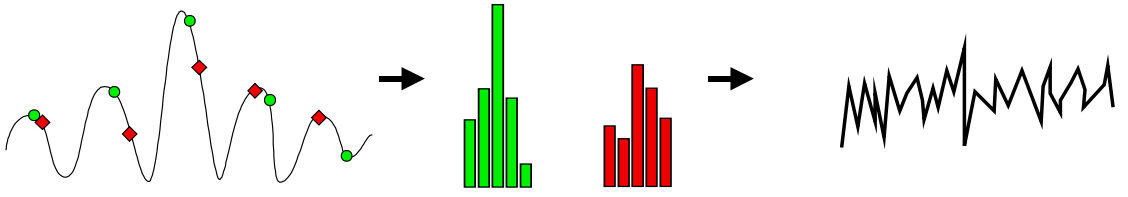

Figure 6 Illustration of the sampling position errors

The fine spectral shape of the NESR curves of Figure 7 depends in part on the random nature of the Monte-Carlo simulations and in part on the shape of the interferogram and, thus, on the spectral

shape of the incoming radiance. However, overall, the shape is spectrally flat and the noise caused by the sampling position error can be considered to be white.

The noise caused by the sampling position error is proportional to the amplitude of the interferogram, so it is proportional to the amplitude of the total incoming radiance. Because the background light is not negligible for small incoming flux, $NESR_\delta$ is only approximately proportional to the signal level. To illustrate this, Figure 8 shows three curves of $NESR_\delta$ for three different signal level. So, if the position error noise is dominant, the SNR is independent of the total signal level.

The noise caused by the sampling position error is proportional to the amplitude of the interferogram. The amplitude of the interferogram is proportional to the total energy reaching the detector, so it is proportional to the system efficiency, ξ, and étendue, Θ. So the noise in term of photon flux is proportional to ξ and Θ. However the gain is inversely proportional to ξ and Θ so that the calibrated noise ($NESR_\delta$) is independent of the efficiency and étendue.

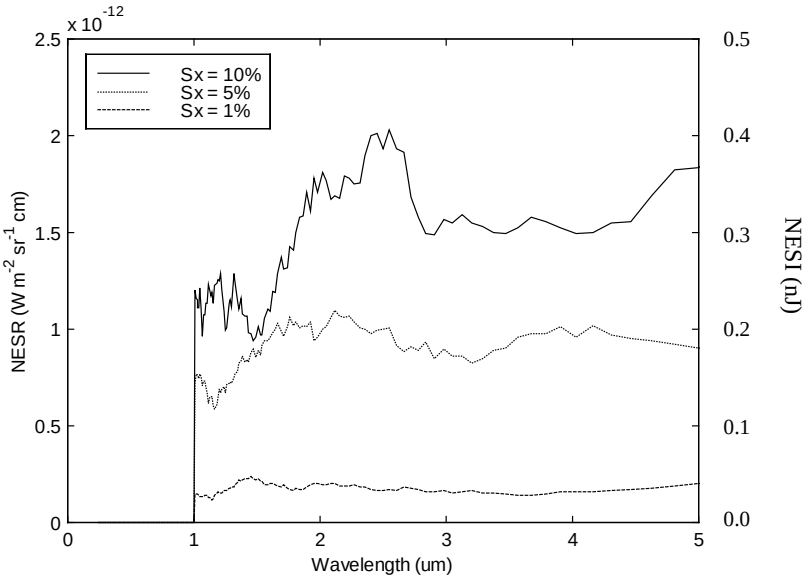

Figure 7 NESR due to the position error for various relative errors of sampling position

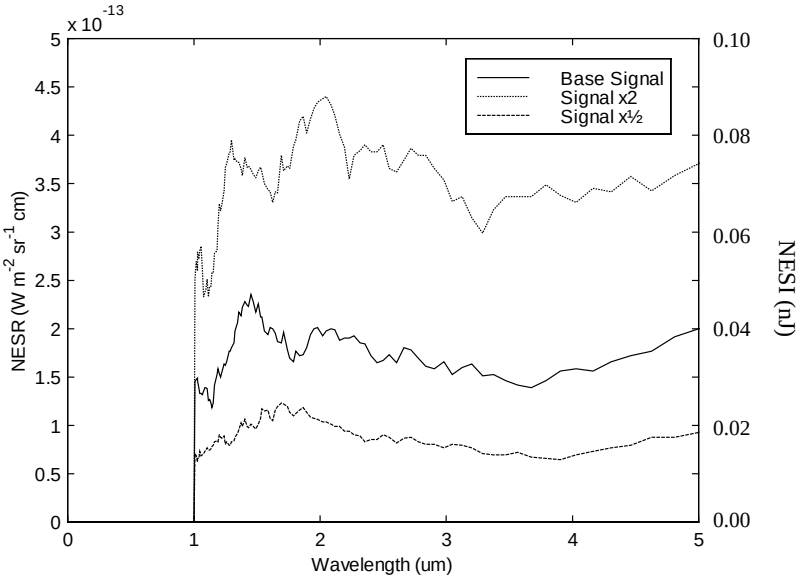

Figure 8 NESR due to the position error for various signal levels and a position error of 1% (rms)

2.4.3 Summary

For the photon noise, analysis of the equations of Section 2.1 and the results shown in Section 2.4.1, lead to the following conclusions:

$$NESR_\gamma \propto \sqrt{\int L\, d\sigma}$$
$$NESR_\gamma \propto R$$
$$NESR_\gamma \propto \frac{1}{\sqrt{t}}$$
$$NESR_\gamma \propto \frac{1}{\sqrt{\xi}}$$
$$NESR_\gamma \propto \frac{1}{\sqrt{\Theta}}$$
$$NESR_\gamma \propto \sigma$$

For the position error noise, analysis of the equations of sections 2.1 and 2.2 and the results shown in Section 2.4.2, lead to the following conclusions:

$$NESR_\delta \propto L$$
$$NESR_\delta \propto s_x$$
$$NESR_\delta \propto R$$
$$NESR_\delta \text{ is spectrally flat}$$
$$NESR_\delta \text{ is independent of } t,\ \xi \text{ and } \Theta$$

Comparison of Figure 3 and Figure 7 indicates that for an irradiance of about 5nJy at a wavelength of 3 μm and a sampling position accuracy of 1%, the photon noise is more than 10 times larger than the position error noise. A position accuracy of 1% is readily achievable with a modern servo-control, so it should not be difficult to achieve a SNR of more than 10 for signals of about 5 nJy with the current design. Having a high efficiency and a high étendue would also rise the SNR for small incoming fluxes.

Because $NESR_\delta$ is proportional to the signal and $NESR_\gamma$ is proportional to the square root of the signal, $NESR_\delta$ increases more rapidly with the signal than $NESR_\gamma$. So, even if $NESR_\gamma$ is much larger than $NESR_\delta$ for small signals, at some point, for larger signals, $NESR_\delta$ will be higher than $NESR_\gamma$. Of course, at this point the SNR may large enough to satisfy most practical applications. Figure 9 shows both $NESR_\delta$ and $NESR_\gamma$ as a function of the signal level. $NESR_\gamma$ exceeds $NESR_\delta$ when the signal is about fifty times the base case signal. Figure 10 shows the corresponding SNR. For figures 8 and 9, all parameters, except *f*, are as stated for the base case of Section 2.4.

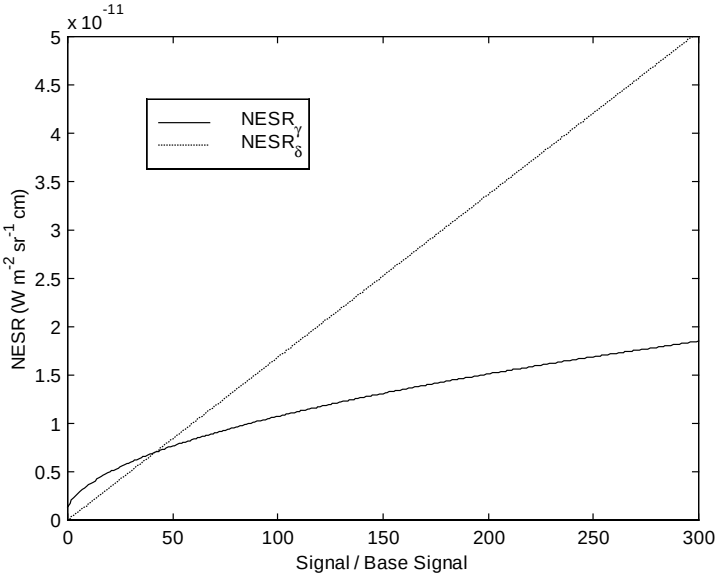

Figure 9 $NESR_\gamma$ and $NESR_\delta$ as a function of the signal level at a wavelength of 3 μm

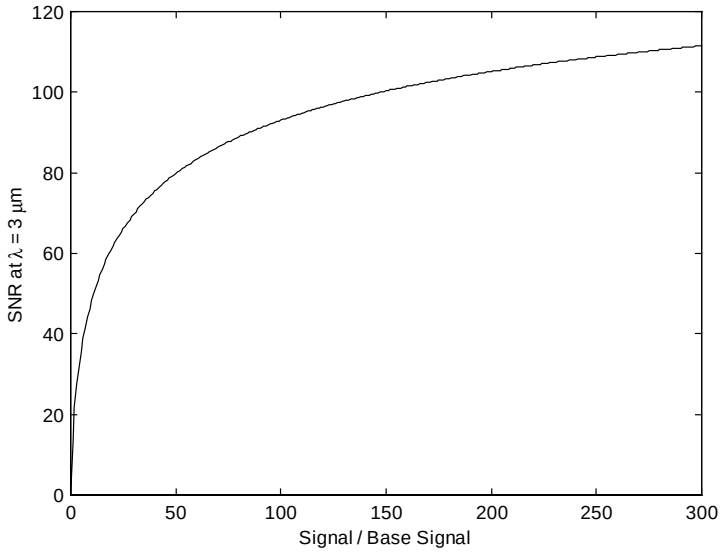

Figure 10 Signal to noise ratio at a wavelength of 3 μm as a function of the signal level

3. IFTS INSTRUMENT LINESHAPE

In this section we describe the instrument lineshape (ILS) simulations made the NGST IFTS. The goal of these activities is both to design the interferometer and to predict the performance.

As a design tool the ILS models are used to determine the maximum angle permissible in the interferometer. For a constant throughput (as set by the NGST telescope), the larger the angles in the interferometer, the smaller the interferometer pupil can be. However there exists a limit beyond which the instrument lineshape degrades and consequently the spectral resolution decreases below the science requirements.

One such example is shown in Figure 11, where the full width at half maximum of the lineshape is plotted against the full angle in the interferometer. If we take the 64x64 example, we can see the lineshape start to degrade for angles larger than 100 mrad. Other cases of larger detectors (256x256 and 1024x1024) show that the same degradation occurs at larger angles, because for the same total angle, there is a smaller angle on each individual pixel.

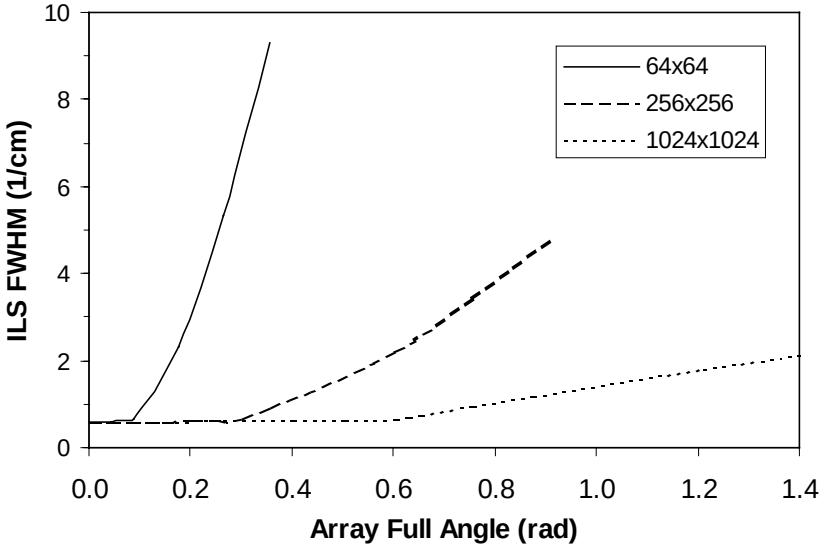

Figure 11 Full-width at half maximum of the instrumental line shape for the corner pixel at 2800 cm^{-1} against the array full angle for a MPD of 1 cm and various detector formats

We used our proprietary ILS model to simulate the lineshape characteristics of the NGST IFTS. We assumed a flat-mirror four-port design. In this configuration the detector layout is as shown in Figure 12. 10% of the detector width is left in between the input and output fields to allow space for a dissector.

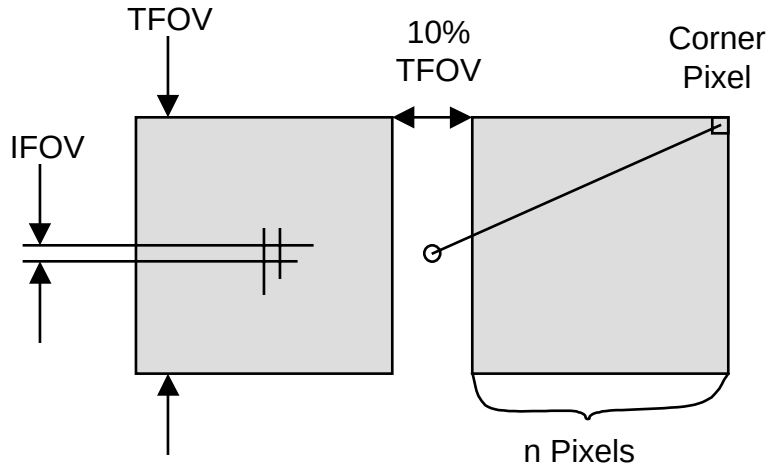

Figure 12 Focal configuration for a flat-mirror four-port interferometer. 10% of the detector width is left in between the input and output fields to allow space for a dissector.

All the simulations we done for the corner pixel which is always worse than any other pixel. The other simulation parameters are listed in Table 2. Several simulations were performed for both the highest wavenumber of both spectral bands, MIR and NIR. The NIR covers the 0.6-5.6 μm range while the MIR covers the 5.6-15 μm range. Various magnification ratio (angle in the interferometer over angle in the scene) were studied with the interferometer aperture varying accordingly.

Table 2: ILS parameters

	MIR	*NIR*
Wavenumber	1786 cm^{-1}	16 666 cm^{-1}
Detector Format	1 k x 1 k	8 k x 8 k
Total Scene Angle	1.7 arcmin	5.3 arcmin
Maximum Path Difference	1 cm	1 cm
Magnification	Various (5-160)	Various (5-160)
Interferometer Pupil	Various (160-5 cm)	Various (160-5 cm)

Figure 13 shows the variation of the linewidth as a function of interferometer aperture diameter. Negligible effects can be seen for aperture sizes as small as 4 cm. Figure 14 show an example of lineshape simulated. Consequently it appears that the angle effects will not be the limiting factor in choosing an interferometer configuration for the NGST IFTS. In fact the interferometer angles corresponding to the interferometer aperture diameter are shown in Figure 15. A reasonable interferometer pupil of 10 cm leads to about 8 degree angles. This is a reasonable choice and it is surprisingly similar to interferometer parameters used for existing of interferometer instruments in development today. This fact tends to reduce the risk.

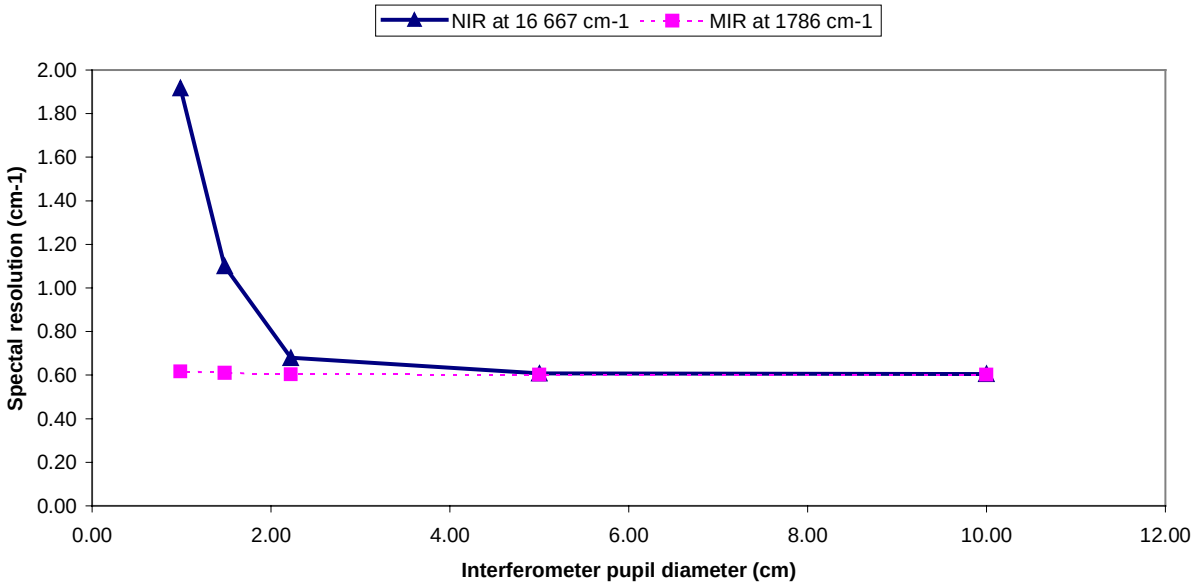

Figure 13 Full-width at half maximum of the instrumental line shape for both the MIR and NIR corner pixels as a function of interferometer aperture

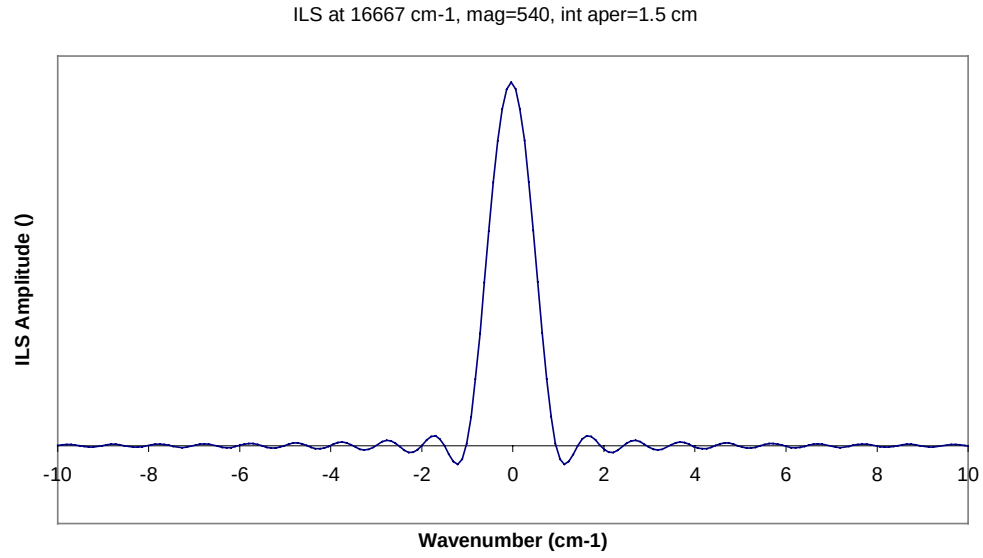

Figure 14 NIR lineshape example of an extreme NGST IFTS configuration, wit a 1.5 cm interferometer pupil.

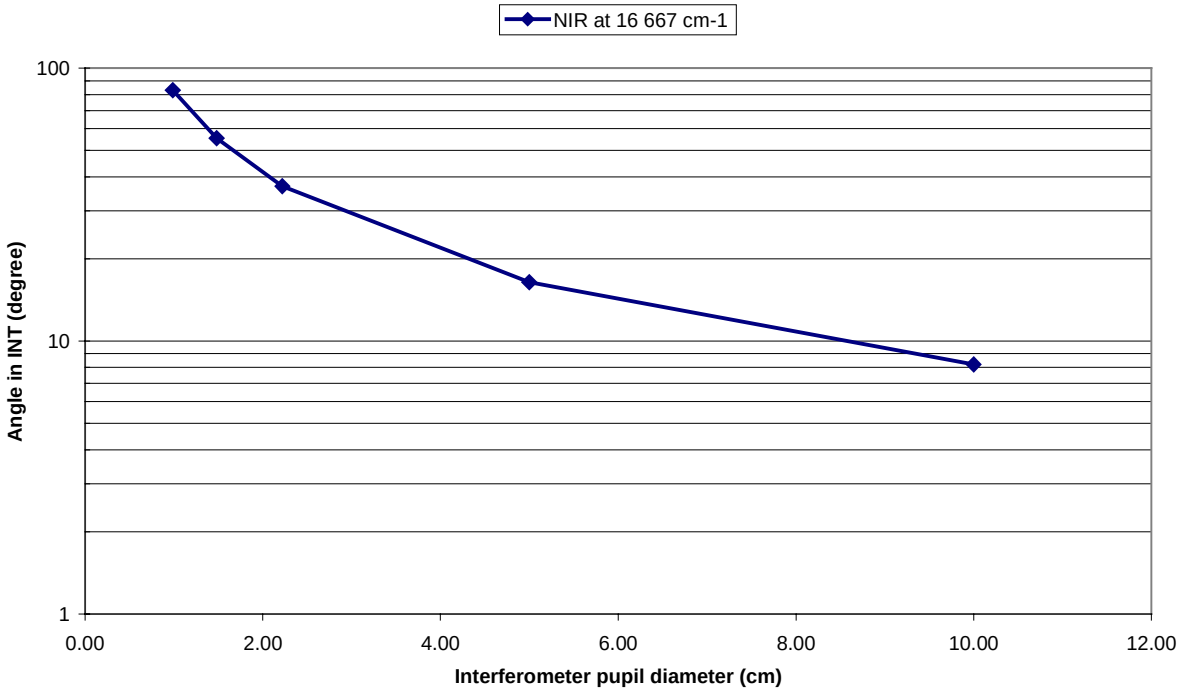

Figure 15 Full-width at half maximum of the instrumental line shape for both the MIR and NIR corner pixels as a function of interferometer aperture

4. IFTS SENSITIVITY COMPARISON

4.1 INTRODUCTION

This section provides a coherent evaluation of the sensitivity of various imaging spectrometers that can be used for NGST. The signal to noise ratio (SNR) is used as the basis of the comparison. The instruments evaluated in this study are spectrometers based on tuneable or dispersive filters, as well as Fourier-transform spectrometers. The performance of the imaging spectrometers is studied for integral field and multi-object spectrographic applications.

The single criterion of the SNR cannot be used alone to favour one option or another. Other aspects such as throughput and resolution must also be considered. Some requirements may moreover form a lock-up specification, forcing the choice to a particular instrument even if it is strongly disadvantaged when one aspect is studied. For example, in this study the spectrometers are compared for a constant throughput and resolution. But for any of these two parameters it can be technically hard or impossible to meet the needed specifications for a given instrument, thus reducing considerably the interest for this option. Pritt *et al.* (PRI97) gives an interesting overview of imaging spectrometers approaches, enumerating many aspects to be considered in order to compare them.

4.2 SENSITIVITY OF IMAGING SPECTROMETERS

In this section we evaluate the signal to noise ratio (SNR) performance of different imaging spectrometer configurations. We consider instruments using tuneable filters (TF), dispersive filters (DF) or Fourier-transform spectrometers (FTS).

Two fundamental applications are studied: Integral Field Spectrographs (IFS) and Multi-Object Spectrographs (MOS). Integral field spectrographs provide contiguous coverage over a two-dimensional (usually square) field of view. On the other hand, a multiple object spectrograph can take advantage of the relatively low density and discreteness of the scene by only looking at a limited number and small parts of the entire (integral) FOV. By placing conveniently, i.e. on a line or a column (using fibres or other mechanisms), the pixels used for imaging, the remaining dimension of the detector array may be used for spectrometry. This makes for a very efficient use of all the available pixels.

4.2.1 Integral Field Spectrographs

This section compares the signal to noise ratio (SNR) of imaging spectrographs in different IFS configurations. This case is more general, i.e. it covers the measurement of the spectral content of all the pixels of an image. These results will be applied to the MOS.

4.2.1.1 Hypotheses

All configurations are compared using the same baseline. It consists in the complete measurement of the spectrum of an image, namely:

- an image consisting in K × L pixels;

- spectrum consisting in N resolved spectral bins of width $\Delta\sigma$ [cm^{-1}] (spectral resolution), extending from the low wavenumber σ_1 [cm^{-1}] to the high wavenumber σ_2 [cm^{-1}], for each pixel, so $N\Delta\sigma = \sigma_2-\sigma_1$;
- $\Phi_S(\sigma)$ is the count rate of the source per unit bandwidth [ph/sec/cm^{-1}];
- $\Phi_B(\sigma)$ is the count rate of the background per unit bandwidth [ph/sec/cm^{-1}], it is expressed in terms of the count rate of the scene $\Phi_B(\sigma) = \gamma\Phi_S(\sigma)$;
- measurement done in the same total duration time T [sec];
- each instrument configuration is assumed to have an efficiency $\eta_{instr}(\sigma)$ [—];
- average value of $\Phi_S(\sigma)$, $\Phi_B(\sigma)$ and $\eta_{instr}(\sigma)$ are used, Φ_S ,Φ_B and η_{instr}; and
- all instruments assumed to have the same throughput, otherwise the signal must be multiplied by the throughput).

Four noise contributions are considered:

1. photon noise from the source (PN);
2. photon noise from the background (BN);
3. detector noise (DN), spectrally white noise often associated with the dark current; and
4. read-out noise (RN).

The read-out noise differs from the detector noise in the sense that it does not depend on the measurement duration (or bandwidth). It is a constant value for each of the read-outs.

4.2.1.2 Tuneable filter

The tuneable filter (TF) instrument uses an optical bandpass filter such as a Fabry-Perot interferometer, or an acousto-optic tuneable filter. It could also be a multiple-filter instrument.

4.2.1.2.1 Characteristics

This configuration enables the measurement of the spectra of all the image pixels by using directly the K × L pixels of the focal plane array (FPA), and measuring alternatively the signal for each spectral bin, while the filter is tuned through each bandwidth to be covered. Common practices in the development of TF instruments make the bin spectral spacing smaller than the resolution, typically by a factor between 0.5 and 0.8. An overlap parameter is used to take into account the increased number of spectral bins needed to cover the full spectral range. Figure 16 shows the transmission curves of a typical TF for different overlap parameters.

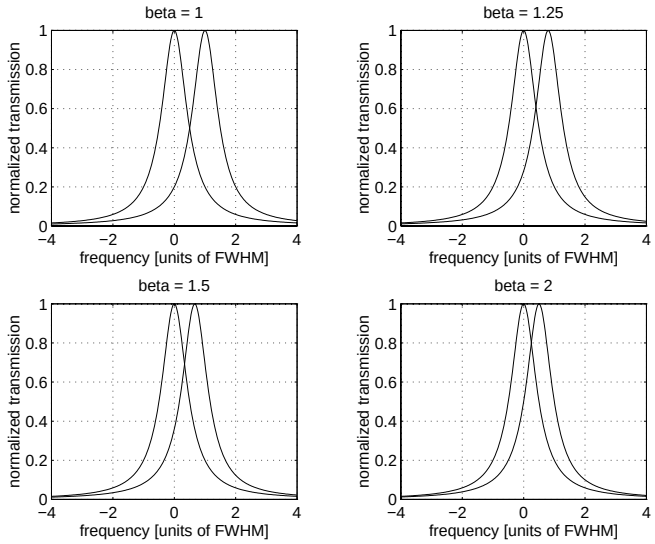

Figure 16 Transmission curves of typical tuneable filter (Fabry-Perot interferometer) for various overlap parameters.

Amongst TF instruments, Fabry-Perot interferometers are characterised by a constant full-width at half maximum (FWHM), so its resolving power varies with the frequency if a wide spectral range is to be covered. Moreover such filters have rather small spectral intervals, the so-called free spectral range (FSR), which limits the achievable spectral range. The FWHM is also proportional to the FSR through the finesse of the interferometer.

4.2.1.2.2 SNR performance

The signal available at each detector Q_{TF} [ph] is proportional to the bandwidth of the filter and to the duration of the measurement,

$$Q_{TF} = \eta_{TF}(\Phi_S + \Phi_B)\frac{\sigma_2 - \sigma_1}{\beta N}\frac{T}{\beta N}, \qquad (23)$$

where η_{TF} is the efficiency of the tuneable filter, Φ_S is the count rate of the scene, Φ_B is the count rate of the background, σ_1 and σ_2 are respectively the lower and the upper frequencies of the bandwidth to be covered, T is the total duration of the measurement (K × L spectra) and β is the overlap parameter.

The photon noise contribution [ph] is (Appendix A)

$$q_{TF_{PN}} = \sqrt{Q_{TF}}\ . \qquad (24)$$

The detector noise contribution [ph] is (Appendix A)

$$q_{TF_{DN}} = \sqrt{\frac{N_0}{2e^2}\frac{T}{\beta N}}, \qquad (25)$$

where N_0 is the level of the current noise power spectral density (single-sided) [A^2/Hz] at the entrance of the preamplifier, due to the detector and preamplifier resistors, and e stands for the elementary charge [C].

The read-out noise contribution [ph] is

$$q_{TF_{RN}} = n_R , \tag{26}$$

where n_R is the RMS value of the read-out noise.

The complete expression for the SNR for the tuneable filter is

$$SNR_{TF} = \frac{\eta_{TF}\Phi_S(\sigma_2 - \sigma_1)T}{\sqrt{\eta_{TF}(\Phi_S + \Phi_B)(\sigma_2 - \sigma_1)T\beta^2 N^2 + \frac{N_0 T}{2e^2}\beta^3 N^3 + n_R^2\beta^4 N^4}} . \tag{27}$$

Since all the pixels of the image are measured simultaneously, the SNR is independent of the size of the image.

4.2.1.3 Dispersive filter

The dispersive filter (TF) instrument is an optical spectrometer using a dispersive element such as a diffraction grating to spread spatially the spectrum.

4.2.1.3.1 Characteristics

This configuration enables the measurement of the spectra of the image by spreading spatially the spectrum of an image column over a K × N pixel FPA, and measuring alternatively the spectra for each column of the image, while the image is scanned across. Common practices in the development of DF instruments make the bin spectral spacing smaller than the resolution, typically by a factor between 0.5 and 0.8. An overlap parameter is used to take into account the increased number of spectral bins needed to cover the full spectral range. Figure 17 shows the transmission curves of a typical DF for different overlap parameters.

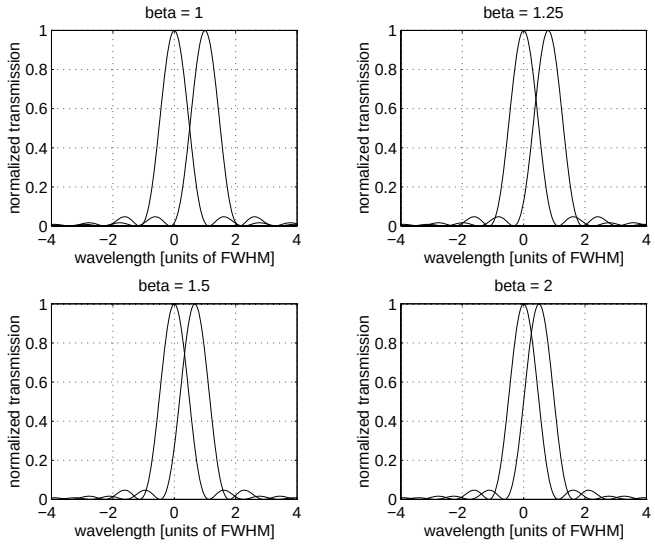

Figure 17 Transmission curves of typical dispersive filter (diffraction grating) for various overlap parameters.

Diffraction gratings are characterised by a constant resolving power in wavelength, so its resolving power varies with the frequency if a wide spectral range is to be covered. Moreover such filters have limited spectral range to octave bandwidth due to higher diffraction orders.

4.2.1.3.2 SNR performance

The signal available at each detector Q_{DF} [ph] is proportional to the bandwidth of the filter and to the duration of the measurement,

$$Q_{DF} = \eta_{DF}(\Phi_S + \Phi_B)\frac{\sigma_2 - \sigma_1}{\beta N}\frac{T}{L}, \tag{28}$$

where η_{DF} is the efficiency of the dispersive filter, Φ_S is the count rate of the scene, Φ_B is the count rate of the background, σ_1 and σ_2 are respectively the lower and the upper frequencies of the bandwidth to be covered, T is the total duration of the measurement (K × L spectra) and β is the overlap parameter.

The photon noise contribution [ph] is (Appendix A)

$$q_{DF_{PN}} = \sqrt{Q_{DF}}\,. \tag{29}$$

The detector noise contribution [ph] is (Appendix A)

$$q_{DF_{DN}} = \sqrt{\frac{N_0}{2e^2}\frac{T}{L}}, \tag{30}$$

where N_0 is the level of the current noise power spectral density (single-sided) [A^2/Hz] at the entrance of the preamplifier, due to the detector and preamplifier resistors, and e stands for the elementary charge [C].

The read-out noise contribution [ph] is

$$q_{DF_{RN}} = n_R, \tag{31}$$

where n_R is the RMS value of the read-out noise.

The complete expression for the SNR for the dispersive filter is

$$SNR_{DF} = \frac{\eta_{DF}\Phi_S(\sigma_2-\sigma_1)T}{\sqrt{\eta_{DF}(\Phi_S+\Phi_B)(\sigma_2-\sigma_1)T\beta NL + \frac{N_0 T}{2e^2}\beta^2 N^2 L + n_R^2\beta^2 N^2 L^2}}. \tag{32}$$

The SNR is strongly dependent of the size of the image.

4.2.1.4 Fourier-transform spectrometer

4.2.1.4.1 Characteristics

In contrast with tuneable and dispersive filters, Fourier-transform spectrometers (FTS) do not measure directly the spectrum. They measure the autocorrelation function of the scene, which is next Fourier-transformed to provide the spectrum. In its simplest form, the Fourier-transform spectrometer instrument is generally a variant of the Michelson interferometer. The autocorrelation function of the scene is measured as the optical path difference in the interferometer is swept. Two approaches are possible. Both sides of the so-called interferogram can be measured to improve the signal processing (double-sided interferogram, DSI), even if only one side (single-sided interferogram, SSI) is strictly needed because the autocorrelation is an even function. So Fourier-transform spectrometers use double-sided interferograms with M points (or single-sided interferograms with M/2 points) in order to achieve the measurement.

This configuration enables the measurement of the spectra of the image by using directly the K × L pixels of the FPA, and measuring alternatively the signal for each optical path difference, while one arm of the interferometer is lengthened / shortened with regard to the other.

4.2.1.4.2 SNR performance

The average signal available at each detector Q_{FTS} [ph] is proportional to the full bandwidth covered by the instrument and to the duration of the measurement,

$$Q_{FTS} = \eta_{FTS}(\Phi_S+\Phi_B)(\sigma_2-\sigma_1)\frac{T}{M\alpha/2}, \tag{33}$$

where η_{FTS} is the efficiency of the spectrometer, Φ_S is the count rate of the scene, Φ_B is the count rate of the background, σ_1 and σ_2 are respectively the lower and the upper frequencies of the bandwidth to be covered, T is the total duration of the measurement (K × L spectra), M is the number

of points of the double-sided interferogram, and α is a parameter which equals 2 for DSI instrument and 1 for SSI instrument.

It is common to understand the FTS as an instrument sending half the signal to the second port, the latter being transmission to a distinct port or reflection back to the scene depending on the particular design. However a close look at the instrument physical principles shows the need to modulate the signal spectrum in order to obtain an interferogram (the interferometer is often called a modulator). The best performance achievable is a 100% modulation, i.e. an interferogram having all the signal at zero path difference (ZPD) and half the signal at maximum OPD (e.g. see Figure 30). Once the Fourier transform is applied to the interferogram, it is seen that half the signal is unmodulated, so it is in the DC component. Meanwhile the other half of the signal is modulated and is located at Fourier frequencies that will be matched to optical frequencies through the sampling frequency and the sweeping velocity. From this modulated part, half of the signal is in the negative frequencies and half is located in the positive frequencies. Therefore the maximum theoretical efficiency of a single port FTS is ½. Dual port devices can be used at the price of doubling the detector hardware.

SSI instruments have twice the integration time per sample for each of their interferogram points, since they have 2 times less points to measure in the same time interval. This results in a factor 2 improvement on the signal side. However other considerations, such as the more difficult calibration procedures, decrease this apparent sensitivity advantage.

To properly sample the interferogram (to satisfy the Nyquist criterion), the number of points of the DSI must exceed two times the ratio of the highest frequency to the spectral resolution,

$$M \geq 2\frac{\sigma_2}{\Delta\sigma} \geq 2\frac{\sigma_2 - \sigma_1}{\Delta\sigma} = 2N\,, \tag{34}$$

which is itself always larger than two times the number of spectral bins. In common practice, some margin is kept between Nyquist rate (half of sampling frequency) and maximum frequency σ_2.

The photon noise contribution [ph] is (Appendix A)

$$q_{FTS_{PN}} = \sqrt{Q_{FTS}}\,. \tag{35}$$

The detector noise contribution [ph] is (Appendix A)

$$q_{FTS_{DN}} = \sqrt{\frac{N_0}{2e^2}\frac{T}{M\alpha/2}}\,, \tag{36}$$

where N_0 is the level of the current noise power spectral density (single-sided) [A^2/Hz] at the entrance of the preamplifier, due to the detector and preamplifier resistors, and e stands for the elementary charge [C].

The read-out noise contribution [ph] is

$$q_{FTS_{RN}} = n_R\,, \tag{37}$$

where n_R is the RMS value of the read-out noise.

The complete expression for the SNR in the interferogram domain is

$$SNR_{FTS_{IGM}} = \frac{\eta_{FTS}(\Phi_S + \Phi_B)(\sigma_2 - \sigma_1)T}{\sqrt{\eta_{FTS}(\Phi_S + \Phi_B)(\sigma_2 - \sigma_1)T\frac{M\alpha}{2} + \frac{N_0}{2e^2}T\frac{M\alpha}{2} + n_R^2\frac{M^2\alpha^2}{4}}}. \quad (38)$$

The SNR in the spectrum and in the interferogram domains are related by the following coefficient (see Appendix B)

$$SNR_{FTS} = \frac{1}{N}\sqrt{\frac{M\alpha/2}{2}}SNR_{FTS_{IGM}}. \quad (39)$$

This last factor takes into account the facts that the total power of the noise samples in the interferogram domain is split in 2 over the negative and positive frequencies and it is also split in 2 over the real and imaginary parts of the spectrum. The latter is a benefit only for double-sided interferograms, since the imaginary part of the spectrum is related directly to the odd part of the noise samples. For SSI, the noise is mirrored, as the signal, so it ends completely in the real part of the spectrum. Moreover the noise power is spread equally over all the frequencies. Since only the positive frequency content of the real part of the spectrum is kept, while the signal is spread over N spectral bins, the factor becomes that of Equation 39.

Thus the complete expression for the SNR for the Fourier-transform spectrometer is

$$SNR_{FTS} = \frac{\eta_{FTS}\Phi_S(\sigma_2 - \sigma_1)T}{\sqrt{2\eta_{FTS}(\Phi_S + \Phi_B)(\sigma_2 - \sigma_1)TN^2 + N_0TN^2 + \alpha n_R^2 MN^2}}, \quad (40)$$

where α is a parameter equal to 2 for double-sided interferograms and it equals 1 for single-sided interferograms. The only difference in SNR performance between DSI and SSI FTS' is the ultimate SNR achieved for read-out noise limited measurements, where SSI dominates by a factor $\sqrt{2}$. So, for most practical cases, they both have the same performance.

SSI instruments are swept at half speed of DSI ones, so the measured interferogram samples are 2 times larger. However SSI instruments take all the noise to the real part of the spectrum, thus resulting in a improvement by a factor $\sqrt{2}$. The latter disappears for photon and detector noises since the noise contributions are also higher by a factor $\sqrt{2}$.

Since all the pixels of the image are measured simultaneously, the SNR is independent of the size of the image.

4.2.1.5 Summary

Table 3 gives a summary of the SNR behaviours for the various configurations and noises. Also listed in Table 3 are other important parameters to be considered to compare the instruments, along with the SNR, namely

- the size of the necessary focal-plane array (FPA);
- the duration of each sample measurement (giving the speed needed for the FPA); and

- the maximum signal level (to be compared with the dark current and the detector saturation levels).

Table 3: Summary of SNR in the photon noise limit (PN), detector noise limit (DN) and the readout noise limit (RN) for the various instruments (TF: tuneable filter; DF: dispersive filter; FTS: Fourier-transform spectrometer (α=2: double-sided interferogram; α=1: single-sided interferogram)

Type	*FPA*	*Sample Duration*	*Maximum Signal*	*SNR-PN*	*SNR-DN*	*SNR-RN*
TF	$K \times L$	$\Delta t \frac{1}{\beta N}$	$Q_0 \frac{\eta_{TF}}{\beta^2 N^2}$	$SNR_{\max_{PN}} \frac{\sqrt{\eta_{TF}}}{\beta N}$	$SNR_{\max_{DN}} \frac{\eta_{TF}}{\beta N \sqrt{\beta N}}$	$SNR_{\max_{RN}} \frac{\eta_{TF}}{\beta^2 N^2}$
DF	$K \times \beta N$	$\Delta t \frac{1}{L}$	$Q_0 \frac{\eta_{DF}}{\beta N L}$	$SNR_{\max_{PN}} \frac{\sqrt{\eta_{DF}}}{\sqrt{\beta N L}}$	$SNR_{\max_{DN}} \frac{\eta_{DF}}{\beta N \sqrt{L}}$	$SNR_{\max_{RN}} \frac{\eta_{DF}}{\beta N L}$
FTS	$K \times L$	$\Delta t \frac{1}{M}$	$Q_0 \frac{\eta_{FTS}}{M}$	$SNR_{\max_{PN}} \frac{\sqrt{\eta_{FTS}}}{\sqrt{2N}}$	$SNR_{\max_{DN}} \frac{\eta_{FTS}}{\sqrt{2}N}$	$SNR_{\max_{RN}} \frac{\eta_{FTS}}{\sqrt{\alpha} N \sqrt{M}}$

In Table 3, the following definition was used

$$Q_o = \Phi_S (\sigma_2 - \sigma_1) T \, . \tag{41}$$

The maximum SNRs are given in Table 4 for each noise contribution.

Table 4: Maximum SNR for each of the noise limits

Photon Noise (scene / background)	*Detector Noise*	*Read-out Noise*
$SNR_{\max_{PN}} = \sqrt{\frac{\Phi_S (\sigma_2 - \sigma_1) T}{1+\gamma}}$	$SNR_{\max_{DN}} = \Phi_S (\sigma_2 - \sigma_1) \sqrt{\frac{2e^2 T}{N_0}}$	$SNR_{\max_{RN}} = \frac{\Phi_S (\sigma_2 - \sigma_1) T}{n_R}$

4.2.1.5.1 Summary for N^3 data cube

In order to compare the instruments for integral field applications, we make comparisons for images with N × N pixels, each having N resolved spectral bins. Thus TF and FTS need a FPA with N × N pixels, while the DF still need a larger FPA. This situation makes full use of the available detectors.

Table 5: Summary of SNR in the photon noise limit (PN), detector noise limit (DN) and the readout noise limit (RN) for the various instruments for integral field applications (TF: tuneable

filter; DF: dispersive filter; FTS: Fourier-transform spectrometer (α=2: double-sided interferogram; α=1: single-sided interferogram)

Type	*FPA*	*Sample Duration*	*Maximum Signal*	*SNR-PN*	*SNR-DN*	*SNR-RN*
TF	$N \times N$	$\Delta t \frac{1}{\beta N}$	$Q_0 \frac{\eta_{TF}}{\beta^2 N^2}$	$SNR_{\max_{PN}} \frac{\sqrt{\eta_{TF}}}{\beta N}$	$SNR_{\max_{DN}} \frac{\eta_{TF}}{\beta N \sqrt{\beta N}}$	$SNR_{\max_{RN}} \frac{\eta_{TF}}{\beta^2 N^2}$
DF	$N \times \beta N$	$\Delta t \frac{1}{N}$	$Q_0 \frac{\eta_{DF}}{\beta N^2}$	$SNR_{\max_{PN}} \frac{\sqrt{\eta_{DF}}}{\sqrt{\beta} N}$	$SNR_{\max_{DN}} \frac{\eta_{DF}}{\beta N \sqrt{N}}$	$SNR_{\max_{RN}} \frac{\eta_{DF}}{\beta N^2}$
FTS	$N \times N$	$\Delta t \frac{1}{M}$	$Q_0 \frac{\eta_{FTS}}{M}$	$SNR_{\max_{PN}} \frac{\sqrt{\eta_{FTS}}}{\sqrt{2} N}$	$SNR_{\max_{DN}} \frac{\eta_{FTS}}{\sqrt{2} N}$	$SNR_{\max_{RN}} \frac{\eta_{FTS}}{\sqrt{\alpha} N \sqrt{M}}$

Framed formulae correspond to typical situations encountered in practice. Because all these instruments cannot reach the same throughput, FTS ones have much higher signal levels and they tend to be more PN limited, whereas TF / DF tend to be more DN / RN limited. It is shown that the different approaches have very different behaviours, when one considers only SNR. FTS appears to be superior for higher spectral resolution imaging applications. Nevertheless a complete numerical evaluation of the SNR, considering simultaneously all the contributions, needs to be done in order to compare the levels achievable with each instrument.

The SNR performance is compared for each of the noise contributions: photon noise (see Figure 18), detector noise (see Figure 19) and read-out noise (see Figure 20).

Figure 18 presents the variation of the SNR with an increase of the number of spectral bins, which corresponds mainly to an increased resolution. For photon noise limited, all instrument types behave about equally, the dispersive filter having a small advantage.

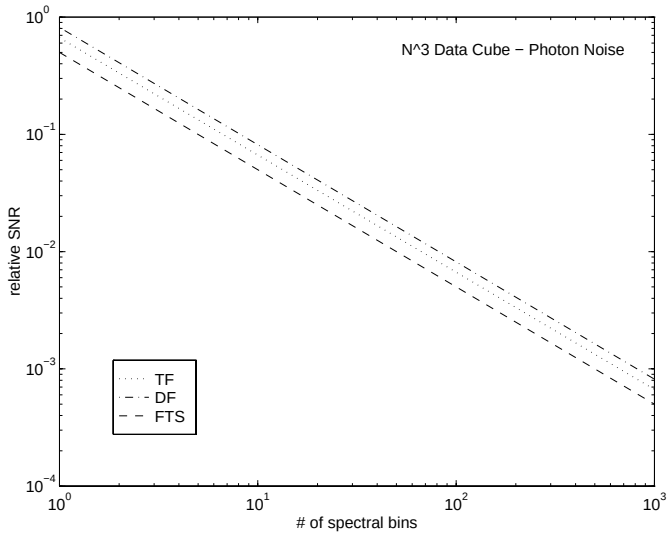

Figure 18 SNR for photon noise limited instruments in integral field applications.

Figure 19 presents the variation of the SNR with an increase of the number of spectral bins, which corresponds mainly to an increased resolution. For detector noise limited, the FTS has a clear advantage (the so-called multiplex advantage) over the other types of instrument.

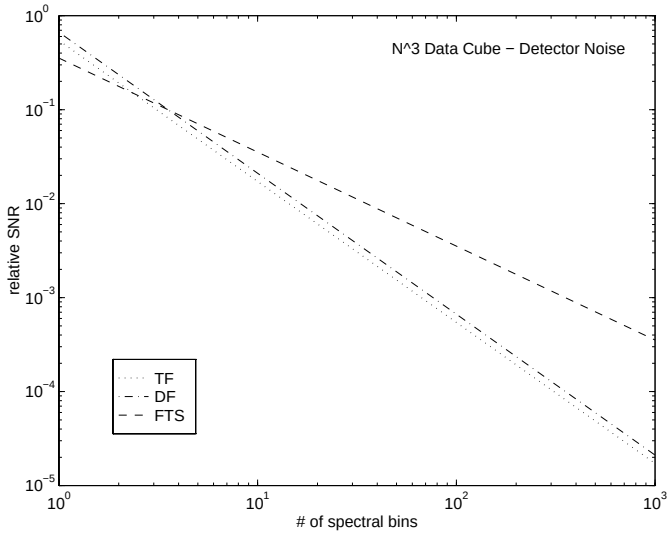

Figure 19 SNR for detector noise limited instruments in integral field applications.

Figure 20 presents the variation of the SNR with an increase of the number of spectral bins, which corresponds mainly to an increased resolution. For read-out noise limited, the FTS has still a clear advantage (the so-called multiplex advantage) over the other types of instrument. SSI instruments have a slight advantage over DSI.

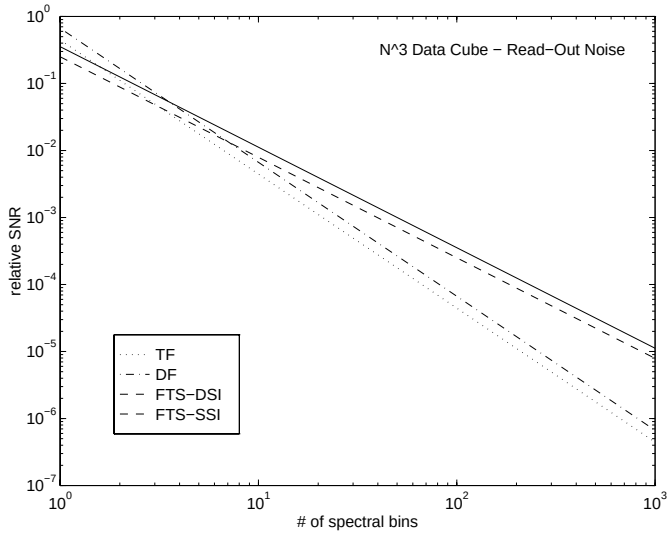

Figure 20 SNR for read-out noise limited instruments in integral field applications.

4.2.1.5.2 Summary for single pixel

In order to compare the instruments for multiple object applications, we make comparisons for images with 1 × 1 pixel, having N resolved spectral bins. Thus each instrument type uses as many detectors as needed, expecting them to be available.

Table 6: Summary of SNR in the photon noise limit (PN), detector noise limit (DN) and the readout noise limit (RN) for the various instruments for multiple object applications (TF: tuneable filter; DF: dispersive filter; FTS: Fourier-transform spectrometer (α=2: double-sided interferogram; α=1: single-sided interferogram)

Type	*FPA*	*Sample Duration*	*Maximum Signal*	*SNR-PN*	*SNR-DN*	*SNR-RN*
TF	1×1	$\Delta t \frac{1}{\beta N}$	$Q_0 \frac{\eta_{TF}}{\beta^2 N^2}$	$SNR_{\max_{PN}} \frac{\sqrt{\eta_{TF}}}{\beta N}$	$SNR_{\max_{DN}} \frac{\eta_{TF}}{\beta N\sqrt{\beta N}}$	$SNR_{\max_{RN}} \frac{\eta_{TF}}{\beta^2 N^2}$
DF	$1\times \beta N$	Δt	$Q_0 \frac{\eta_{DF}}{\beta N}$	$SNR_{\max_{PN}} \frac{\sqrt{\eta_{DF}}}{\sqrt{\beta N}}$	$SNR_{\max_{DN}} \frac{\eta_{DF}}{\beta N}$	$SNR_{\max_{RN}} \frac{\eta_{DF}}{\beta N}$
FTS	1×1	$\Delta t \frac{1}{M}$	$Q_0 \frac{\eta_{FTS}}{M}$	$SNR_{\max_{PN}} \frac{\sqrt{\eta_{FTS}}}{\sqrt{2N}}$	$SNR_{\max_{DN}} \frac{\eta_{FTS}}{\sqrt{2}N}$	$SNR_{\max_{RN}} \frac{\eta_{FTS}}{\sqrt{\alpha}N\sqrt{M}}$

Framed formulae correspond to typical situations encountered in practice. Because all these instruments cannot reach the same throughput, FTS ones have much higher signal levels and they tend to be more PN limited, whereas TF / DF tend to be more DN / RN limited. It is shown that the different approaches have relatively similar behaviour, when one considers only SNR for single pixel applications. Nevertheless a complete numerical evaluation of the SNR, considering simultaneously all the contributions, needs to be done in order to compare the levels achievable with each instrument.

Since it needs many detectors to be efficient, DF is taking advantage of the numerous detectors available. This is not the case for the TF / FTS. TF and FTS achieve the same SNR for a N^3 data cube or for a single pixel.

The SNR performance is compared for each of the noise contributions: photon noise (see Figure 21), detector noise (see Figure 22) and read-out noise (see Figure 23).

Figure 21 gives the variation of the SNR with an increase of the number of spectral bins, which corresponds mainly to an increased resolution. For photon noise limited, the DF has still a clear advantage (taking benefit of the extraneous detectors available) over the other types of instrument.

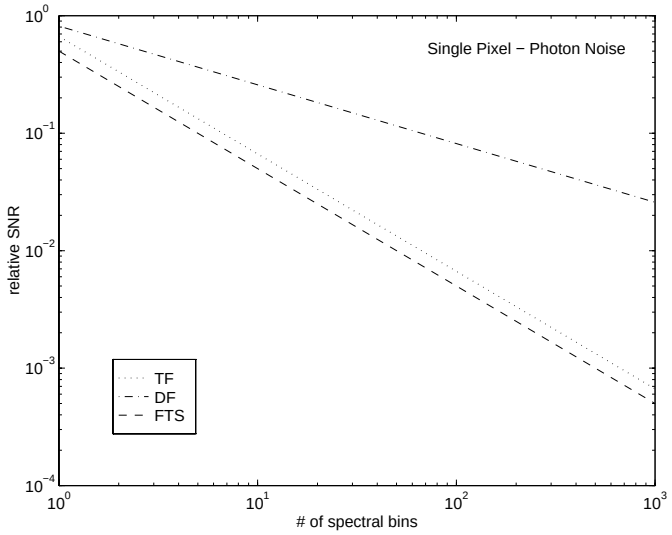

Figure 21 SNR for photon noise limited instruments in multiple object applications.

Figure 22 gives the variation of the SNR with an increase of the number of spectral bins, which corresponds mainly to an increased resolution. For detector noise limited, the DF and FTS have a net advantage over the TF instrument. DF achieves slightly higher SNR than FTS, at the cost of using many detectors.

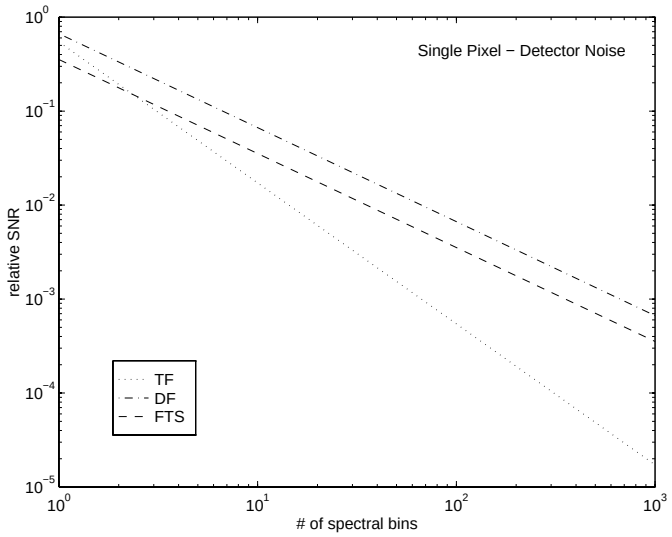

Figure 22 SNR for detector noise limited instruments in multiple object applications.

Figure 23 gives the variation of the SNR with an increase of the number of spectral bins, which corresponds mainly to an increased resolution. For read-out noise limited, the DF has the best sensitivity (taking benefit of the extraneous detectors available).

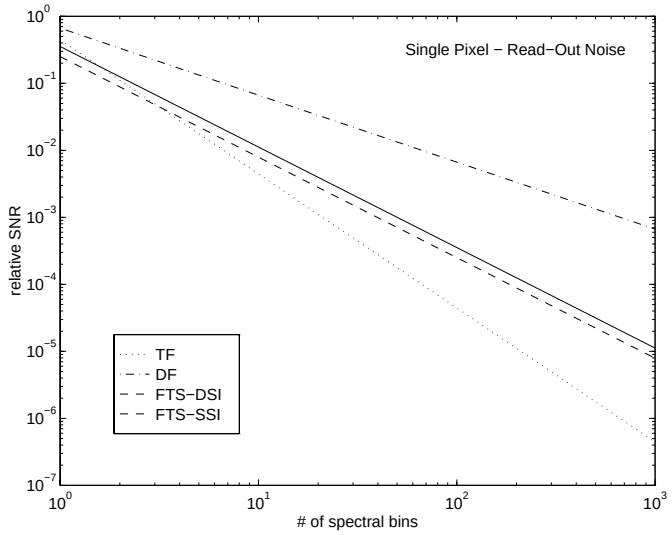

Figure 23 SNR for read-out noise limited instruments in multiple object applications.

4.2.2 Multi-Object Spectrographs

All the results of Section 4.2.1 can be applied directly to the case of multi-object spectrograph, by simply replacing L by 1. This has been done in Section 4.2.1.5.2.

In this case, the dispersive spectrometer enjoys a relative improvement due to the fact that it uses a multi-detector group (that provide the spectral information along the dispersion axis) for each of the object in the field, as opposed to the other instruments that only use one pixel to build the spectrum (using time modulation).

5. IFTS SWEEP STRATEGIES

5.1 INTRODUCTION

This section analyses various approaches for optimising the sensitivity of the IFTS. The main motivation is to investigate means of making the FTS more attractive, because it is believed to have sensitivity disadvantage as compared to dispersive spectrometers. Please refer to Sections 2 and 4 for more details on the sensitivity calculations.

5.2 PROPOSED METHODS

5.2.1 Uneven integration time versus OPD

It has been suggested by a number of people that using a uneven integration time versus OPD may be a way to improve the signal-to-noise ratio of a FTS measurement. The idea is to spend more time in some area of the optical path difference in order to locally improve the noise in that section of the interferogram. This is illustrated in Figure 24 where we consider a step-scan FTS equipped with an integrating detector for simplicity. Similar discussions can be held for a rapid-scan FTS equipped with an AC-coupled, band-limited detector. The most "natural" way to perform the interferogram samples is to use equal integration time for all OPD samples (dash line). However we would like to investigate the efficiency of uneven integration times such as the example shown in Figure 24 (solid line).

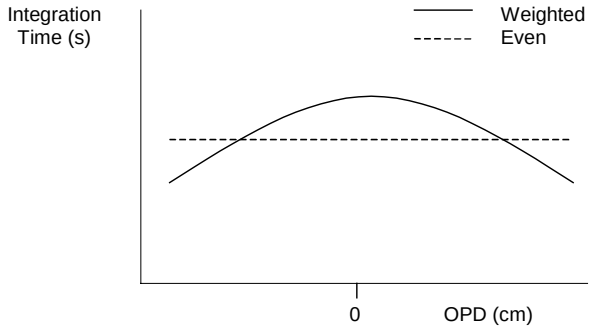

Figure 24 Integration time schemes

In order to derive some quantitative comparison, let us define the following terms. Let

T be the total integration time

N be the total number of interferogram (IGM) samples

τ_i be the integration time on IGM sample *i*, with *i = 0 to N-1*

so that the total time is

$$T = \sum_{i=0}^{N-1} \tau_i \tag{42}$$

If the integration time is constant along the OPD we have

$$T = \sum_{i=0}^{N-1} \tau_i = \sum_{i=0}^{N-1} \bar{\tau} = N\bar{\tau} \tag{43}$$

With $\bar{\tau}$ the constant integration time for each sample

On the other hand for uneven integration times τ_i' defined as $\tau_i' = \rho_i \bar{\tau}$, where ρ_i are positive numbers we have

$$T = N\ \bar{\tau} = \sum_{i=0}^{N-1} \tau_i' = \sum_{i=0}^{N-1} \rho_i\ \bar{\tau} = \bar{\tau} \sum_{i=0}^{N-1} \rho_i \tag{44}$$

which implies that

$$\sum_{i=0}^{N-1} \rho_i\ = N \tag{45}$$

We will now analyse the problem by separating the noise ε_x from the signal S_x in the interferogram, as illustrated in Figure 25.

$$IGM = S_x + \varepsilon_x \tag{46}$$

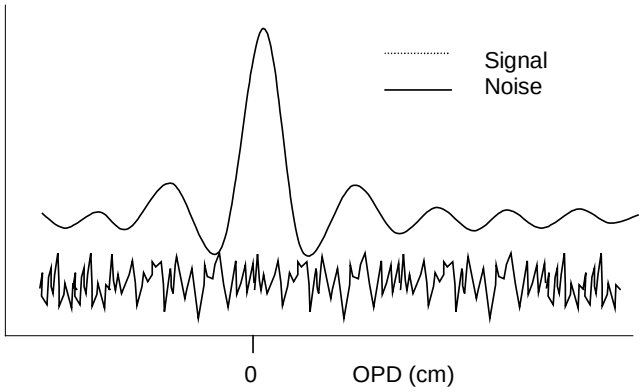

Figure 25 Decomposing the interferogram in signal and noise

Of course the end goal is to obtain the optimum SNR in the spectral domain, where we can also separate the signal and the noise in a similar manner.

$$SPC = S_\sigma + \varepsilon_\sigma \tag{47}$$

Because of the linearity of the Fourier transform we can consider that the signal in the spectral domain is the FT of the signal in the interferogram domain; $S_\sigma = \Im[S_x]$ and correspondingly that the noise in the spectral domain is the FT of the noise in the interferogram domain; $\varepsilon_\sigma = \Im[\varepsilon_x]$.

We will now consider the case illustrated in Figure 26. This figure considers two cases: a) a "classical" constant integration time and b) a triangular integration time such that the total time is equal for both cases. In the first case we obtain in c) a generic-looking interferogram signal and noise. Strictly speaking the example illustrated in Figure 26 would be either detector dark noise or readout noise dominated rather than photon noise dominated, because of the uniform noise amplitude across the OPD. However the mathematical development presented here does not assume or require OPD-independent noise and is general (applicable to photon noise for example). Separate Fourier Transform of the signal and noise yield the spectral signal and noise as shown in d).

With a weighted integration time illustrated in b) we get the distorted signal and noise as shown in e). With this triangular weighting the signal is increased around Zero Path Difference (ZPD) and decreased at the OPD extremities, both linearly with integration time. The noise on the other hand varies with the square root of the integration time, whether the noise is due to photon noise or dark noise. This is graphically represented in e).

In order to perform a equitable comparison between the weighted versus constant integration time case, one must normalize the signal and noise of the former case. If this is not done, the spectral signal would correspond to numerically apodizing the interferogram, and the spectral resolution would be affected. Changing the spectral resolution clearly has an effect on the SNR as explained in Section 5.2.2. In this section we want to study the effect of changing the integration times alone for a constant spectral resolution so we want to remove the apodization of the signal. This is shown in Figure 26 f) where both the signal and noise have been divided by the integration time profile as shown in b). This as the effect of making the signal equal to the even integration time case b). This also has the effect of changing the noise distribution as shown in f). The noise thus has a global scaling inversely proportional to the square root of the integration time. Once transformed to the spectral domain, the noise appear white g) but it is not because it is now affected by a degree of correlation. This arises because the noise in g) is really the white noise of d) convolved with the Fourier Transform of the envelope function that relates the noise in f) as compared to the noise in c).

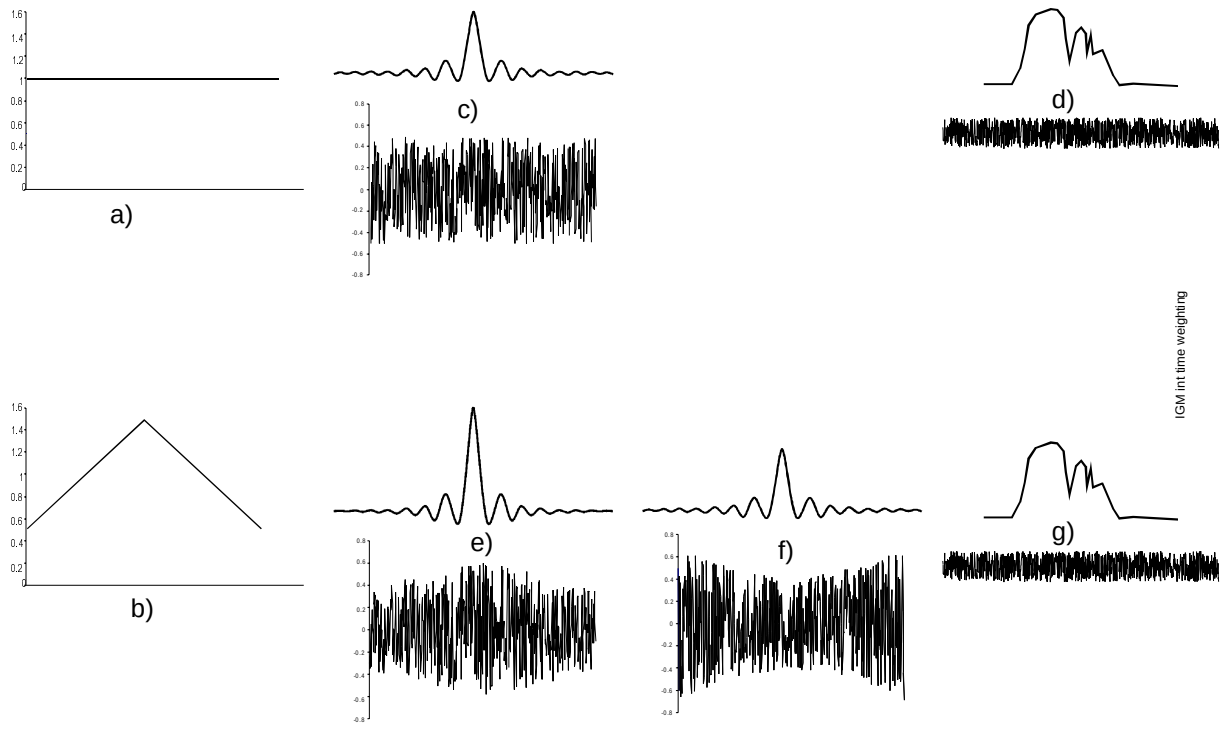

Figure 26 Comparison of even and uneven integration time approaches

To estimate the increase or decrease of the amplitude of noise for the weighted integration time case, we will use the formulation of Parseval's theorem given in Equation 48.

$$\langle \varepsilon_\sigma \rangle = \sqrt{\frac{\Delta x}{\Delta \sigma}} \langle \varepsilon_x \rangle \tag{48}$$

where Δx is the maximum path difference (cm)

$\Delta\sigma$ is half the sampling frequency (cm^{-1})

$\langle\ \rangle$ is the standard deviation operator applied to the vector, respectively in the spectral or interferogram domain.

Since Δx and $\Delta\sigma$ are constant for both the constant (superscript c) and weighted (superscript w) integration time cases, we can write

$$\frac{\langle \varepsilon_\sigma^w \rangle}{\langle \varepsilon_\sigma^c \rangle} = \frac{\langle \varepsilon_x^w \rangle}{\langle \varepsilon_x^c \rangle} \tag{49}$$

Following the explanations describing Figure 26 we can also write that on a small portion OP of the OPD,

$$\left\langle \varepsilon_x^w \right\rangle_{OP} = \frac{\left\langle \varepsilon_x^c \right\rangle_{OP}}{\sqrt{\rho_i}} \tag{50}$$

Equation 50 can be reasoned as follows, on a small portion of the OPD where the integration time can be considered constant for a smooth and slowly changing weighting function, the noise in the weighted integration time case is simply inversely proportional to the ratio of the integration time ρ_i . Equation 50 also makes the assumption of ergoticity, i.e. that the amplitude of the noise is the same statistically (for example for several experiments) or for neighbouring points in the vector in the spectral or interferogram domain.

Using Equation 50, Equation 49 can be rewritten as

$$\frac{\left\langle \varepsilon_\sigma^w \right\rangle}{\left\langle \varepsilon_\sigma^c \right\rangle} = \frac{\sqrt{\frac{1}{N}\sum_{wholeOPD}\left(\varepsilon_x^w\right)^2}}{\left\langle \varepsilon_x^c \right\rangle} = \frac{\sqrt{\frac{1}{N}\sum_{OP1}\left(\varepsilon_x^w\right)^2 + \frac{1}{N}\sum_{OP2}\left(\varepsilon_x^w\right)^2 + \frac{1}{N}\sum_{OP3}\left(\varepsilon_x^w\right)^2 + \ldots}}{\left\langle \varepsilon_x^c \right\rangle}$$

$$\frac{\sqrt{\left\langle \varepsilon_\sigma^w \right\rangle_{OP1}^2 + \left\langle \varepsilon_\sigma^w \right\rangle_{OP2}^2 + \left\langle \varepsilon_\sigma^w \right\rangle_{OP3}^2 + \ldots}}{\sqrt{\left\langle \varepsilon_\sigma^c \right\rangle_{OP1}^2 + \left\langle \varepsilon_\sigma^c \right\rangle_{OP2}^2 + \left\langle \varepsilon_\sigma^c \right\rangle_{OP3}^2 + \ldots}} = \frac{\sqrt{\frac{1}{\rho_{OP1}}\left\langle \varepsilon_\sigma^c \right\rangle_{OP1}^2 + \frac{1}{\rho_{OP2}}\left\langle \varepsilon_\sigma^c \right\rangle_{OP2}^2 + \frac{1}{\rho_{OP3}}\left\langle \varepsilon_\sigma^c \right\rangle_{OP3}^2 + \ldots}}{\sqrt{\left\langle \varepsilon_\sigma^c \right\rangle_{OP1}^2 + \left\langle \varepsilon_\sigma^c \right\rangle_{OP2}^2 + \left\langle \varepsilon_\sigma^c \right\rangle_{OP3}^2 + \ldots}} \tag{51}$$

It can be shown that Equation 51 is always > 1.

This means that the noise (standard deviation) in any weighted approach is larger or at best equal to the noise in a constant integration time approach. This shows that in general the weighted approach is worse than using the usual constant integration time approach and that it does not constitute an obvious candidate for improving the SNR of an FTS measurement.

This however does not mean that there is no value in using a weighted approach. Apart from increasing the total noise, a weighted approach will "colour" the noise so that it is possible to favor low frequency or high frequency noise, in a manner decoupled from the signal itself (which is usually treated by performing numerical apodization). In other words it provides a extra degree of liberty in signal processing, allowing to treat the noise separately from the signal. If a particular science application is highly dependent on a particular type of noise, it is conceivable to use the weighted integration time approach to reduce this type of noise at the detriment of another type of noise. This judgement however is beyond the scope of this study.

5.2.2 Optimization of OPD and Numerical Apodization

The figure of merit commonly used for the sensitivity of spectroradiometer is the Noise Equivalent Spectral Radiance (NESR).

$$NESR(\sigma) = \frac{I_N(\sigma)}{R_{AC}(\sigma)\tau(\sigma)M(\sigma)\Theta\sqrt{t}\Delta\sigma\ F} \qquad (52)$$

where $I_N(\sigma)$ is the noise current (A $Hz^{-1/2}$)

$R_{AC}(\sigma)$ is the detector responsivity (A W^{-1})

$\tau(\sigma)$ is the system transmission ()

$M(\sigma)$ is the system modulation ()

Θ is the system Étendue (sr cm^2)

t is the acquisition time (s)

$\Delta\sigma$ is the spectral interval (cm^{-1}) = 1/(2MPD)

F is a factor dependant on the numerical apodization factor

According Equation 52, with everything else being constant, the NESR is inversely proportional to the spectral resolution. The spectral interval $\Delta\sigma$ is directly related to the spectral resolution[1] and simply the inverse of twice the maximum OPD (MPD). The factor *F* is a number larger than 1 for most numerical apodization functions. It is easy to see that the noise in the spectrum will be decreased if the noise in the interferogram is decreased by a numerical apodization function (see Equation 50).

From Equation 52, we see that one can reduce the noise in the spectrum by reducing MPD and/or performing numerical apodization on the interferogram. However both of these methods lead to a decrease of spectral resolution or information. This behaviour is expected of all spectrometers in general and not only of FTS.

For all missions, there should be a trade study performed to find the optimum spectral resolution to achieve the maximum science by trading noise and spectral resolution.

[1] The term spectral resolution is ill defined. Several definitions exist and tend to vary from one scientific domain to the other.

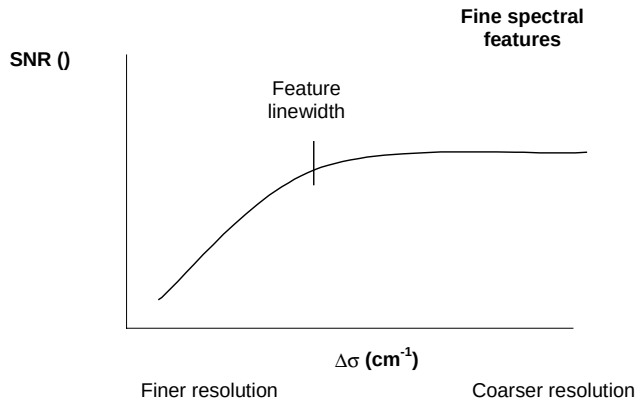

Figure 27 SNR versus Spectral Interval

Figure 27 shows the behaviour of the SNR of fine spectral features. The left side of Figure 27 illustrates the statement that the SNR decreases when the spectral resolution is decreased. This holds when the spectral resolution is better than the spectral feature, i.e. when the feature is resolved. If the feature is not resolved, the data points at the peak of the feature will decrease linearly with the spectral resolution, offsetting any reduction of noise, leading to a constant SNR. This underlines the fact that Equation 52 considers only the noise and not the possible change of signal, so it holds for spectrally resolved features.

6. APPENDIX A: NOISE CONTRIBUTIONS

This section describes the noise processes present in photon counting experiments, namely shot noise and additive white noise.

6.1 SHOT NOISE IN A PHOTON COUNTING PROCESS

In this appendix, photon counting is studied as a random process such that the photons produce the following current:

$$n(t) = \sum_i e\delta(t - t_i), \tag{53}$$

where e is the electron charge and t_i are the random instants of arrival of photons which is known to follow a Poisson distribution [PAP91]. The mean arrival rate is:

$$\lambda = (\Phi_S + \Phi_B)(\sigma_2 - \sigma_1) = \frac{I_0}{e}. \tag{54}$$

The expectation value of n(t) can then be evaluated:

$$E\{n(t)\} = \lambda e = I_0. \tag{55}$$

The autocorrelation function and the doubled-sided power spectral density of n(t) are respectively:

$$R_n(\tau) = e^2\lambda^2 + e^2\lambda\delta(t) \tag{56}$$

and

$$S_n(f) = e^2\lambda^2\delta(f) + e^2\lambda. \tag{57}$$

Now, the process n(t) is altered in some way by the detector. Let $n_f(t)$ be the detected process and let define $n_f(t)$ so that:

$$n_f(t) = h(t) \otimes n(t), \tag{58}$$

where h(t) is the impulse response of the detector and $\otimes$ stands for the convolution. The expectation and variance of $n_f(t)$ are accordingly:

$$E\{n_f(t)\} = e\lambda \int_{-\infty}^{\infty} h(t)dt \tag{59}$$

and

$$\sigma_{n_f}^2 = e^2\lambda \int_{-\infty}^{\infty} h^2(t)dt. \tag{60}$$

6.2 CHARGE-ACCUMULATING DETECTION

6.2.1 Shot noise

If the detector is accumulating charges, such as a CCD, the function h(t) is a unitary boxcar of duration Δt, that is $h(t)=u(t)-u(t-\Delta t)$ (see Figure 28).

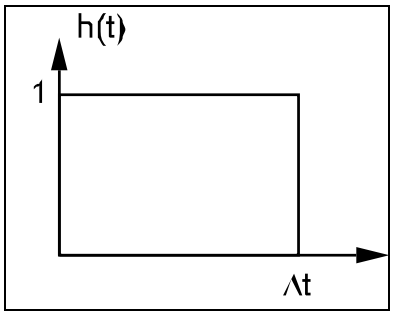

Figure 28 Impulse function of a charge-accumulating detector

The expectation and variance of $n_f(t)$ are in this case:

$$E\{n_f(t)\} = e\lambda\Delta t = I_0\Delta t = Q_0 \tag{61}$$

and

$$\sigma_{n_f}^2 = e^2\lambda\Delta t = eI_0\Delta t = eQ_0 . \tag{62}$$

The signal to noise ratio can finally be calculated:

$$SNR = \frac{e\lambda\Delta t}{\sqrt{e^2\lambda\Delta t}} = \sqrt{\lambda\Delta t} . \tag{63}$$

This result shows that the signal to noise is the square root of the average number of photons detected in the time interval Δt, as it is expected for standard photon counting experiment.

6.2.2 Additive white noise

If the system is limited by a constant single-sided white noise level N_0 (in A^2/Hz), the noise variance would instead be:

$$\sigma_{n_f}^2 = \frac{N_0}{2}\Delta t . \tag{64}$$

6.3 PHOTOCURRENT DETECTION

6.3.1 Shot noise

For a photocurrent detector followed by a normalised electrical integrator, the impulse response is a unitary area boxcar of duration Δt.

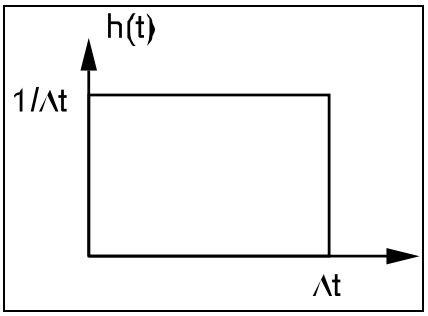

Figure 29 Impulse response of a photocurrent detector followed by a normalised integrator.

Here h(t) = (u(t)-u(t-Δt))/Δt. The expectation and variance of $n_f(t)$ are in that case:

$$E\{n_f(t)\} = e\lambda = I_0 \tag{65}$$

and

$$\sigma_{n_f}^2 = \frac{e^2\lambda}{\Delta t} = \frac{eI_0}{\Delta t}. \tag{66}$$

The signal to noise ratio can finally be calculated:

$$SNR = \frac{e\lambda}{\sqrt{e^2\lambda/\Delta t}} = \sqrt{\lambda \Delta t}. \tag{67}$$

This result shows that the signal to noise ratio is the same for both detector types.

6.3.2 Additive white noise

If the system is limited by a constant single-sided white noise level N_0 (in A^2/Hz), the noise variance would instead be:

$$\sigma_{n_f}^2 = \frac{N_o}{2}\frac{1}{\Delta t}. \tag{68}$$

7. APPENDIX B: EFFECT OF A DISCRETE FOURIER TRANSFORMATION ON SNR

The aim of this appendix is to establish the effects on the signal to noise ratio when applying a discrete Fourier transformation (DFT) on a temporal signal. The goal is to be able to deduce to spectral signal to noise ratio for a given value of the SNR on a time signal.

7.1 DOUBLE-SIDED INTERFEROGRAMS

Let's start with a widely used definition of the DFT, its inverse and the discrete Parseval theorem for a real signal of length M [OPP89]:

$$DFT: X[k] = \sum_{n=0}^{M-1} x[n] e^{j2\pi \frac{k}{M} n}, \tag{69}$$

$$DFT^{-1}: x[n] = \frac{1}{M} \sum_{k=0}^{M-1} X[k] e^{-j2\pi \frac{k}{M} n} \tag{70}$$

and

$$\sum_{n=0}^{M-1} x^2[n] = \frac{1}{M} \sum_{k=0}^{M-1} \left| X[k] \right|^2 . \tag{71}$$

These definitions apply to double-sided interferograms and double-sided spectra. They include the fact that the data must be realigned before it is processed. So a double-sided interferogram ends starting with zero-path difference (ZPD) up to one end, followed by the points at the other end of the sweep and finishing with the points close to ZPD. This is coherent with the fact that the fast-Fourier transform (FFT) algorithm works with the hypothesis that both the signal and the spectrum are periodic. More specifically, the pattern observed from 0 to M-1 is repeated from M to 2M-1, and so on or conversely the pattern from –M/2+1 to M/2 is repeated from M/2+1 to 3M/2, and so on. Therefore the negative frequency side, being mapped from –M/2+1 to –1, is also mapped from M/2+1 toM-1.

Suppose that the spectrum X[k] is non zero only for one spectral bin, k_0, such that:

$$X[k] = \delta[k + k_0] + \delta[k - k_0], \tag{72}$$

The use of the DFT implies that this sequence is periodic with a period M. In fact the DFT maps a periodic "time" sequence into a periodic spectral sequence. This real and even spectrum corresponds to a real and even time signal, which is:

$$x[n] = \frac{2}{M} \cos\left(2\pi \frac{k_0}{M} n \right). \tag{73}$$

Now, if the spectrum is flat over a given spectral band and zero outside this band, the discrete spectrum is a collection of N adjacent non-zero spectral bins having the same value:

$$X[k] = \sum_{k_1=k_0}^{k_0+N-1} \left(\delta[k+k_1] + \delta[k-k_1]\right), \tag{74}$$

where all non-zero spectral bins are assigned a unitary value. The corresponding time signal is therefore:

$$x[n] = \sum_{k_1=k_0}^{k_0+N-1} \frac{2}{M} \cos\left(2\pi \frac{k_1}{M} n\right). \tag{75}$$

This interferogram has its maximal value at n=0. It is given by:

$$x[0] = \sum_{k_1=k_0}^{k_0+N-1} \frac{2}{M} \cos(0) = \frac{2}{M}(k_0 + N - 1 - k_0 + 1) = \frac{2N}{M} \tag{76}$$

This shows that for N out of M/2 unitary spectral bins, the maximal interferogram value is 2N/M. Conversely if the maximal value of the time signal is one, the N non-zero spectral bins will have a M/2N value. Here we use the fact that the time signal has no DC component. If it has been present, it theoretically should be a level of 1 in the interferogram domain, corresponding to a level M for the spectral bin at 0. This is depicted in Figure 30 for a band-limited spectrum and its interferogram. It must be noticed that both the interferogram and its spectrum are folded in order to be easier to interpret.

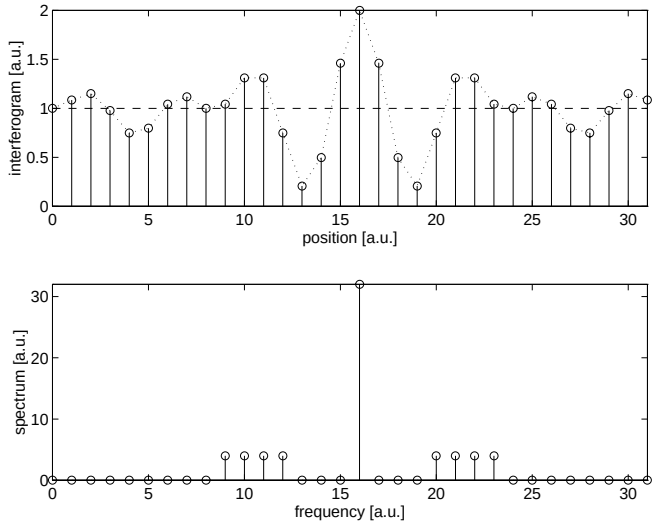

Figure 30 Interferogram and associated band-limited spectrum.

If x[n] =e[n] where e[n] is a zero-mean white noise with variance σ_e^2, the transformed signal will also be zero-mean white noise. The point is to evaluate the noise variance in this domain. Using Parseval's relation one has:

$$E\left\{\sum_{n=0}^{M-1} e^2[n]\right\} = E\left\{\frac{1}{M}\sum_{k=0}^{M-1}\left|E[k]\right|^2\right\}. \tag{77}$$

By interchanging the order of operators and expressing $|E[k]|^2$ with its real and imaginary components, one obtains:

$$\sum_{n=0}^{M-1} E\left\{e^2[n]\right\} = \frac{1}{M}\sum_{k=0}^{M-1}\left(E\left\{E_r^2[k]\right\} + E\left\{E_i^2[k]\right\}\right), \tag{78}$$

since the real and imaginary values of the DFT are uncorrelated. All the expectations in this equation are variances. The transformed noise will be equally split between the real an imaginary parts so that:

$$\sum_{n=0}^{M-1}\sigma_e^2 = \frac{1}{M}\sum_{k=0}^{M-1}(\sigma_{E_r}^2 + \sigma_{E_i}^2) = \frac{2}{M}\sum_{k=0}^{M-1}\sigma_{E_r}^2 \ . \tag{79}$$

Thus the variance of the real part of the DFT becomes:

$$\sigma_{E_r} = \sqrt{\frac{M}{2}}\sigma_e . \tag{80}$$

Combining all the results, one can then say that if an interferogram has a unitary maximal value, its SNR will be (at n=0):

$$SNR_{IGM} = 1\big/\sigma_e \ . \tag{81}$$

It is now also possible to calculate the spectral SNR for the non-zero spectral bins:

$$SNR_{SPC} = \frac{M\big/2N}{\sqrt{M\big/2}\sigma_e} = \frac{1}{N}\sqrt{\frac{M}{2}}\frac{1}{\sigma_e} = \frac{1}{N}\sqrt{\frac{M}{2}}SNR_{IGM} , \tag{82}$$

which is the desired result. We have thus related the spectral SNR to the interferogram SNR at ZPD.

7.2 SINGLE-SIDED INTERFEROGRAMS

Single-sided interferograms could be measured instead of full double-sided ones since the interferogram is theoretically even. So, in principle, a single-sided interferogram is simply mirrored prior to the evaluation of the DFT:

$$x[n] = \begin{cases} x_{SSI}[n], & 0 \le n \le \dfrac{M}{2} \\ x_{SSI}[M-n], & \dfrac{M}{2}+1 \le n \le M-1 \end{cases} . \tag{83}$$

The DFT becomes

$$X[k] = \sum_{n=0}^{\frac{M}{2}} x_{SSI}[n] e^{j2\pi \frac{k}{M} n} + \sum_{n=\frac{M}{2}+1}^{M-1} x_{SSI}[M-n] e^{j2\pi \frac{k}{M} n} \tag{84}$$

By reordering the last sum and by rearranging terms, one finally finds

$$X[k] = 2 \sum_{n=0}^{\frac{M}{2}-1} x_{SSI}[n] \cos\left(2\pi \frac{k}{M} n \right) - x_{SSI}[0] + (-1)^k x_{SSI}[M/2]. \tag{85}$$

This last result clearly shows that the DFT is real, which corresponds to an even time sequence. So a given level of interferogram, double-sided or mirrored single-sided, gives the same level in the spectrum domain.

Given Parseval's relation, the noise contribution is

$$E\left\{ \sum_{n=0}^{\frac{M}{2}} e_{SSI}^2[n] + \sum_{n=\frac{M}{2}+1}^{M-1} e_{SSI}^2[M-n] \right\} = E\left\{ \frac{1}{M} \sum_{k=0}^{M-1} \left| E[k] \right|^2 \right\}. \tag{86}$$

By interchanging the order of operators and expressing $|E[k]|^2$ only with its real component, since the time sequence is still even, one obtains:

$$\sum_{n=0}^{\frac{M}{2}} E\left\{ e_{SSI}^2[n] \right\} + \sum_{n=\frac{M}{2}+1}^{M-1} E\left\{ e_{SSI}^2[M-n] \right\} = \frac{1}{M} \sum_{k=0}^{M-1} E\left\{ E_r^2[k] \right\}. \tag{87}$$

All the expectations in this equation are variances since the stochastic processes are zero-mean,

$$\sum_{n=0}^{M-1} \sigma_e^2 = \frac{1}{M} \sum_{k=0}^{M-1} \sigma_{E_r}^2 . \tag{88}$$

Thus the variance of the real part of the DFT becomes:

$$\sigma_{E_r} = \sqrt{M} \sigma_e . \tag{89}$$

Combining all the results, one can then say that if an interferogram has a unitary maximal value, its SNR will be (at n=0):

$$SNR_{IGM} = 1 / \sigma_e . \tag{90}$$

It is now also possible to calculate the spectral SNR for the non-zero spectral bins:

$$SNR_{SPC} = \frac{M/2N}{\sqrt{M}\sigma_e} = \frac{1}{2N}\sqrt{M}\,\frac{1}{\sigma_e} = \frac{1}{2N}\sqrt{M}\,SNR_{IGM}\,, \qquad (91)$$

which is the desired result. We have thus related the spectral SNR to the interferogram SNR at ZPD. The last result shows a factor $\sqrt{2}$ with the relation obtained for the double-sided case (Equation 82), because the mirroring operation made all the noise even and put all its contribution in the real part of the spectrum.

— End of document —